Development of NMR Methodologies to Study Site Specific Zinc-Protein Interactions

by

Amy Musgrave Benton

July 2021

Director of Thesis: Colin S. Burns, Ph.D.

Major Department: Chemistry

Abstract

Found in all three biological domains of life and the second most abundant metal in the human body, zinc (Zn^{2+}) is essential to various cellular processes like the metabolism of DNA and RNA, gene expression, and the regulation of apoptosis. However, as a d^{10} metal, Zn^{2+} is spectroscopically silent; electromagnetic radiation cannot induce d-to-d transitions. Current methodologies used to study zinc-binding proteins (ZBPs) include x-ray crystallography, NMR chemical shift monitoring, and amino acid substitutions studies. However, these all have limitations, like the inability to crystallize irregular and unstructured proteins, spectral overlap in NMR prohibiting assignment of residues, and the need to express of chemically synthesize several mutants. With the exception of x-ray crystallography, NMR and the study of mutants provide indirect information about the Zn^{2+} coordination sphere.

The purpose of this research was to determine if the quadrupolar nucleus zinc-67 ($^{67}Zn^{2+}$) could be used in NMR experiments to more directly identify Zn^{2+}-binding ligands. Two approaches were explored here, one based on ^{13}C spin-lattice relaxation measurements (T_1) and

the other on the observation of spin-spin splitting in 1D ^{1}H and ^{13}C spectra. The model systems used for these experiments were ethylenediaminetetraacetic acid (EDTA), a carboxyl containing Zn^{2+} chelator; glycine (Gly), a simple amino acid; and PK9-H, a portion of the vacuolar cation-transporting ATPase (YPK9) protein shown to bind zinc. NMR studies of Zn-EDTA yielded ^{13}C T_1 values of 7.653 s (± 0.415), 409.650 ms (± 26.063), and 343.033 ms (± 38.171) for the carbonyl, lateral, and central carbons, respectively. ^{67}Zn-EDTA had T_1 values of 8.480 s (± 0.579), 454.167 ms (± 56.329), and 395.266 ms (± 66.944). The differences between Zn-EDTA and ^{67}Zn-EDTA T_1 values were statistically insignificant, indicating that $^{67}Zn^{2+}$ did not significantly alter the spin-lattice relaxation of the nearby carbon atoms. No J-couplings between ^{67}Zn and nearby atoms were readily observable in the 1D ^{1}H and ^{13}C spectra. If there is J-coupling, then it is likely very small ($\ll$ 1 Hz). The NMR studies of Gly showed that the addition of Zn^{2+} resulted in various Zn^{2+}-bound species in solution and a loss in the carbonyl carbon signal. Therefore, it was deemed to be a poor system to use for these studies. Despite previous NMR research suggesting that the PK9-H peptide of YPK9 bound Zn^{2+}, our CD and fluorescence studies showed no evidence of a binding interaction. However, a ^{13}C NMR spectrum was recorded and the conditions for running solvent-suppressed ^{1}H NMR and 2D ^{1}H-^{1}H TOCSY were optimized so that these experiments could be more easily completed in the future. In conclusion, there is no evidence that the utilization of ^{67}Zn provides binding information about ligating atoms as it does not induce new splitting in NMR spectra and does not impact T_1 values of atoms two or three bonds away from ^{67}Zn. It is not recommended to pursue a heteronuclear TOCSY methodology using quadrupolar ^{67}Zn. Further, Gly and YPK9 do not appear to be suitable model systems for these studies, as the former forms multiple Zn-bound species in solution and the latter shows little evidence of Zn-binding.

Development of NMR Methodologies to Study Site Specific Zinc-Protein Interactions

A Thesis

Presented to the Faculty of the Department of Chemistry

East Carolina University

In Partial Fulfillment of the Requirements for the Degree

Master of Science Degree in Chemistry

by

Amy Musgrave Benton

July 2021

Development of NMR Methodologies to Study Site Specific Zinc-Protein Interactions

by

Amy Musgrave Benton

APPROVED BY:

DIRECTOR OF

THESIS: _____

Colin S. Burns, Ph.D.

COMMITTEE MEMBER: _____

Sambuddha Banerjee, Ph.D.

COMMITTEE MEMBER: _____

Anne M. Spuches, Ph.D.

COMMITTEE MEMBER: _____

Patrick J. Horn, Ph.D.

CHAIR OF THE DEPARTMENT

OF CHEMISTRY: _____

Andrew T. Morehead, Jr., Ph.D.

DEAN OF THE

GRADUATE SCHOOL: _____

Paul J. Gemperline, Ph.D.

Dedicated to Grandmama and Granddaddy

Thank you for everything.

I love you.

Acknowledgements

Foremost, I would like to express the deepest appreciation for my thesis advisor, Dr. Colin S. Burns, for his continued support allowing me to complete this master's degree. His guidance, patience, and reassurance has allowed this to be possible. My sincere thanks go to the members of my thesis committee – Dr. Banerjee, Dr. Horn, and Dr. Spuches – for their willingness to share their knowledge and their encouragement throughout my pursuit of this degree. I would also like to thank Dr. Hvastkovs for having so much faith in me as a freshman in his advising office and continuing to guide me throughout my higher education career. I am grateful for David Halatek, my lab mate who has kept me levelheaded throughout the past year.

I would like to thank Kristin Tyson and Caitlin Palmer Willett, who have continued to pick me up and dust me off throughout my undergraduate and graduate education. Unquestionably, I would not be here without their numerous pep talks and unwavering support. I love you both. I want to express my appreciation for Allyson Brown, my best friend who has continued to love and support me since we were children. Thank you for continuing to proofread my papers after all this time. I love you. I would like to express my gratitude for my sister, Kristina, mother, grandmother, and grandfather for their uncompromising love and encouragement. Lastly, I would like to thank my loving husband for his continuous love and support. Thank you for believing in me even when I didn't believe in myself. I love you, honey.

Table of Contents

List of Tables ..... **viii**

List of Figures ..... **x**

List of Abbreviations ..... **xiii**

Chapter 1: Introduction **1**

1.1 The Biological Relevance of Zinc 1

1.2 Chemical Properties & Protein Interactions of Zinc 2

1.3 Current Methodologies to Determine Spectroscopically Silent Metal-Protein Interactions 4

1.3.1 X-ray Crystallography 4

1.3.2 NMR Chemical Shift Monitoring 8

1.3.3 Point Mutations 11

1.4 NMR, Zinc, & T_1 Relaxation Mechanism 12

1.5 Inversion Recovery Experiment 19

1.6 Previous Research in the Burns Lab 22

1.7 Project Aims 25

1.8 Vacuolar Cation-transporting ATPase 26

Chapter 2: Materials and Methods **33**

2.1 Preparation of EDTA Solutions & NMR Studies 33

2.2 Glycine Solution Preparation & NMR Studies 34

2.3 Peptide Synthesis & Purification 35

2.4 Peptide Solution Preparation & Circular Dichroism Spectropolarimetry 36

2.5 Peptide Solution Preparation & Fluorescence Spectroscopy 37

2.6 Peptide Solution Preparation & Nuclear Magnetic Resonance Spectroscopy 37

Chapter 3: Results 38

3.1 EDTA Studies 38

3.1.1 T_1 Measurements 38

3.1.1 J-couplings 51

3.2 Glycine Studies 55

3.3 PK9-H Peptide Studies 59

Chapter 4: Conclusions & Future Directions 69

References 73

Appendix A: Fitting Data of EDTA Solutions 79

Appendix B: Averages, Standard Deviations, and P-Values of EDTA Solutions 91

List of Tables

Table 1. NMR Spin Activity of Nuclei Properties 13

Table 2. NMR Properties of ^{67}Zn 14

Table 3. Spin-lattice Relaxation Rates (R_1), Chemical Shift Anisotropy (R_1^{CSA}) and Spin Rotation (R_1^{SR}) Contributions for apo-EDTA at 298 K and 125.2 MHz.[30] 23

Table 4. Spin-lattice Relaxation Rates (R_1), Chemical Shift Anisotropy (R_1^{CSA}) and Spin Rotation (R_1^{SR}) Contributions for Zn-EDTA at 298 K and 125.2 MHz.[30] 24

Table 5. Activation Energies of Carbonyl, Lateral, and Central Carbons of apo-EDTA and Zn-EDTA at 298 K and 125.2 MHz.[30] 24

Table 6. Summary of EDTA Solutions for NMR 34

Table 7. Comparison of ^{13}C T_1 Values from Intensity Fit of Carbonyl Peak of apo-EDTA (a) and (b) 41

Table 8. Comparison of ^{13}C T_1 Values from Intensity Fit of Carbonyl Peak of Zn-EDTA (a) and (b) 41

Table 9. Comparison of ^{13}C T_1 Values of Area and Intensity Fits of Carbonyl Peak of apo-EDTA (a) & (b) 42

Table 10. Comparison of T_1 Values of Intensity Fit of Lateral Peak of Deoxygenated apo-EDTA (a) and (b) with Oxygenated apo-EDTA (c) 45

Table 11. Intensity Fit T_1 Values of Carbonyl Carbon of apo-EDTA (a) 45

Table 12. Intensity Fit T_1 Values of Lateral Carbon of apo-EDTA (a) 46

Table 13. Intensity Fit T_1 Values of Central Carbon of apo-EDTA (a) 46

Table 14. Comparison of T_1 Values of Intensity Fit of Carbonyl Peak of apo-EDTA (a), (b), and (c) with Zn-EDTA (a), (b), and (c) 47

Table 15. Comparison of T_1 Values of Intensity Fit of Lateral Peak of Zn-EDTA (a) and (b) with Zn-EDTA (d) Made with Synthesized $ZnCl_2$ 48

Table 16. Comparison of T_1 Values of Intensity Fit of Carbonyl Peak of apo-EDTA (a), (b), and (c) with ^{67}Zn-EDTA (e) 50

Table 17. Comparison of T_1 Values of Intensity Fit of Carbonyl Peak of Zn-EDTA (a), (b), and (c) with ^{67}Zn-EDTA (e) 51

Table 18. T_1 Measurements of Carboxyl Peak of apo-Gly 57

Table 19. T_1 Measurements of Alpha Peak of apo-Gly 58

Table 20. T_1 Measurements of Zn-Gly..... 59

List of Figures

Figure 1. Structural, catalytic, and cocatalytic coordination diagrams of zinc. Single letter amino acid code used with H_2O being shown in purple. For catalytic and cocatalytic, the H_2O is labile with substrate ligands allowing for catalysis. 3

Figure 2. X-ray crystal structure of apo-Syt1 in gray and Pb-Syt1 in purple, with the Pb^{2+} depicted as an orange sphere.[11] 6

Figure 3. (a) Enlargement of the ^{15}N-^{1}H HSQC of the Pb^{2+} titrations into the C2A domain. Pb^{2+} concentrations ranged from 0 to 2.5 mM, with peak shift occurring because of two Pb^{2+} binding events, both shown with arrows. **(b)** Composite chemical shift changes, Δ (ppm), of $^{1}H_N$-^{15}N backbone of the C2A domain upon the addition of low and high concentrations of Pb^{2+}.[11] 7

Figure 4. Ribbon diagram of the loop region of C2A with its three Ca^{2+} binding sites and select residues identified. Pb^{2+} interactions with Ca^{2+} binding sites 2 and 3 shown.[11] 8

Figure 5. (a) ^{1}H-^{15}N HSQC spectra of ProTα in the without (red) and with (blue) 3 mM of Zn^{2+}. The GRR region is located in the dashed line box. **(b)** Composite $^{1}H_N$ and ^{15}N chemical shift changes, $\Delta\delta_{comp}$ (Hz), of ProTα upon the addition of 3 mM of Zn^{2+}.[14] The GRR region, shown in grey between 50-80 ppm, has very few assignable resonances.[14] 10

Figure 6. Structure of Zn^{2+} bound EDTA with labeled bond lengths. 18

Figure 7. Pulse sequence of the inversion recovery experiment. 19

Figure 8. Stack plot of ^{1}H inversion recovery experiment of pamoic acid (shown on right), with ^{1}H signals corresponding to labels on the structure.[29] 20

Figure 9. Curve resulting from an inversion recovery experiment showing T_1 and its relationship to M_0. 21

Figure 10. Structures of **(a)** apo-EDTA and **(b)** Zn-EDTA complexes expected in aqueous solution at pH 7.2. Carbon types – carbonyl, lateral, and central labeled as A, B, and C on the apo-structure.[30] 23

Figure 11. ^{1}H-^{1}H TOCSY NMR spectra of the aromatic region of 2.5 mM Ac-PDEKHEL-Am peptide (pH 6.2, 298 K) with (blue) and without (orange) 1.0 equivalents of Zn^{2+}.[34] 28

Figure 12. (a) ^{1}H and **(b)** ^{13}C chemical shift variations ($\Delta\delta = \delta_{holo} - \delta_{apo}$) for Ac-PDEKHEL-Am caused by 1.0 equivalents of Zn^{2+}.[34] 29

Figure 13. Aromatic region of ^{1}H–^{13}C HSQC NMR spectra of PK9-H peptide, 2.5 mM, pH 7, 298 K, in the absence (red) and presence (blue) of 1 equivalent of Zn^{2+}.[35] 30

Figure 14. Selected aromatic regions of ^{1}H–^{1}H TOCSY NMR spectra of the PK9-H peptide, 2.5 mM, pH 7, 298 K, in the absence (red) and in the presence (blue) of 1 equivalent of Zn^{2+}. The signals experiencing chemical shift changes are shown in blue.[35] 31

Figure 15. (a) ^{1}H and **(b)** ^{13}C chemical shift variations ($\Delta\delta = \delta_{holo} - \delta_{apo}$) for PK9-30 due to the addition of Zn^{2+} at pH 7.3.[36] 32

Figure 16. Overlay of ^{13}C NMR of apo-EDTA and Zn-EDTA in black and red, respectively. Inset shows (A) carbonyl, (B) lateral, and (C) central carbons, which correspond to peak labels on spectra. 39

Figure 17. ^{13}C NMR stacked plots of **(a)** apo-EDTA and **(b)** Zn-EDTA with the variable delay times shown on the y-axis. 40

Figure 18. (a) Intensity and **(b)** area fits of the carbonyl carbon of apo-EDTA (a) with line of best fit equations. **(a)** RSS: 0.1581, SD: $2.791 \cdot 10^{-2}$, $T_1 = 9.492$ s. **(b)** RSS: 1.030, SD: $6.344 \cdot 10^{-2}$, $T_1 = 10.135$ s. 44

Figure 19. ^{13}C NMR of apo-EDTA in black, Zn-EDTA in red, and ^{67}Zn-EDTA in blue with peaks labeled. 49

Figure 20. Overlay of ^{1}H NMR with solvent suppression of apo-EDTA in black and Zn-EDTA in red with labeled peaks that correspond to the Zn-EDTA structure shown at right. 53

Figure 21. Overlay of ^{1}H NMR with solvent suppression of Zn-EDTA in red and ^{67}Zn-EDTA in blue with labeled peaks and integral values. 54

Figure 22. Enlarged overlay of ^{1}H NMR with solvent suppression of Zn-EDTA in red and ^{67}Zn-EDTA in blue. 55

Figure 23. (a) apo-Gly and **(b)** Zn-Gly with the (A) carboxyl and (B) alpha carbons labeled. 56

Figure 24. ^{13}C NMR of apo-Gly in black and Zn-Gly in red with (A) carboxyl and (B) resonances labeled. 57

Figure 25. HPLC of PK9-H with UV-Vis absorbance at 214 nm shown in red and 280 nm shown in blue.Percent acetonitrile shown in gray. Fraction collected from 15 to 20 minutes. 60

Figure 26. ESI-MS of PK9-H with the base peak at an *m/z* of 1093.3683 corresponding to the expected *m/z* shown. 60

Figure 27. CD spectra and HT of apo-PK9-H at pH 6.2 in purple, Zn-PK9-H at pH 6.2 in green, and Zn-PK9-H at pH 7.4 in blue. 62

Figure 28. Fluorescence spectra of PK9-H (15 μM, pH 7.4) upon the addition of 0 to 20 equivalents of Zn^{2+} 63

Figure 29. Fluorescence fits of Zn^{2+} titrations into PK9-H (15 μM, pH 7.4) where m1 = K_a. 64

Figure 30. (a) Structure of PK9-H peptide with select carbon atoms identified. **(b)** ^{13}C NMR of PK9-H peptide with select regions and signals identified. 65

Figure 31. ^{1}H NMR of PK9-H peptide with solvent suppression using 1D excitation sculpting and W5. 66

Figure 32. ge-2D ^{1}H-^{1}H TOCSY of PK9-H using excitation sculpting with MLEV-17 and ES element. 68

Figure 33. 1D Selective TOCSY pulse sequence. 72

List of Abbreviations

ZBPs Zinc Binding Proteins…….19

Zn^{2+} Zinc……20

Zn^{1+} Zinc……20

HSAB Hard-Soft Acid-Base Theory……..…20

EPR Electron Paramagnetic Resonance Spectroscopy……...22

ENDOR Electron-Nuclear Double Resonance Spectroscopy……..……22

NMR Nuclear Magnetic Resonance Spectroscopy……...……22

Pb^{2+} Lead……23

Syt1 Synaptotagmin 1…….23

ProTα Prothymosin-α……...26

IDP Intrinsically Disordered Protein…….26

GRR Glutamate Rich Region……..…27

CD Circular Dichroism Spectroscopy……..….29

PCET Proton-Coupled Electron Transfer…….29

I Spin Quantum Number……...30

Q Quadrupole Moment……..……31

μ Magnetic Moment……..…32

γ	Gyromagnetic Ratio……...32
T_1	Spin-Lattice Relaxation Time……33
M_0	Total Nuclear Magnetic Moment……...……33
$T_{1(DD)}$	Internuclear Dipole-dipole Interaction Mechanism……33
$T_{1(CSA)}$	Chemical Shift Anisotropy Mechanism…….……33
$T_{1(SR)}$	Spin Rotation Mechanism……..……34
$T_{1(Q)}$	Quadrupolar Interaction Mechanism……..……34
$T_{1(SC)}$	Scalar Coupling Mechanism……..…34
TOCSY	Total Correlation Spectroscopy NMR……36
vd	Variable Delay……..….38
E_a	Energy of Activation……..…39
δ	Chemical Shift……40
R_1	Spin-Lattice Relaxation Rate……..……40
R_1^{CSA}	Chemical Shift Anisotropy Relaxation Rate……...…40
R_1^{SR}	Spin Rotation Relaxation Rate……...……40
R_1^{DD}	Dipole-dipole Relaxation Rate……...……40
YPK9	Vacuolar Cation-transporting ATPase……...……43
ATP13A2	Human ATPase Cation Transporting 13A2……44

PARK9 Human ATPase Cation Transporting 13A2……44

PK9-H Ac-PDEKHEL-NH_2……...……44

PK9-C Ac-FCGDGANDCG-Am……..44

PK9-30 Ac-SPDEKHELMIQLQKLDYTVGFCGDGANDCG-Am……..……48

Fmoc Fluorenylmethoxycarbonyl……52

HPLC High Performance Liquid Chromatography……...……52

ESI-MS Electrospray Ionization Mass Spectrometry……...…52

Chapter 1: Introduction

1.1 The Biological Relevance of Zinc

As an essential metal, zinc is found in all three domains of life – archaea, bacteria, and eukarya, with most of it contained in proteins.[1] The largest amount of zinc binding proteins (ZBPs) are seen in eukaryotes with an average relative abundance in their proteome of 8.8%.[1] ZBPs constitute 4.9% and 6.0% of proteins in bacteria and archaea proteomes, respectively.[1] In general, larger proteomes contain a larger number of ZBPs, however bioavailability of zinc and the temperature of their environments can affect the number of ZBPs an organism has. In bacteria and archaea zinc is important to the stabilization of enzymes and allowing for reactions of various substrates. Eukaryotes utilize zinc for the stabilization of enzymes and gene expression.[1] Some ZBPs can be seen in all three domains of life like alcohol dehydrogenases, which convert alcohols into aldehydes and ketones for subsequent chemical reactions, and zinc-dependent aminoacyl-tRNA synthetases.[1] A possible reason for the ubiquitous nature of these proteins is that they likely carry out essential zinc-dependent functions that were able to endure evolutionary changes.[1]

In humans, zinc is the second most abundant metal in the body, subsequent only to iron. Approximately 10% (~ 3,000) of proteins encoded in the human genome contain zinc as a metallic cofactor, including over 300 enzymes and 1,000 transcription factors.[1-3] It plays a role in biological processes like immune function, synthesis of DNA and RNA, signal transduction, and gene expression.[4] Zinc is imperative to ensure prenatal and postnatal development with the largest amounts found in bone and muscle tissues.[1,5] A deficiency of zinc can cause inhibited growth and impaired brain development.[5]

1.2 Chemical Properties & Protein Interactions of Zinc

There a several factors that allow zinc be so prevalent in proteins. It is readily available in the environment with significant bioavailability and its chemical properties allow it to be utilized in proteins. Zinc is the 24th most abundant metal in the Earth's crust as it has a concentration of approximately 75 ppm.[6] Soil, seawater, and the atmosphere contain 5 to 770 ppm, 30 ppb, and 0.1 $\mu g/m^3$ of zinc, respectively.[6]

Zinc is a transition metal whose only bioavailable oxidation state to the transition metal is 2+ (Zn^{2+}), ensuring that is redox inert, unlike other metals like iron that is reactive under redox-altering conditions.[4,7] While an oxidation state of 1+ is possible (Zn^{1+}), this is rarely seen in nature.[6] The redox resistance zinc has is key to the overall stability it offers proteins. It is often seen coordinating 4, 5, and 6 ligands; however, it can coordinate between 2 and 8 ligands.[4,7] The flexible coordination geometry allows it to ensure proteins can remain dynamic. Its ability to adopt various coordination shapes and remain redox inert, allows it to play various roles in proteins.

The various roles zinc can play in proteins – catalytic, cocatalytic, and structural – cause it to be prevalent in biological systems.[4,8] Possible coordination spheres for the three different types of zinc cofactors can be seen in **Figure 1**. Structurally zinc is able to stabilize the secondary and tertiary structures of proteins – like when bound to four cysteines to provide support.[4] Zinc can act as a Lewis acid and accept a pair of electrons from a donor, functioning as a catalytic factor and accepting a pair of nonbonding electrons from a water molecule.[1,7] As a cocatalytic factor, it can be located near another metallic cofactor allowing them to work cohesively with one another in a similar manner to the catalytic function.[4]

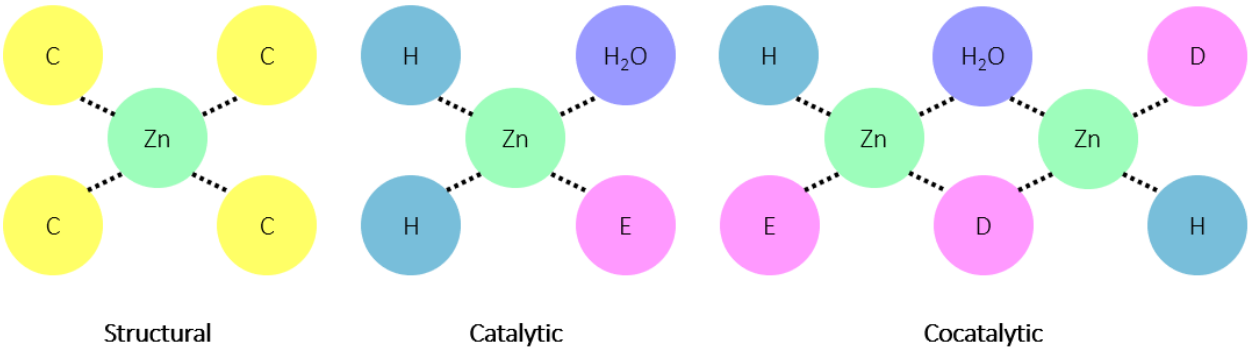

Figure 1. Structural, catalytic, and cocatalytic coordination diagrams of zinc. Single letter amino acid code used with H_2O being shown in purple. For catalytic and cocatalytic, the H_2O is labile with substrate ligands allowing for catalysis.

According to hard-soft acid-base theory (HSAB), zinc is a borderline Lewis acid that can coordinate with both soft and hard bases.[7] In proteins, zinc most often coordinates with cysteine, histidine, aspartic acid, and glutamic acid residues. Its intermediate behavior allows it to interact with the soft sulfhydryl offered by cysteine, the imidazolyl nitrogen of histidine, and the hard carboxyl oxygens in aspartic and glutamic acid residues.[2,3,8] Zinc can form interactions with the carbonyls of the C-terminus, polypeptide backbone, and sidechains; and the nitrogens of the amide bonds and N-terminus. It tends to bind in a tetrahedral or square pyramidal geometry, with the sulfur of the thiolate group of cysteine more often seen in the tetrahedral coordination, and oxygen and nitrogens often coordinating in the square pyramidal coordination spheres.[7] In enzymes, the multiple roles zinc can play allow it to be utilized in all six of the classical enzyme classes – oxidoreductases, transferases, hydrolases, lyases, isomerases, and ligases – the only metallic cofactor to do so.[4,7,8] With the various roles zinc can have in proteins and the different types of proteins zinc can be found in, it is a metal cofactor that occupies different coordination sites with their own coordinating ligands and geometries.

In the 2+ state, zinc maintains full d-shell orbitals and is therefore spectroscopically silent.[9] It is not the only spectroscopically silent element – other essential metals including copper (Cu^{1+}) and calcium (Ca^{2+}) along with the toxic metal lead (Pb^{2+}), are spectroscopically silent because they have either completely empty or filled d-shell orbitals.[9] The lack of available electronic transitions ensures that spectroscopically silent elements like zinc have no signature in the UV/Vis or microwave regions of the electromagnetic spectrum.[9] Therefore, techniques like absorption spectroscopy, electron paramagnetic resonance spectroscopy (EPR), and electron-nuclear double resonance spectroscopy (ENDOR) are ineffective for studying zinc. Most often, x-ray crystallography and nuclear magnetic resonance spectroscopy (NMR) are used to study zinc cofactors in proteins.

1.3 Current Methodologies to Determine Spectroscopically Silent Metal-Protein Interactions

There are many methodologies used to study spectroscopically silent metal-protein interactions, like those between zinc and proteins, but only a few will be discussed here. X-ray crystallography, NMR chemical shift monitoring, and point mutations all have their own advantages and disadvantages.

1.3.1 X-ray Crystallography

X-ray crystallography is one of the most prevalently used techniques to study the structure and interaction of proteins. A purified sample of the protein of interest can be crystallized and diffraction patterns from exposure to x-ray waves can be translated into

structural information.[10] Although, in order to utilize x-ray crystallography to study proteins, a relatively high concentration of a homogeneous, soluble protein is needed to ensure crystal growth.[10] As a result, it can be difficult to study some proteins using this method. If a protein is structurally dynamic or has glycosylations, it can be difficult if not impossible to crystalize.[10] Larger proteins like hydrophobic integral proteins can be troublesome to crystalize. The results of x-ray crystallography also show a stationary view of the protein and does not always reflect the dynamic properties and interactions of proteins.

A common target of toxic Pb^{2+} in the brain is Zn^{2+} and Ca^{2+} coordination sites in proteins.[11,12] Synaptotagmin 1 (Syt1), a calcium dependent trigger of the release of neurotransmitters, is one such potential target of Pb^{2+}.[11] In order to begin understanding Pb-Syt1 interaction, researchers utilized x-ray crystallography of the two domains of the protein – C2A and C2B. The resulting x-ray structure of the C2A domain complexed with Pb^{2+} is shown below in **Figure 2**.[11] The x-ray crystallography data demonstrated that there are apparent structural differences between the metal free Syt1 structure and Pb-Syt1 and Syt1 is able to bind one Pb^{2+} ion at the first Ca^{2+} binding site.[11]

Figure 2. X-ray crystal structure of apo-Syt1 in gray and Pb-Syt1 in purple, with the Pb^{2+} depicted as an orange sphere.[11]

Using the x-ray crystallography data as a basis for further research into the Pb^{2+}-binding behavior of Syt1 in solution, Igumenova and coworkers monitored changes in chemical shifts in ^{1}H-^{15}N HSQC spectra as Pb^{2+} was titrated into the protein.[11] The shift of resonance peaks observed near the binding sites were a function of Pb^{2+} titrated into the C2A domain, as shown in **Figure 3a**, and the total calculated chemical shift is shown graphically in **Figure 3b**.[11] The behavior of the resonance peaks caused by nearby amino acids demonstrated that there were two binding events occurring.[11] Upon the second Pb^{2+} binding, the chemical shift changed direction confirming that once saturated, two Pb^{2+} were bound to Syt1.[11] This taken with the calcium-bound and lead-bound crystal structures of Syt1 allowed determination of the Pb^{2+} binding sites, shown in **Figure 4**.

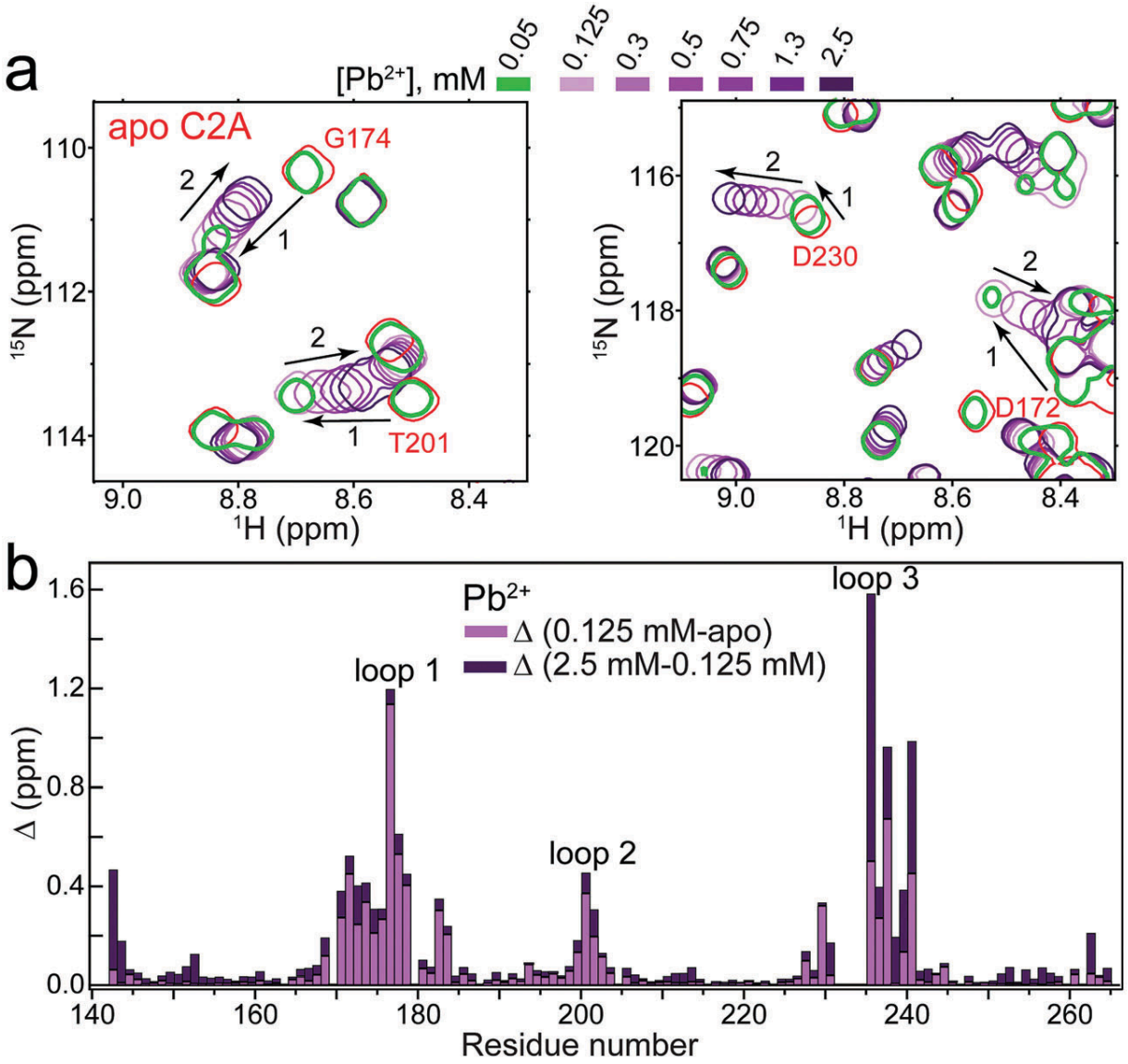

Figure 3. (a) Enlargement of the ^{15}N-^{1}H HSQC of the Pb^{2+} titrations into the C2A domain. Pb^{2+} concentrations ranged from 0 to 2.5 mM, with peak shift occurring because of two Pb^{2+} binding events, both shown with arrows. **(b)** Composite chemical shift changes, Δ (ppm), of $^{1}H_{N}$-^{15}N backbone of the C2A domain upon the addition of low and high concentrations of Pb^{2+}.[11]

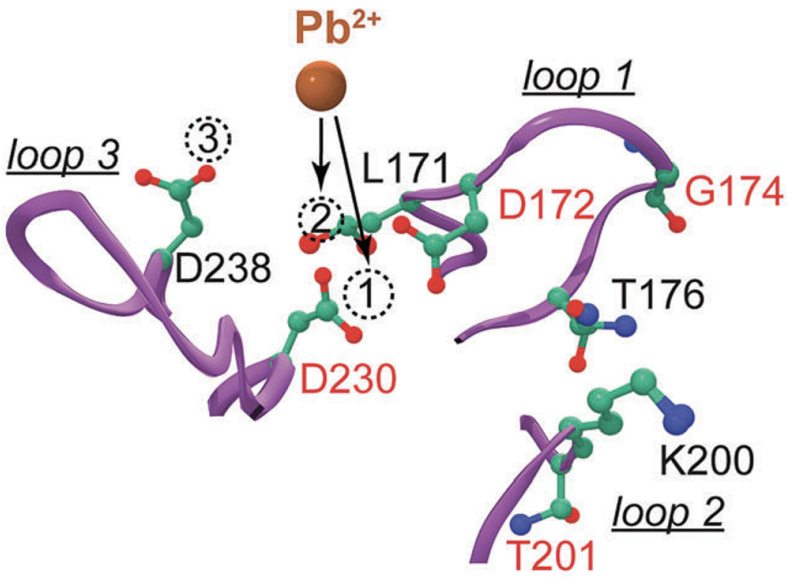

Figure 4. Ribbon diagram of the loop region of C2A with its three Ca^{2+} binding sites and select residues identified. Pb^{2+} interactions with Ca^{2+} binding sites 2 and 3 shown.[11]

While the x-ray crystallography data demonstrated that there was a single Pb^{2+} binding site, further research using chemical shift monitoring of ^{1}H-^{15}N HSQC NMR demonstrated that there was a second Pb^{2+} binding site.[11] This second binding site was not seen in the x-ray structure, because of its relative low affinity with the C2A domain, which prevented it from cocrystallizing with the protein. This highlights how potentially important binding events which occur in solution may be missed in solid-state experiments.

1.3.2 NMR Chemical Shift Monitoring

NMR chemical shift monitoring utilizes the movement of resonance peaks as the result of the addition of the ligand of interest. As discussed in 1.3.1, researchers used chemical shift monitoring of ^{1}H-^{15}N HSQC NMR to determine Pb^{2+} binding interactions with Syt1.[11] The use of ^{1}H-^{15}N HSQC NMR provided essential information which was not attainable from the x-ray

crystallography data alone. This method can be a helpful technique to utilize in order to understand the stoichiometry surrounding binding events, but it comes with limitations.

As seen in **Figure 3**, there are resonance peaks associated with amino acids that are not directly involved in the Pb^{2+} binding event, that still drift as Pb^{2+} is added, such as T201.[11] The movement of resonance peaks is not because the amino acid responsible for it is involved in binding, instead it is because the residue is experiencing a new chemical environment as a result of the conformational change induced by Pb^{2+}. Here, the crystal structure was essential in guiding interpretation of which amino acids were coordinating the Pb^{2+} ion.

A similar methodology was utilized with a saturating concentration of Zn^{2+} and prothymosin-α (ProTα), an intrinsically disordered protein (IDP) believed to play a role in immune function.[13,14] The resulting ^{1}H-^{15}N HSQC spectra are overlaid in **Figure 5a**, and the total chemical shifts of each residue are shown graphically in **Figure 5b**.[14] Using HNCACB, CBCA(CO)NH, CCC-TOCSY, HNCACO, and HNCO triple-resonance NMR experiments, researchers could only assign 66 amide signals of the 109 residues in the protein.[14] The unassigned residues are shown in the dashed box of **Figure 5a**.[14] The amino acid sequence of ProTα is shown in **Scheme 1**. A portion of the protein called the glutamate rich region (GRR) is shown underlined. It contains a large number of Glu and Asp residues. Of the unassigned residues, 25 Glu and 11 Asp are within the zinc binding GRR.

10	20	30	40
MSDAAVDTSS	EITTKDLKEK	KEVVEEAENG	RDAPANGNAE
50	60	70	80
NEENGEQEAD	NEVDEEEEEG	GEEEEEEEEG	DGEEEDGDED
90	100	110	
EEAESATGKR	AAEDDEDDDV	DTKKQKTDED	D

Scheme 1. Amino acid sequence of ProTα, with the GRR underlined.

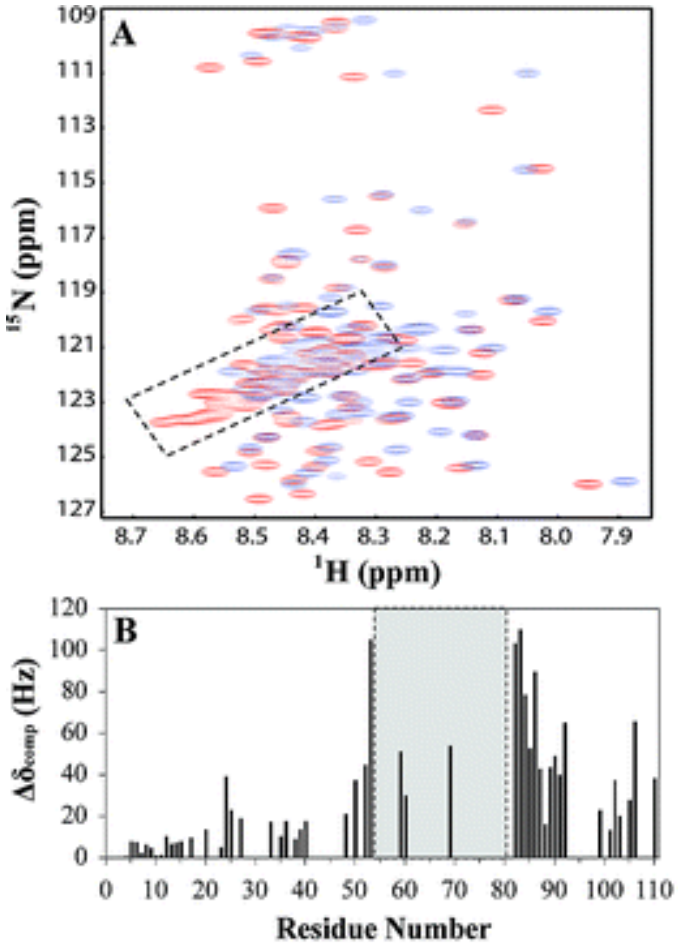

Figure 5. (a) ^{1}H-^{15}N HSQC spectra of ProTα in the without (red) and with (blue) 3 mM of Zn^{2+}. The GRR region is located in the dashed line box. **(b)** Composite $^{1}H_N$ and ^{15}N chemical shift changes, $\Delta\delta_{comp}$ (Hz), of ProTα upon the addition of 3 mM of Zn^{2+}.[14] The GRR region, shown in grey between 50-80 ppm, has very few assignable resonances.[14]

The homogeneity of the GRR and lack of secondary structure of ProTα resulted in the considerable spectral overlap of the NMR signals seen. Despite using various NMR experiments, a large number of resonances arising from the GRR were unable to be identified. Using chemical shift monitoring of ^{1}H-^{15}N HSQC NMR to determine ligand binding events is difficult when resonances overlap because of a dynamic structure, homogeneity of sequence, or because of pure coincidence.

1.3.3 Point Mutations

Often biochemists will utilize point mutations in proteins in order to understand more about binding interactions with ligands.[15] Using knowledge from the Protein Data Bank (PDB) and hard-soft acid-base (HSAB) theory, researchers can often narrow down possible residues involved in binding. For example, knowing Zn^{2+} is an intermediate Lewis acid suggests that it is binding to Cys, His, Glu, and Asp residues in proteins. Often this is sufficient information when determining potential sites to mutate. Amino acids with a similar size and hydrophobic character, but lacking key ligating atoms, can be substituted in and the binding ability of the protein can be assayed and compared to the native protein. [15,16] Methods like isothermal titration calorimetry (ITC) and circular dichroism polarimetry (CD) can then be used to determine whether a measurable change in the thermodynamics or secondary structure associated with metal binding were altered.[17] A change in the measured value, when compared to the native protein, indicates that the mutated site plays some role in binding.[15] Although this approach is powerful, it does not always reveal which residues are directly involved in metal binding because nearby non-ligating residues still may influence the binding affinity or structure. If the native residue was needed for structural stability or allowed for a chemical reaction like proton-coupled electron transfer

(PCET) to occur, the results of a mutation might falsely indicate that it is directly involved in binding.

This technique is useful and can be used to study any ligand of interest, but it has its own hindrances. For example, several protein samples often need to be prepared by expression or chemical synthesis to scan amino acid mutations through several potential ligand sites and each in turn needs to be assayed.[15] Thus, the process can be laborious.

While the methods discussed are often sufficient to provide information regarding ligand-protein interactions, there is a potential need for new experimental methods that allow for better information regarding the interactions of proteins with spectroscopically silent elements. Although there are numerous spectroscopically silent metals of interest, this research will focus on those of zinc.

1.4 NMR, Zinc, & T_1 Relaxation Mechanism

The spinning of certain nuclei generates a small magnetic field due to their positively charged nature.[18] Under normal circumstances, the nuclei are randomly oriented in space. If a large outside magnetic field is introduced, then the magnetic fields of the nuclei can either align with the field or align against it.[18] There is an inherent energy difference, although small, between the opposed and aligned nuclei with those aligned with the field at a lower energy level than those opposed.[19] The more energetically favorable spin state of being aligned with the external magnetic field ensures that more nuclei remain aligned with the field.[18] NMR spectroscopy utilizes the ability of nuclei to "flip" from low to high energy spin states when they absorb electromagnetic radiation, typically in the radio frequency range, that matches the

difference in energy levels.[18,19] Generally, nuclei in different chemical environments will require different wavelengths of radio frequency energy to induce a spin flip.

Electrons, protons, and neutrons have their own individual spins that contribute to the overall spin of the atom.[18] In some atoms, the spins counteract each other so that the nucleus has no overall spin. These nuclei are deemed NMR spin-inactive because they lack an overall spin.[18,19] For a nucleus to be spin-active – observable in NMR – it must have a nonzero spin quantum number (I) which describes the number of allowed spin states.[18] Nuclei are classified into spin-active or spin-inactive according to the rules in **Table 1**. If the number of neutrons and the number or protons is even, then the nucleus has no spin. This is the case for atoms like ^{12}C and ^{16}O. If the sum of neutrons and protons is odd, then the nucleus has a half-integer spin such as ^{13}C or ^{1}H that has an I of ½.[18] Lastly, if a nucleus has an odd number of neutrons and an odd number of protons, then the nucleus has a spin that is an integer like ^{2}H or ^{14}N that have I values of ½.[18]

Table 1. NMR Spin Activity of Nuclei Properties

Mass Number	Atomic Number	Spin Quantum Number	NMR Activity
Odd	Odd or Even	Half integral	Active
Even	Odd	Integral	Active
Even	Even	Zero	Inactive

There are five naturally occurring isotopes of zinc with abundances ranging from approximately half a percent to almost 50%.[20] The most abundant isotope of zinc is ^{64}Zn, which

accounts for approximately 49.17% of zinc in the environment.[20] There is also ^{66}Zn, ^{67}Zn, ^{68}Zn, and ^{70}Zn. All isotopes of zinc are NMR spin-inactive except ^{67}Zn which has an I of 5/2 due to its odd atomic mass. [20] Other relevant NMR properties of ^{67}Zn are shown below in **Table 2**. Since ^{67}Zn has an I of greater than ½, it has a quadrupole moment (Q) that describes the shape of its electric and magnetic fields.[20,21] The Q of ^{67}Zn is 15.0 fm^2, which indicates that it has a prolate (or elongated) quadrupolar nucleus. This irregular shape compared to a more spherical charge distribution provides ^{67}Zn with more relaxation mechanisms by which it can return to equilibrium faster and can subsequently cause faster relaxation in nearby nuclei through spin-lattice relaxation. [21] On the NMR spectrum, this is seen as broad spectral peaks over a wide range of chemical shifts, especially compared to nuclei like ^{1}H and ^{13}C which have spins of ½ and quadrupolar moments of 0. [22,23] The magnetic moment (μ) and gyromagnetic ratio (γ) are directly related and provide insight to the sensitivity of the nucleus and describe how easy it is to obtain an NMR signal from the nucleus. [19] The values seen for ^{67}Zn are considered moderate meaning that its NMR signal should be observable, however it might not be as strong as ^{1}H for example. [24]

Table 2. NMR Properties of ^{67}Zn

Nuclei	**I**	**Q (fm^2)**	**μ (μ_N)**	**γ (10^7 rad s^{-1} T^{-1})**
^{67}Zn[a]	5/2	15.0	1.036	1.677

a. Solid State Nuclear Magnetic Resonance (2002) **22**, 458–483.

Nuclei with a spin greater than ½, quadrupolar nuclei like ^{67}Zn, are difficult to study. They have nonspherical charge distributions and must be treated as either prolate (elongated) or oblate (widened) spinning bodies.[19] Their nonspherical distribution of charge as the nuclei spin causes them to have an asymmetric electric and magnetic field. Subsequently, the nucleus has an electric quadrupole.[18] These are not seen in NMR spectroscopy studying ^{1}H and ^{13}C because they have I = ½, giving them a spherical distribution of charge.[18] As a result, their electric and magnetic fields are spherical, homogeneous, and isotropic in all directions.

Quadrupolar nuclei return to equilibrium faster because they have more relaxation mechanisms available to them.[21] In the NMR spectra, they are responsible for broad spectral peaks because of the rapid spin-lattice relaxation (T_1) that the nuclei undergo.[21] T_1 describes the point at which the total nuclear magnetic moment (M_0) returns to 63% of its original intensity. As M_0 returns to equilibrium, it has to release energy into the surroundings via spin-lattice relaxation mechanisms.[18,19,25] The contributions of the possible relaxation mechanisms are described in ***Equation 1***.[26] They are assumed to be additive and contribute to the overall T_1 of the nucleus that is measured.[26] There are other mechanisms that are not highlighted by the equation, as they arise only in limited cases, but the most significant contributors are shown.

$$\frac{1}{T_1} = \frac{1}{T_{1(DD)}} + \frac{1}{T_{1(CSA)}} + \frac{1}{T_{1(SR)}} + \frac{1}{T_{1(Q)}} + \frac{1}{T_{1(SC)}} \ldots \qquad \textbf{\textit{Equation 1}}$$

Internuclear dipole-dipole interaction ($T_{1(DD)}$) describes the relaxation mechanism that occurs between the nucleus and a directly bonded second nucleus that has a magnetic spin.[26] The nuclei have the ability to relax via dipolar relaxation as they experience a small magnetic field

because of the dipolar interaction between them.[26] The effects of dipolar interaction depend on several variables – the magnitude of the two dipoles, the orientation of their interaction relative to the magnetic field, and the distance between the two dipoles.[26] For ^{13}C bonded directly to protons or for protons that are located near other protons, this is often the largest, if not only, contributor to T_1.[26]

Due to the anisotropic electron distribution in chemical bonds, nuclei are able to relax via chemical shift anisotropy ($T_{1(CSA)}$) mechanisms.[26] Due to the uneven charge distribution, the local magnetic field experienced by a nucleus, and subsequently its chemical shift, is affected.[26] This process depends on the orientation of the bond relative to the applied magnetic field.[26] The rapid tumbling of molecules in solution typically averages out the chemical shift anisotropy resulting in one signal, however, if the fluctuating field about the bond is strong enough, it can allow the nucleus to undergo relaxation.[26] The large chemical shift range seen for some nuclei like ^{19}F and ^{31}P are often due to chemical shift anisotropy.[26]

As molecules and atoms rotate very rapidly in solution, they create small magnetic fields due to their charge.[26] As this field fluctuates due to events like molecular collisions, nuclei can undergo relaxation.[26] This process is known as spin rotation mechanisms ($T_{1(SR)}$).[26]

Quadrupolar interaction mechanisms ($T_{1(Q)}$), which are only experienced by quadrupolar nuclei with their quadrupolar moment interact with the electric field.[26] This is the dominant relaxation mechanism for quadrupolar nuclei as they tumble and induce spin flips in other spin states to allow themselves to relax.[26] Unlike other T_1 mechanisms, quadrupolar relaxation depends on the electric field instead of the magnetic field.[26]

Quadrupolar nuclei can affect the T_1 and spectra of spin ½ nuclei through scalar coupling mechanisms ($T_{1(SC)}$).[26] The coupling of a nucleus to another spin results in 2I+1 signals in an NMR spectrum.[26] An example of this is the triplet that appears in the ^{13}C spectra of deuterated chloroform ($CDCl_3$).[26] Deuterium with a spin of 1 is a quadrupolar nucleus that is connected to ^{13}C by a coupling constant of 32 Hz. This can exist for other quadrupolar nuclei and spin ½ nuclei.[26] However, this coupling can be lost if the quadrupolar nucleus relaxes at a rate that is relatively fast compared to the magnitude of the coupling.[26] Couplings between a quadrupolar nucleus and spin ½ nucleus are more likely to be seen if they are in a highly symmetrical environment because of the slower relaxation that the quadrupolar nucleus will experience.[26] This leads to an increase in the lifetime of the spin states in the quadrupolar nucleus permitting J-coupling to be observed.[19] An increase in temperature can also allow the quadrupolar nucleus to undergo slower relaxation, which increases the chance that couplings can be observed.[26] However, quadrupolar scalar couplings can often difficult to observe in NMR spectra.[26]

For our research purposes, quadrupolar interactions and scalar couplings will be of the most interest. The use of $^{67}Zn^{2+}$ has the potential to impact T_1 values of nearby spin active nuclei as well as cause irregular splitting patterns to appear in spectra. As mentioned previously, in proteins, Zn^{2+} is often coordinated by oxygen, sulfur, and nitrogen atoms. Often the sulfur and nitrogen of Cys and His, respectively, are easier to study than the oxygens of Asp and Glu, so the oxygens were a focus of this research. With the low natural abundance of ^{17}O, the only spin active isotope of oxygen, and its spin of 5/2 causing broad signals, this nucleus was unlikely to be an acceptable indicator of Zn^{2+} binding.[27] In residues like Asp and Glu, a carbon atom is adjacent to the coordinating oxygen atom and an additional two bond lengths away is a proton. This is similar to the structure of ethylenediaminetetraacetic acid (EDTA) bound to Zn^{2+} as

shown in **Figure 6**. With its irregularly shaped magnetic field, $^{67}Zn^{2+}$ has the potential to induce relaxation in the nearby ^{13}C and ^{1}H atoms via quadrupolar interactions decreasing the overall measured T_1.

The means by which ^{67}Zn has the potential to induce relaxation is via scalar couplings. Although two or three bond lengths seems to be a large distance, it is not uncommon to observe these types of scalar couplings. For instance, ^{13}C and ^{1}H have a coupling constant of approximately 125 Hz when separated by a single bond.[19] With two or three intervening bonds, the coupling decreases to a few Hz, but is still measurable and is the basis for 2D HMBC NMR experiments. In the literature, ^{13}C and ^{67}Zn had a measured coupling constant of 88 Hz at a distance of one bond length by solid-state NMR.[28] This is not much smaller than the coupling constant between ^{13}C and ^{1}H. There is the potential that at larger bond lengths, scalar coupling exists between ^{67}Zn and spin active nuclei like ^{1}H and ^{13}C. If there is a scalar coupling between the ^{67}Zn and ^{1}H or ^{13}C, then there is the potential for an irregular splitting pattern to arise in resulting spectra.

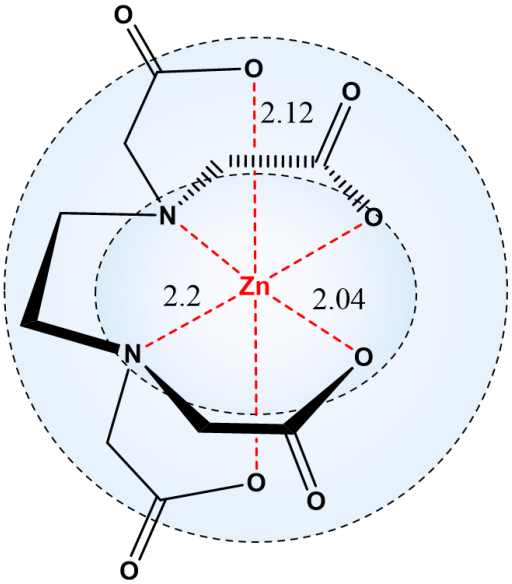

Figure 6. Structure of Zn^{2+} bound EDTA with labeled bond lengths.

An observation of a spin coupling between ^{67}Zn and ^{1}H or ^{13}C in a liquid-state NMR would provide evidentiary support for the development of a more advanced 2D NMR experiment, such as a heteronuclear total correlation spectroscopy (TOCSY) experiment. As a spin-active nucleus, ^{67}Zn has the potential to be utilized for a TOCSY experiment which would cause a transfer of magnetization from ^{67}Zn to nuclei within the same spin system, if the J-coupling has sufficient strength. This would provide direct evidence of atoms involved in Zn-coordination.

1.5 Inversion Recovery Experiment

In order to make T_1 measurements, whether for ^{1}H, ^{13}C, or other NMR spin active nuclei, researchers utilize the inversion recovery experiment.[25] A sample at thermal equilibrium is subjected to a 180° inversion pulse that causes a spin flip, and the signal resulting after various delay periods is used to approximate T_1. The delay periods, τ, can range from 0 seconds to up to 5 times the anticipated value of T_1.[25] After the delay period, the sample is excited with a 90° pulse and the resulting signal is measured. This pulse sequence depicted in **Figure 7**.

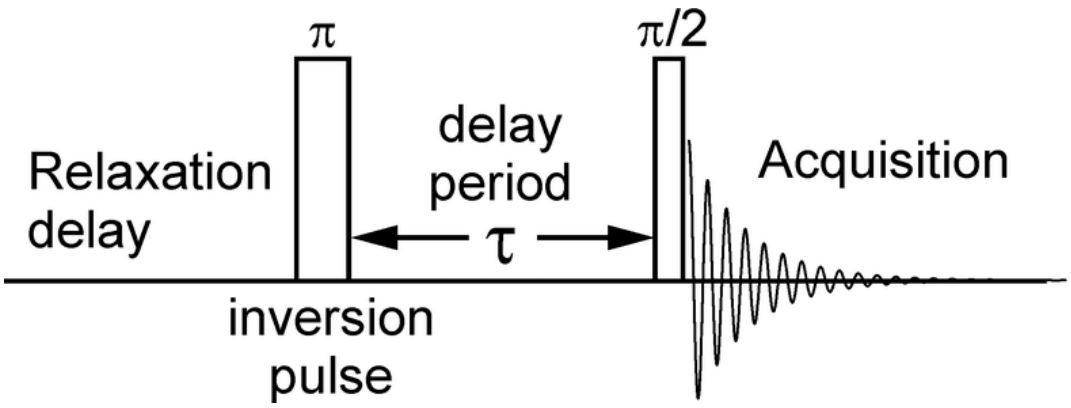

Figure 7. Pulse sequence of the inversion recovery experiment.

The intensity of the signal recorded is plotted against the values of τ to create a signal recovery curve. T_1 is the point at which the signal has recovered approximately 63% of its original intensity and can be determined by fitting the signal recovery curve.[25] The resulting NMR spectra recorded at the various values of τ can be plotted as a stack plot, like the one for pamoic acid shown in **Figure 8**.[29] Although this is a ^{1}H NMR, an inversion recovery experiment can be performed on any NMR spin-active nucleus including ^{13}C.

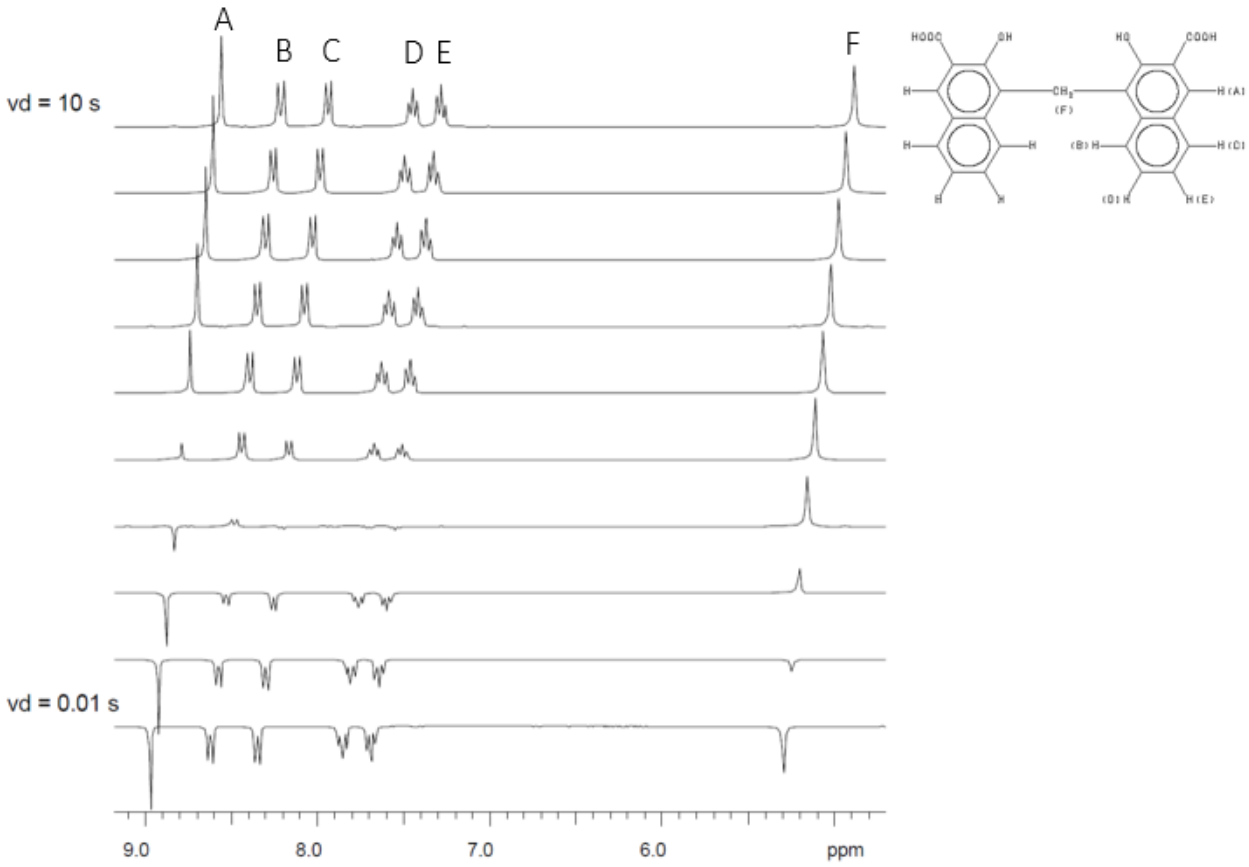

Figure 8. Stack plot of ^{1}H inversion recovery experiment of pamoic acid (shown on right), with ^{1}H signals corresponding to labels on the structure.[29]

Pamoic acid had six sets of chemically equivalent protons – labeled in **Figure 8** as A, B, C, D, E, and F. At the time point vd = 0.01 s, where vd stands for variable delay, the signals are

at their maximum negative intensity. As the vd increases, the peaks become less negative and eventually transition over the baseline to positive intensity. The final vd chosen is typically at least 5 times the value of T_1 allowing the signals ample time to return to equilibrium.

The results of an inversion recovery experiment can then be graphed for each signal using either the intensity or area values as a function of increasing time, as shown in **Figure 9**. The change can be described with an equation of the form shown in ***Equation 2***, which relates the change in intensity (or area) to the change in time. M naught (M_0) is the magnitude of the magnetization vector at equilibrium and can be referred to as either an intensity or area. T_1 can be determined as the point at which M_0 has recovered 63% of its original intensity.

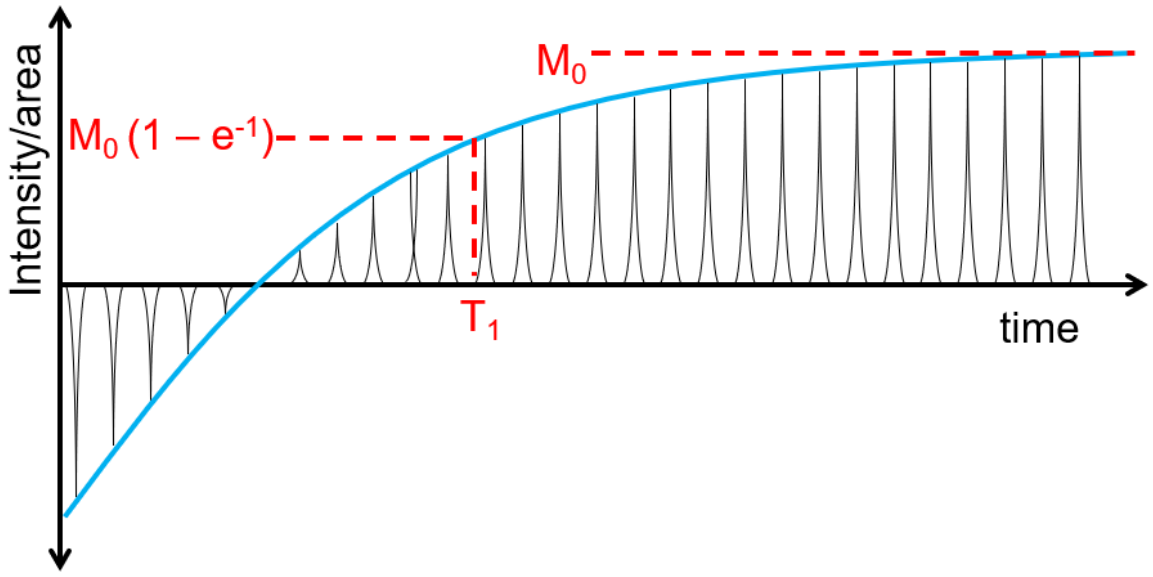

Figure 9. Curve resulting from an inversion recovery experiment showing T_1 and its relationship to M_0.

$$M_z(t) = M_0\left(1 - 2e^{-t/T_1}\right) \qquad \textit{Equation 2}$$

1.6 Previous Research in the Burns Lab

Ethylenediaminetetraacetic acid (EDTA) is a carbonyl containing high affinity metal chelator that acts as a multidentate ligand. Previous research in the Burns lab has focused on making ^{13}C relaxation measurements on EDTA complexed with and without Zn^{2+} for its three different carbon types – carbonyl, central CH_2, and lateral CH_2 – as a function of temperature and field strength.[30] By varying field strength and temperature, the contributions of individual relaxation mechanisms – chemical shift anisotropy, spin rotation, and dipole-dipole – to the overall relaxation rates of individual carbons were determined.[30] The activation energies (E_a) for the motions of the different carbons were determined by studying the temperature effects of temperature variation.[30]

The hexadentate complex with octahedral symmetry formed between EDTA and Zn^{2+} can be seen in **Figure 10**, along with the labeled carbon types.[30] Unbound EDTA produces three ^{13}C NMR signals – 175, 57, and 51 ppm. The furthest downfield signal, 175 ppm, is due to the carbonyl carbon. The peaks at 57 and 51 ppm are a result of the lateral and central carbons, respectively. Upon binding Zn^{2+}, the resonances shift further downfield to 178, 61, and 56 ppm. Although the carbons in EDTA do not directly coordinate Zn^{2+} binding, they are near enough to the coordinating atoms, N and O, to experience changes in their chemical shifts (δ) and spin-lattice relaxation rates (R_1) upon formation of the Zn-EDTA complex.[30]

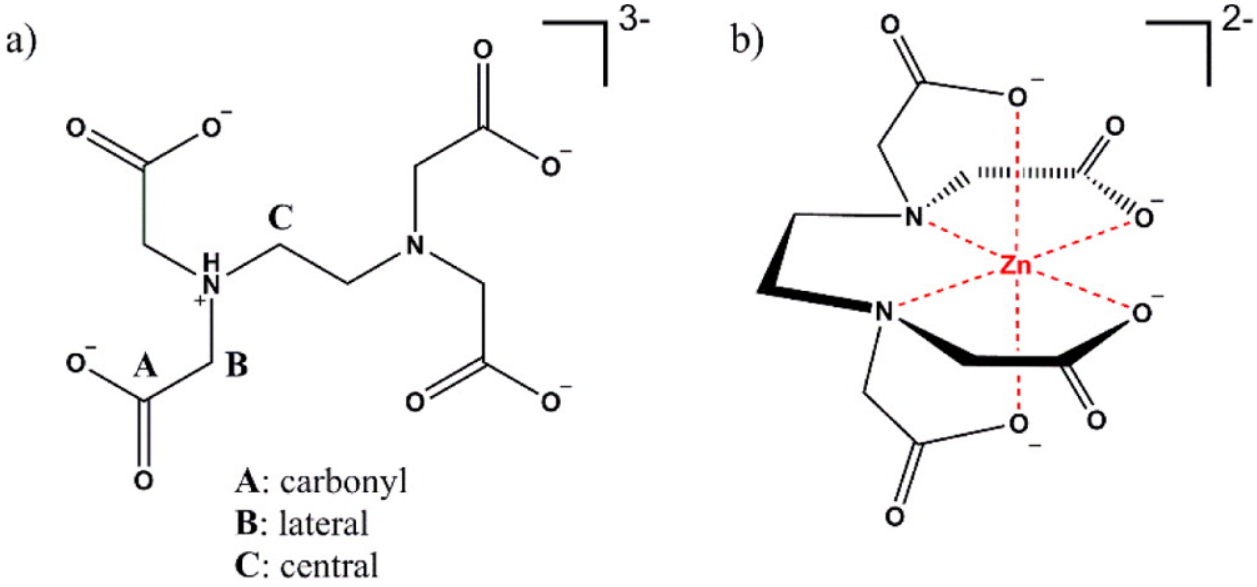

Figure 10. Structures of **(a)** apo-EDTA and **(b)** Zn-EDTA complexes expected in aqueous solution at pH 7.2. Carbon types – carbonyl, lateral, and central labeled as A, B, and C on the apo-structure.[30]

R_1, chemical shift anisotropy relaxation rates (R_1^{CSA}), spin rotation relaxation rates (R_1^{SR}) and dipole-dipole relaxation rates (R_1^{DD}) contributions for the three carbon types in apo-EDTA and Zn-EDTA are shown in **Table 3** and **4**, respectively.[30] E_a values of the carbonyl, central, and lateral carbons of EDTA with and without Zn^{2+} are shown in **Table 5**.[30]

Table 3. Spin-lattice Relaxation Rates (R_1), Chemical Shift Anisotropy (R_1^{CSA}) and Spin Rotation (R_1^{SR}) Contributions for apo-EDTA at 298 K and 125.2 MHz.[30]

Carbon types	R_1 (1/s)	R_1^{CSA} (1/s)	R_1^{SR} (1/s)	R_1^{DD} (1/s)	% CSA	% SR	% DD
Carbonyl	0.175 (5.8×10^{-4})	0.150 (0.006)	0.025 (0.006)	–	85.7	14.3	–
Lateral	2.94 (0.05)	–	0.62 (0.05)	2.32 (0.05)	–	21.1	78.9
Central	2.94 (0.05)	–	1.14 (0.2)	1.80 (0.2)	–	38.8	61.2

Table 4. Spin-lattice Relaxation Rates (R_1), Chemical Shift Anisotropy (R_1^{CSA}) and Spin Rotation (R_1^{SR}) Contributions for Zn-EDTA at 298 K and 125.2 MHz.[30]

Carbon types	R_1 (1/s)	R_1^{CSA} (1/s)	R_1^{SR} (1/s)	R_1^{DD} (1/s)	% CSA	% SR	% DD
Carbonyl	0.214 (0.005)	0.195 (0.042)	0.019 (0.019)	–	91.1	8.9	–
Lateral	3.13 (0.34)	–	2.76 (0.21)	0.37 (0.21)	–	88.2	11.8
Central	4.00 (0.34)	–	1.60 (0.35)	2.40 (0.35)	–	40.0	60.0

Table 5. Activation Energies of Carbonyl, Lateral, and Central Carbons of apo-EDTA and Zn-EDTA at 298 K and 125.2 MHz.[30]

Carbon type	Activation energy (kJ/mol)	
	apo-EDTA	Zn-EDTA
Carbonyl	33.7	40.3
Lateral	22.1	20.4
Central	9.7	11.4

Chemical shift anisotropy and spin rotation mechanisms are the most significant contributors to the relaxation rates of carbonyl carbons.[30] The two hydrogens located on each of the central and lateral carbons of EDTA lead to dipole-dipole interactions. The dipole-dipole and spin-rotation mechanisms are the methods by which the lateral and central carbons undergo spin-lattice relaxation.[30]

For the carbonyl carbon, R_1 and the percent contribution of CSA increases upon EDTA binding Zn^{2+}, as seen in **Table 3** and **4**.[30] **Table 5**, shows that its E_a also increases upon Zn^{2+} coordinating with EDTA.[30] The data in **Table 3** and **4** confirms that the spin-lattice relaxation of

the central and lateral carbons of EDTA is largely due to their dipole-dipole interactions, with the spin-rotation mechanism making a small contribution.[30] The activation energy of the lateral carbon decreases upon Zn^{2+} binding, while it increases for the central carbon, as shown in **Table 5**.[30]

Taken together, this data suggests that the lateral carbon is able to rotate more freely upon EDTA forming a complex with Zn^{2+}. In order for this to occur, there must be a point in the binding interaction in which bonds are broken between EDTA and Zn^{2+}, allowing a bridged complex to form between EDTA and two Zn^{2+} ions.[30] As a result, a Zn^{2+} ion would be coordinated by a five membered ring allowing for the lateral carbon to have more rotation freedom.[30] This would also explain the increased contribution of the spin rotation mechanism to the overall relaxation rate of the lateral carbon as the motion of the carbonyl and central carbons becomes more constricted.[30]

1.7 Project Aims

The purpose of this research is to establish NMR methodologies that could provide site-specific information about zinc-binding interactions which can be used to study a considerable number of proteins or other biomolecules. This includes those that have been historically difficult to examine like proteins that are homogeneous in sequence or lacking secondary structure. Ultimately, the aim is the development of a novel TOCSY methodology that utilizes spin-spin coupling between ^{67}Zn and other NMR spin active nuclei to determine site-specific binding information of zinc in proteins directly. As a first step towards this long-term goal, ^{13}C T_1 measurements were made on carbonyl-containing metal chelator EDTA without zinc, in the presence of zinc, and in the presence of isotopically enriched ^{67}Zn. This proof-of-concept

experiment was performed to demonstrate the basic feasibility of a relaxation-based approach to identify Zn-binding ligands directly.

A model peptide, a portion of Vacuolar cation-transporting ATPase (YPK9), was synthesized and its Zn-binding properties characterized to extend the relaxation-based approach to a more biologically relevant system. The YPK9 peptide was studied using CD, fluorescence, and NMR to characterize its zinc binding capability. Key ^{13}C NMR signals were assigned to residues of YPK9 using various NMR methods like DQF-COSY and TOCSY. Although, this peptide was not utilized for ^{13}C T_1 measurements, an effective method of NMR water suppression was established. This technique has the potential to be utilized with homogeneous and unstructured proteins, which are difficult to study using traditional methods.

1.8 Vacuolar Cation-transporting ATPase

Vacuolar cation-transporting ATPase (YPK9) is a transmembrane P-type transport ATPase vacuolar protein in *Saccharomyces cerevisiae* that is believed to sequester heavy metals like manganese and zinc.[31,32] YPK9 is a homolog of human ATPase cation-transporting 13A2 (ATP13A2 or PARK9), both of which belong to the P_5 ATPase subfamily.[32] The two have 58% similarity and are 38% identical.[31]

YPK9 catalyzes the hydrolysis of ATP for energy to transport ions and phospholipids across cellular membranes. Mutations of ATP13A2 have been shown to cause Parkinson disease and similar diseases like Kufor-Rakeb syndrome due to its manganese detoxification ability.[33] YPK9 is 1472 residues long, and a portion of its amino acid sequence is shown in **Scheme 1** with the two possible zinc-binding regions shown underlined. The first zinc-binding region,

PDEKHEL (PK9-H), is the one that is of interest to this research as it contains several Glu residues and an Asp residue, both of which are sometimes seen coordinating Zn^{2+} and are often seen in IDPs. The second zinc-binding region, FCGDGANDCG (PK9-C), does not have any Glu residues, only Asp residues.

```
      1170       1180       1190       1200
ARMSPDEKHE LMIQLQKLDY TVGFCGDGAN DCGALKAADV
```

Scheme 1. Amino acid sequence of YPK9 with the zinc-binding regions of interest shown underlined.

Researchers used 1D and 2D NMR methods to study the coordination of PK9-H and PK9-C with Mn^{2+} and Zn^{2+}.[34] Shown in **Figure 11**, is the ^{1}H-^{1}H TOCSY NMR spectra of 2.5 mM PK9-H at pH 6.2 and 298 K with and without 1 equivalent of Zn^{2+}.[34] The ^{1}H and ^{13}C chemical shift changes due to Zn^{2+} in the HSQC NMR are shown in **Figure 12**.[34] The imidazolic ^{1}H and ^{13}C of the His residue shifted upfield upon Zn^{2+} binding to PK9-H. No new resonances appeared in the HSQC upon Zn^{2+} binding, which suggests that the spectral broadening is due to an intermediate exchange rate between the apo-PK9-H and Zn-PK9-H.[34] It is believed that N_{δ} of His is the atom involved in Zn^{2+} binding. ^{1}H signals due to the Asp and Glu residues shifted downfield upon Zn^{2+} binding to PK9-H. Lys and Leu signals underwent a downfield shift, likely due to Zn^{2+} binding causing them to experience a new chemical environment.[34]

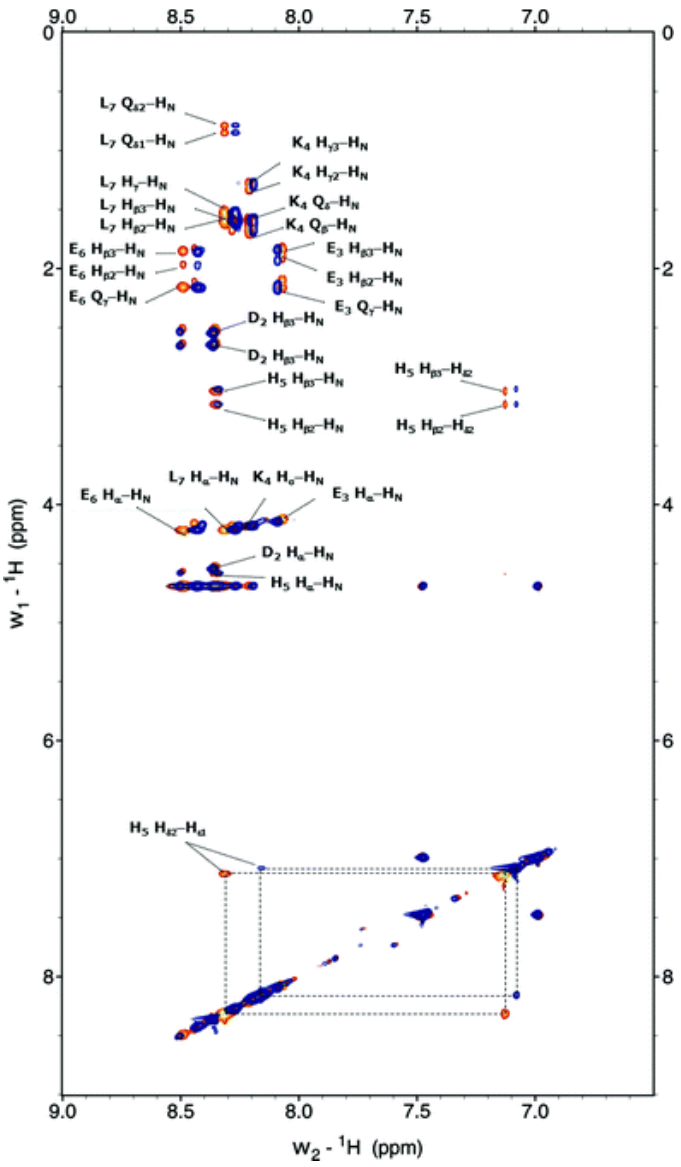

Figure 11. ^{1}H-^{1}H TOCSY NMR spectra of the aromatic region of 2.5 mM Ac-PDEKHEL-Am peptide (pH 6.2, 298 K) with (blue) and without (orange) 1.0 equivalents of Zn^{2+}.[34]

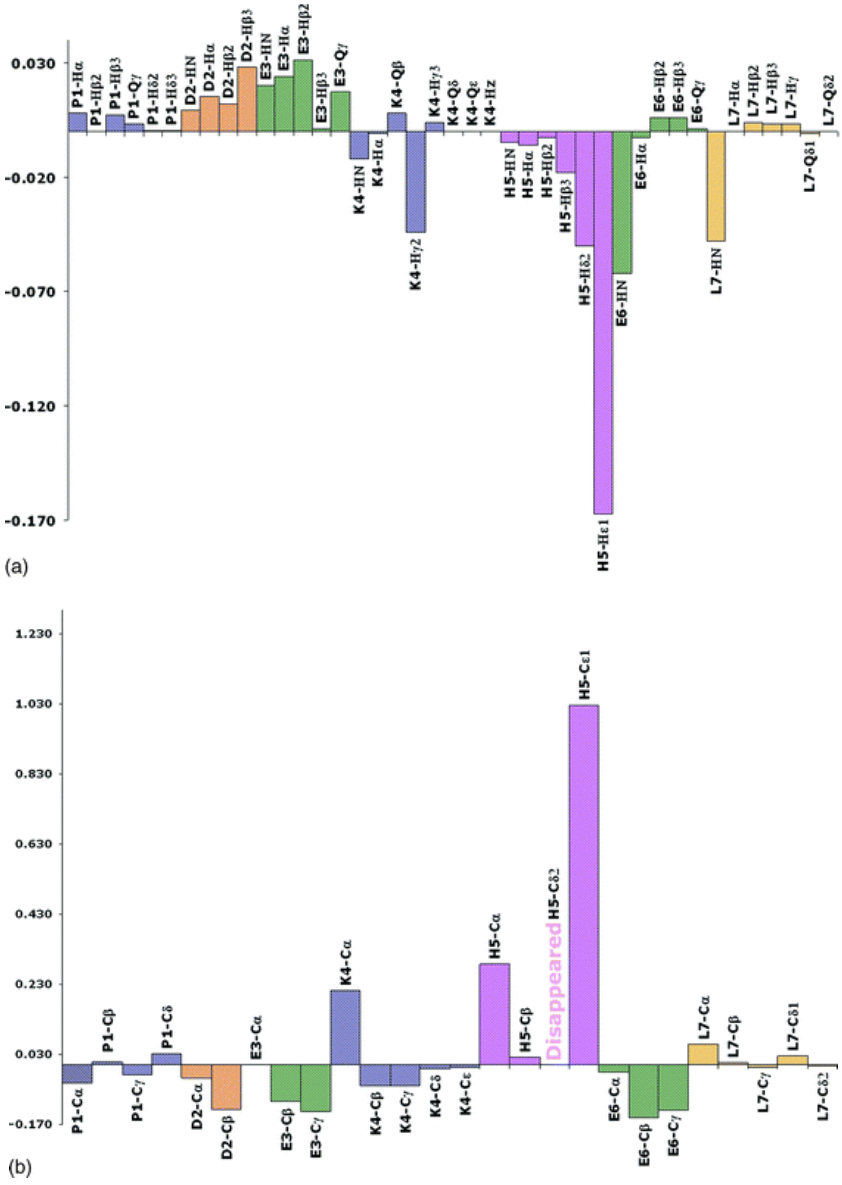

Figure 12. (a) ^{1}H and **(b)** ^{13}C chemical shift variations ($\Delta\delta = \delta_{holo} - \delta_{apo}$) for Ac-PDEKHEL-Am caused by 1.0 equivalents of Zn^{2+}.[34]

Researchers used potentiometric and UV-Vis measurements with 1D and 2D NMR spectroscopy to study the interactions between PK9-H and divalent cations Cu^{2+}, Zn^{2+}, and manganese (Mn^{2+}).[35] The aromatic region of the ^{1}H-^{13}C HSQC of PK9-H with and without 1 equivalent of Zn^{2+} can be seen in **Figure 13** and the aromatic region of the ^{1}H-^{1}H TOCSY can be seen in **Figure 14**.[35] The signals corresponding to the ^{1}H of the imidazole ring of the His residue

underwent downfield shifts. Chemical shifts were also seen for the ^{1}H of the Glu residue in position 6 as well as the Asp and Lys residue.[35] These residues are believed to be around the Zn^{2+} anchoring site in PK9-H.[35]

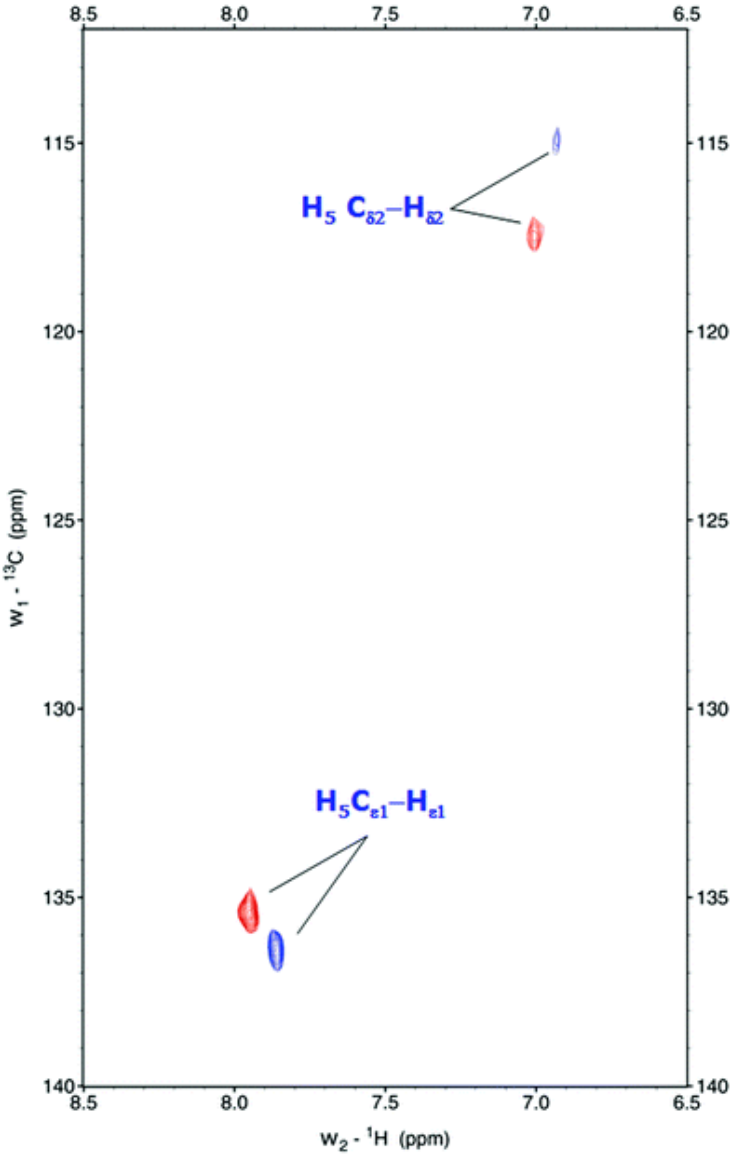

Figure 13. Aromatic region of $^{1}H–^{13}C$ HSQC NMR spectra of PK9-H peptide, 2.5 mM, pH 7, 298 K, in the absence (red) and presence (blue) of 1 equivalent of Zn^{2+}.[35]

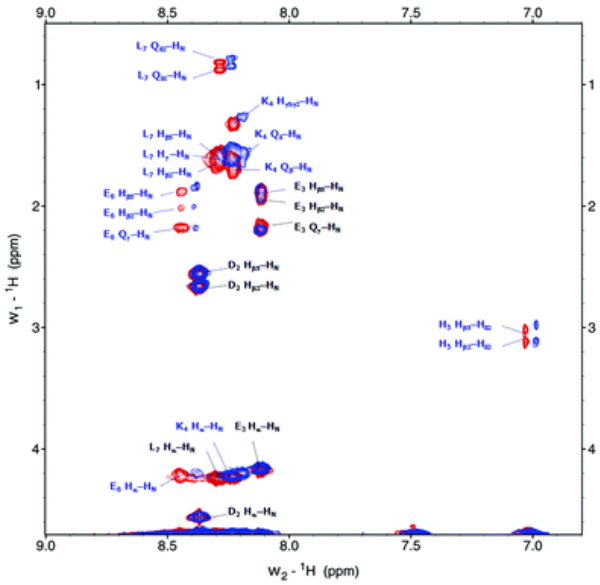

Figure 14. Selected aromatic regions of ^{1}H–^{1}H TOCSY NMR spectra of the PK9-H peptide, 2.5 mM, pH 7, 298 K, in the absence (red) and in the presence (blue) of 1 equivalent of Zn^{2+}. The signals experiencing chemical shift changes are shown in blue.[35]

Researchers used potentiometric measurements, EPR spectroscopy, and 1D and 2D NMR methods to study the coordination of the SPDEKHELMIQLQKLDYTVGFCGDGANDCG (PK9-30) peptide, which contains both binding regions, with Mn^{2+} and Zn^{2+}.[36] A summary of the chemical shift changes of the ^{1}H and ^{13}C signals as a result of Zn^{2+} binding at pH 7.3 can be seen in **Figure 15**. The ^{13}C signals due to the His and Glu residues of PK930, the same residues as PK9-H, decrease in intensity upon Zn^{2+} binding.[36] Researchers believed that this is due to the rapid chemical exchange of the protein fragment undergoing confirmational changes compared to the NMR timescale, because of the numerous Zn^{2+} binding sites in PK9-30.[36] Although the chemical shift changes of YPK9 residues are relatively small, signals due to the later portion of YPK9 due undergo larger chemical shifts, especially those due to the Cys residues.[36]

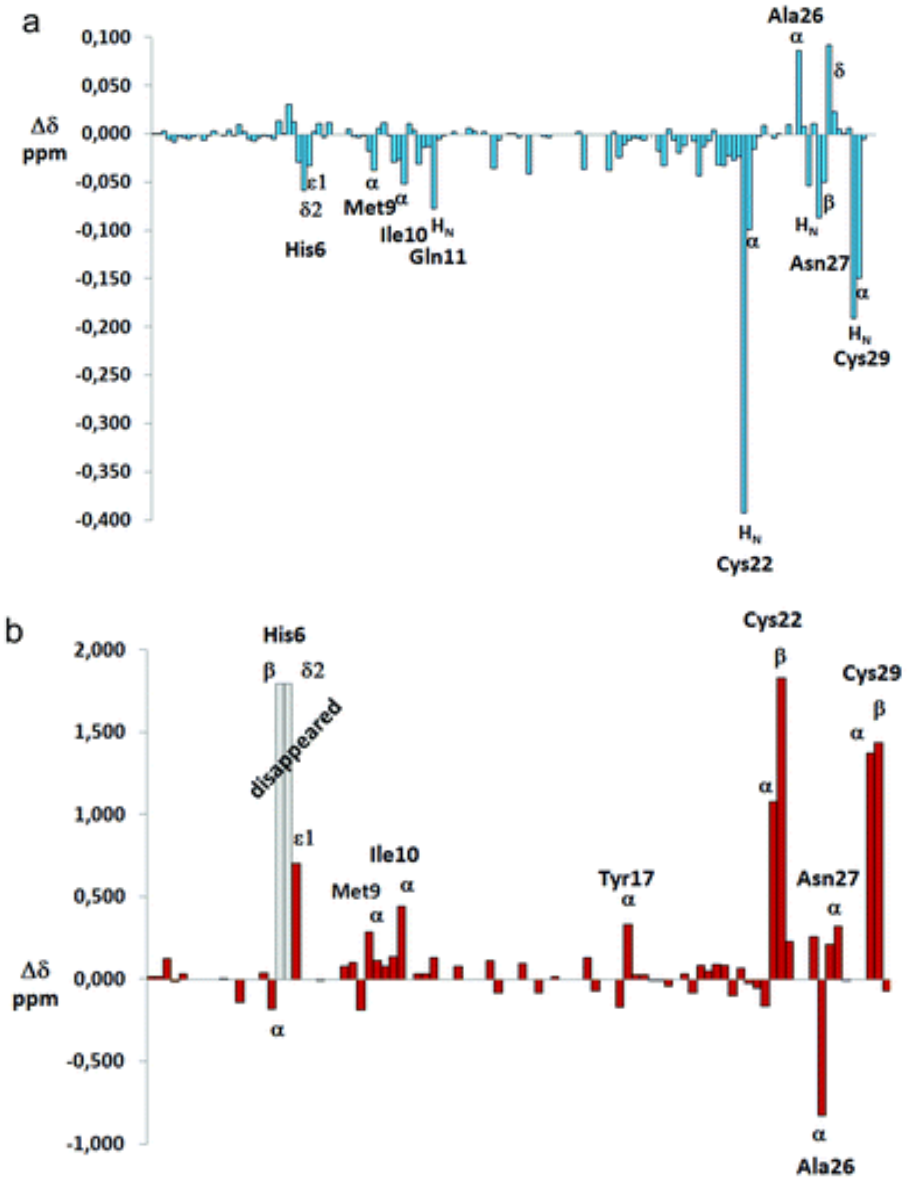

Figure 15. (a) ^{1}H and **(b)** ^{13}C chemical shift variations ($\Delta\delta = \delta_{holo} - \delta_{apo}$) for PK9-30 due to the addition of Zn^{2+} at pH 7.3.[36]

Chapter 2: Materials and Methods

2.1 Preparation of EDTA Solutions & NMR Studies

Ethylenediaminetetraacetic acid (EDTA, ≥ 99%) and deuterium oxide (99.9% atom D) were purchased from Sigma-Aldrich (St. Louis, MO). Sodium phosphate monobasic (> 98%), sodium phosphate dibasic (> 98%), and zinc dichloride (A. C. S. Certified) were purchased from Fisher Scientific (Waltham, MA). Zinc dust (nitrogen flushed) was purchased from Acros Organics (Fair Lawn, NJ). Zinc-67 metal (94.80%) was purchased from Cambridge Isotope Laboratories (Andover, MA). Compounds did not undergo further purification. All EDTA NMR solutions contained 50 mM EDTA in 50 mM phosphate buffer at pH 7.4. Samples containing Zn^{2+} used 1.1 equivalents of $ZnCl_2$. Excess hydrochloric acid (HCl, 6 M) was added to zinc dust (6:0.791) in order to synthesize a sample of $ZnCl_2$, prior to use with zinc-67 metal to determine feasibility. The synthesized $ZnCl_2$ solution was placed on vacuum with a liquid nitrogen cooled trap to collect solid $ZnCl_2$. 50 mM Zn-EDTA solution was made using 1.1 equivalents of synthesized $ZnCl_2$. Upon NMR confirmation, 6 M HCl was added to zinc-67 metal to make $^{67}ZnCl_2$. 50 mM ^{67}Zn-EDTA solution was made using 1.1 equivalents of synthesized $^{67}ZnCl_2$. Select EDTA NMR samples were degassed using freeze-thaw cycles until they no longer effervesced. All EDTA NMR samples were flame sealed. Contents of the EDTA NMR solutions are summarized in **Table 6**.

Table 6. Summary of EDTA Solutions for NMR

Solution type	apo-EDTA	Zn-EDTA	^{67}Zn-EDTA
Deoxygenated[a]	(a), (b)	(a), (b)	
Oxygenated	(c)	(c), (d)[b]	(e)[b]

[a]Deoxygenated using freeze, pump, thaw method

[b]Synthesized $ZnCl_2$

NMR spectra were collected on a 100.6 MHz (B_0 = 9.4 T, 400 MHz ^{1}H frequency) Bruker spectrometer (Billerica, MA). ^{1}H and ^{13}C spectra were collected for each sample. Inversion recovery experiments were completed in triplicate.

2.2 Glycine Solution Preparation & NMR Studies

Zinc dichloride (A. C. S. Certified) and reagent grade glycine were purchased from Fisher Scientific (Waltham, MA). Deuterium oxide (99.9% atom D) was purchased from Sigma-Aldrich (St. Louis, MO). Compounds did not undergo further purification. All glycine NMR solution contained 60 mM glycine in 90% (v/v) water/D_2O at pH 7.4. Phosphate buffer was not used as it competed with Gly for Zn^{2+}. Samples containing Zn^{2+} used 1.1 equivalents of $ZnCl_2$. Solutions were not degassed but were flame sealed.

NMR spectra were collected on a 100.6 MHz (B_0 = 9.4 T, 400 MHz ^{1}H frequency) Bruker AVANCE III spectrometer (Billerica, MA). ^{1}H and ^{13}C spectra were collected for each sample. Inversion recovery experiments were completed in triplicate. The accompanying program, TopSpin 3.6.1 was used for analysis.

2.3 Peptide Synthesis & Purification

The model peptide Ac-WPDEKHEL-NH_2 (PK9-H) was prepared using standard fuorenylmethoxycarbonyl (Fmoc) solid-phase synthesis with few modifications on an automated PS3 synthesizer (Protein Technologies, Inc). The peptide represents residues 1164 through 1171 of the larger YPK9 protein. The serine at position 1164 was substituted for a tryptophan in order to allow for concentration determination using UV-Vis spectroscopy. Although the addition of the tryptophan residue may modify the behavior of the peptide, this is unlikely due to its location outside of the binding region of the short sequence. The peptide was synthesized on rink amide MBHA resin with the proline and tryptophan residues being double coupled to ensure their attachment.

The resulting peptide containing solution was purified using reverse phase high performance liquid chromatography (HPLC) with a C18 column (250 x 4.6 mm, 5 μm, VyDAC, Grace Division Discovery Sciences) on a BioLogic DuoFlow chromatography system. Acetonitrile and water containing 0.1% trifluoroacetic acid (TFA) to ensure total ionization of the peptide and consistency between runs, were used as the mobile phase. A UV/Vis detector was used to monitor the absorbance at 214 and 280 nm.

Peaks which eluted from the column were collected for characterization by electrospray ionization mass spectrometry (ESI-MS). A small aliquot was diluted 10-fold in a solution of 50:50 water/acetonitrile with 0.1% formic acid. A Waters Acquity UPLC was used for separation prior to recording the MS, where 10 μL of the analyte solution was injected. The UPLC used 50:50 water/acetonitrile with 0.1% formic acid as the mobile phase with a flow rate of 0.05 L min^{-1}. MS were collected on a Micromass Q-ToF Micro using positive ionization. Capillary voltage was 3000 V, sample cone voltage was 30 V, extraction cone voltage was 2.0 V, source

and desolvation temperatures were 90 and 350 °C respectively. The cone and desolvation gases were both nitrogen with flow rates of 20 L hr^{-1} and 500 L hr^{-1} respectively. Resulting spectra were analyzed to confirm the presence of a peak at an *m/z* of 1093.508 indicating the peptide was present.

The remaining peptide containing HPLC solution was flash frozen and lyophilized on a Labconco FreeZone 4.5. The resulting solid peptide was dissolved in 18 MΩ·cm water, flash frozen, and lyophilized for further purification.

Approximately 10 mg samples of solid peptide were dissolved in 18 MΩ·cm water to make stock solutions. Concentration determination of aqueous peptide solutions was completed using an Agilent Technologies Cary 8454 UV-Vis Spectrophotometer with a fused quartz cuvette that had a 1 cm pathlength. Absorbance was measured at 280 nm due the absorbance of the aromatic sidechain of tryptophan and subsequent calculations were made using the molar extinction coefficient of tryptophan in 6.0 M guanidinium hydrochloride at 280 nm, 5690 M^{-1} cm^{-1}.[37]

2.4 Peptide Solution Preparation & Circular Dichroism Spectropolarimetry

CD spectra of 200 μM peptide solutions (pH 6.2 and 7.4) with and without 1.1 equivalents of Zn^{2+} were collected on a J-810 spectrometer (Jasco) at room temperature (20-24 °C) with a bandwidth of 1 nm in a 1 mm cell. The PMT high voltage (HT) was below 600 V for the range of 190 to 260 nm. To ensure accuracy and reproducibility, background spectra of the buffer were collected, and all spectra were collected in quadruplicate.

2.5 Peptide Solution Preparation & Fluorescence Spectroscopy

15 μM peptide solution (pH 7.4) and 3 mM $ZnCl_2$ (pH 7.4) was used to perform fluorescence titration experiments. Upon completion, 20 equivalents of Zn^{2+} had been added to the peptide solution.

All fluorescence experiments were performed using a PTI single photon counting spectrofluorometer and a 1 cm quartz cuvette at room temperature (20-24 °C) . Fluorescence experiments utilized an excitation wavelength of 290 nm and recorded emissions between 300 and 850 nm. The step size was 1 nm and integration time was 0.25 s. Titration experiments were run in triplicate.

2.6 Peptide Solution Preparation & Nuclear Magnetic Resonance Spectroscopy

5 mM peptide solution (pH 6.2) was made in 90/10 (v/v) H_2O/D_2O for NMR studies. Solutions utilized 90:10 (v/v) water D_2O for resonance locking. Solutions containing zinc used $ZnCl_2$. All NMR experiments were performed on a Bruker AVANCE III 400 MHz NMR using the accompanying program, TopSpin 3.6.1, for analysis at room temperature (20-24 °C). ^1H NMR with solvent suppression was achieved using 1D excitation sculpting using W5, a watergate variant. 2D ^1H-^1H ge-TOCSY using excitation sculpting with MLEV-17 and ES element was acquired.

Chapter 3: Results

3.1 EDTA Studies

The results of the NMR experiments on the carbonyl containing Zn^{2+} chelator, EDTA, will be discussed in the following, including T_1 measurements and the investigation new splitting patterns resulting from potential J-couplings between ^{67}Zn and ^{1}H and ^{13}C atoms.

3.1.1 T_1 Measurements

Deoxygenated and flame sealed samples previously prepared by SriRamya Garapati were used to validate methodology surrounding T_1 measurements.[38] ^{1}H, ^{13}C, and HSQC NMR were recorded for each of the three samples – apo-EDTA, Zn-EDTA (1:1), and Zn-EDTA (1:0.5) – to which demonstrated that they were uncontaminated. This supported the use of the same methodology as that used by Garapati. Resonance peaks appeared where expected and ^{13}C T_1 measurements of the samples agreed with those previously published.[30]

^{13}C NMR spectra of newly prepared apo-EDTA and Zn-EDTA solutions were recorded, and the resonance peaks appeared in the same positions as those seen in samples prepared by Garapati. An overlay of these spectra can be seen in **Figure 16**. Zn^{2+} caused the peaks to shift downfield as the nuclei responsible became less shielded.

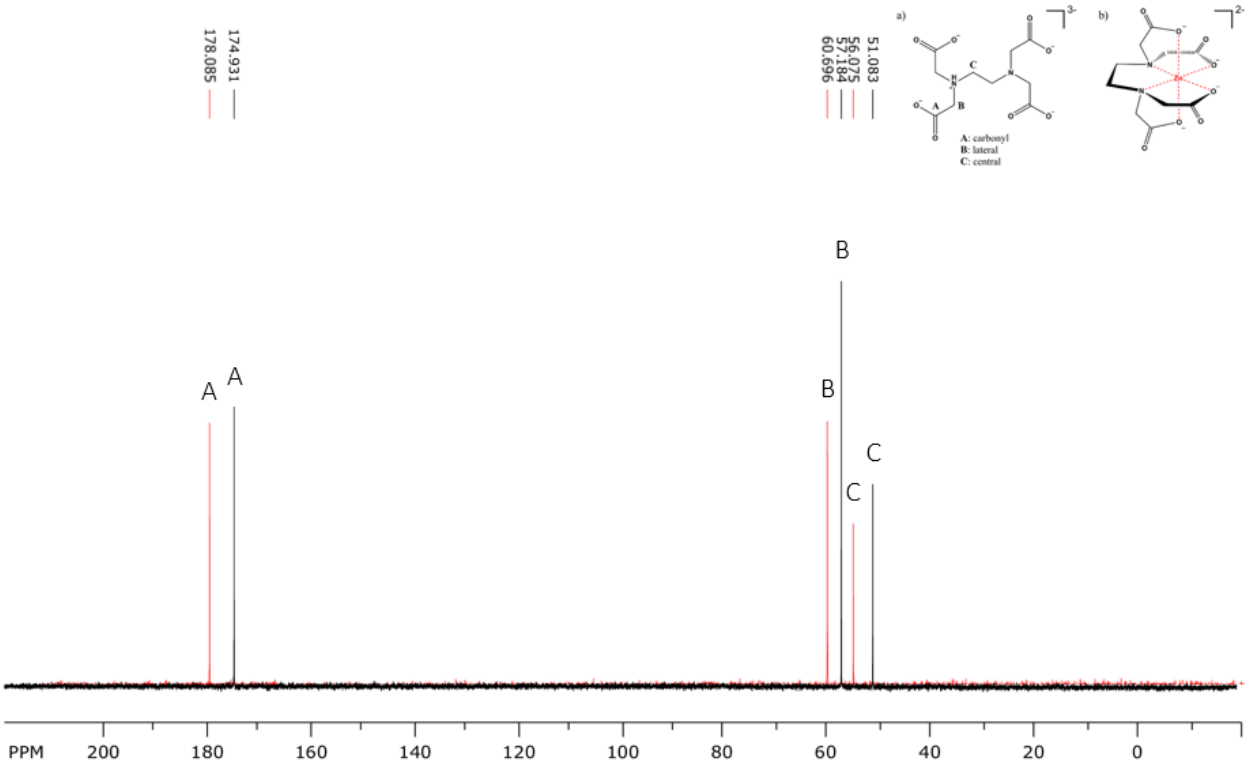

Figure 16. Overlay of ^{13}C NMR of apo-EDTA and Zn-EDTA in black and red, respectively. Inset shows (A) carbonyl, (B) lateral, and (C) central carbons, which correspond to peak labels on spectra.

The ^{13}C NMR stacked plots, generated through inversion recovery experiments, of apo-EDTA and Zn-EDTA are shown in **Figure 17**. The peaks initially are at maximum negative intensity at the shortest τ and then increase towards a maximum positive intensity as the system returns to equilibrium. For each inversion-recovery experiment, spectra were recorded for 8 delay times (0.25, 0.5, 1, 2, 4, 8, 16, and 32 s) to properly sample the recovery curves. The spectrum for each of the timepoints were collected 32 times, and the experiment was repeated three times for each of the independently prepared solutions. This was then fit with using the Bruker TopSpin software. All ^{13}C T_1 measurements of the EDTA solutions can be found in **Appendix A**, including averages, standard deviations, and fitting constants associated with the line of best fit.

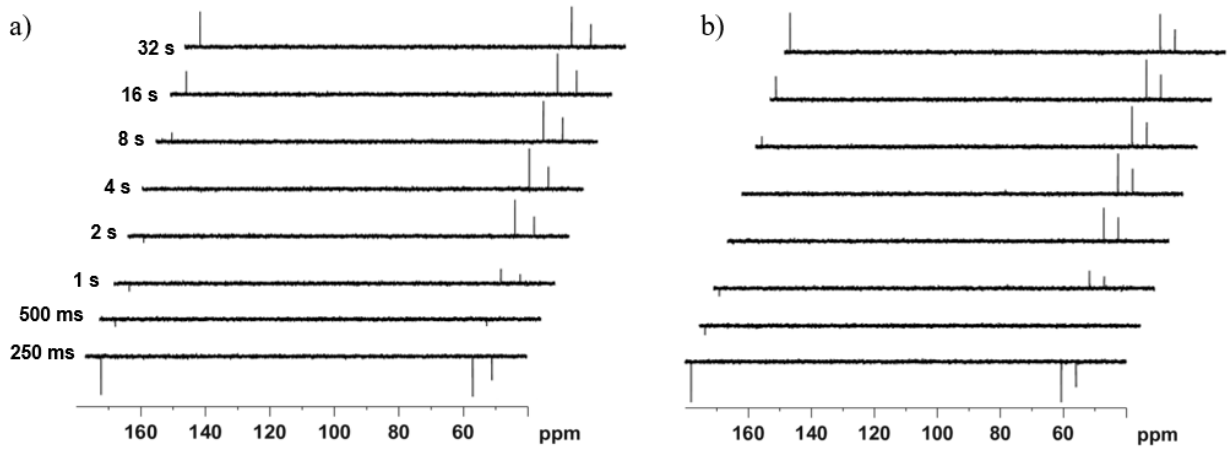

Figure 17. ^{13}C NMR stacked plots of **(a)** apo-EDTA and **(b)** Zn-EDTA with the variable delay times shown on the y-axis.

In order to determine reproducibility in sample preparation, T_1 measurements were made on two matched sets of solutions: deoxygenated apo-EDTA (a) and apo-EDTA (b) solutions and Zn-EDTA (a) and Zn-EDTA (b). As an example, the T_1 values determined for the carbonyl carbon of the apo-EDTA solutions are shown in **Table 7** and those of Zn-EDTA solutions are shown in **Table 8**. The average T_1 value using the intensity fit for the apo-EDTA solutions was 10.017 s and 10.411 s, for apo-EDTA (a) and apo-EDTA (b), respectively. According to the results of student's t test, the differences seen in measurements were not statistically significant ($P = 0.5018$). The Zn-EDTA solutions had an average T_1 value of 7.781 s for Zn-EDTA (a) and 7.525 s for Zn-EDTA (b). The differences seen for these solutions were not statistically significant ($P = 0.5136$). Likewise, the differences seen in the T1 values for the central and lateral carbons, excluding the central peak of apo-EDTA, were found not to be statistically significant. The origin of the single outlier is not known, however the averaging of more experimental runs should resolve the issue. This suggests that there is internal consistency in the sample preparation methodology used and allows the data sets to be grouped accordingly.

Table 7. Comparison of ^{13}C T_1 Values from Intensity Fit of Carbonyl Peak of apo-EDTA (a) and (b)

Run	apo-EDTA (a) (s)	apo-EDTA (b) (s)
1	10.210	11.320
2	10.350	10.110
3	9.492	9.803
Average	10.017	10.411
Standard deviation	0.460	0.802

Table 8. Comparison of ^{13}C T_1 Values from Intensity Fit of Carbonyl Peak of Zn-EDTA (a) and (b)

Run	Zn-EDTA (a) (s)	Zn-EDTA (b) (s)
1	7.949	6.848
2	7.774	7.971
3	7.619	7.756
Average	7.781	7.525
Standard deviation	0.165	0.344

Since magnetization cannot be directly measured by NMR, either signal intensity or signal area are used as proxies. To determine if one fit method was superior to the other, the T_1 values generated by each were subjected to the student's t test. The T_1 values for measurements of the carbonyl peak of apo-EDTA (a) and (b) using fits of both peak intensity and area are shown in **Table 9**. For a data set consisting of 6 runs, t intensity fitting method resulted in an average T_1 of 10.214 s and the area fitting method yielded a T_1 of 10.231 s. According to

student's t test, the difference seen between these data sets is not significantly different (P = 0.9643). This was determined to be the case for the carbonyl and central peak of the apo-EDTA solutions as well. The lateral peak at 57 ppm did show a difference that is considered statistically significant (P = 0.0104). T_1 measurements are sensitive to changes in temperature, and it is possible that inconsistencies between measurements could have caused the range of this data to increase.

Table 9. Comparison of ^{13}C T_1 Values of Area and Intensity Fits of Carbonyl Peak of apo-EDTA (a) & (b)

Run	Intensity (s)	Area (s)
1	10.210	9.790
2	10.350	10.720
3	9.492	10.135
4	11.320	10.790
5	10.110	9.157
6	9.803	10.760
Average	10.214	10.231
Standard deviation	0.623	0.661

Graphs of the area and intensity fit T_1 values for the carbonyl carbon of apo-EDTA (a) can be seen in **Figure 18**. Both sets of data were fit to the equation $I[t] = I[0]\left(1 - 2Ae^{(-t/T1)}\right)$, where I[0] is the intensity at $\tau = 0$ and A is an exponential factor estimated by the Bruker TopSpin program. For the intensity fit and area fit, T_1 was found to be 9.492 s and 10.135 s, respectively. The results of the student's t test demonstrated that there was no statistical

difference in all the peaks ($P > 0.05$) except for the lateral carbon. The average T_1 value for the intensity fit of the lateral carbon was 508.599 ms (± 28.661) and the area fit was 469.417 ms (± 10.487). An iteration of the experiment on the apo-EDTA (b) solution yielded a T_1 value of 560.000 ms. Although this value is larger than the other measurements ($P = 0.127$), it is not an outlier according to Grubb's test which deems that an outlier must have a $P < 0.05$. Because of this, it was still included in data fitting. It is possible that the sensitivity of T_1 measurements to changes in temperature could explain the difference, but this cannot be said with certainty.[39]

Despite the similarity of T_1 values using the area and intensity fits, the relative sum of squares (RSS) and standard deviation (SD) were smaller for the intensity fits, thus intensity fit values were used for the remaining analyses. The origin of the difference between the fitting methods appears to be that signal intensity is less sensitive to issues of spectral phasing than signal area. Since the same phasing is applied to all the spectra collected in a single inversion-recovery experiment, variations between scans cannot be corrected individually.

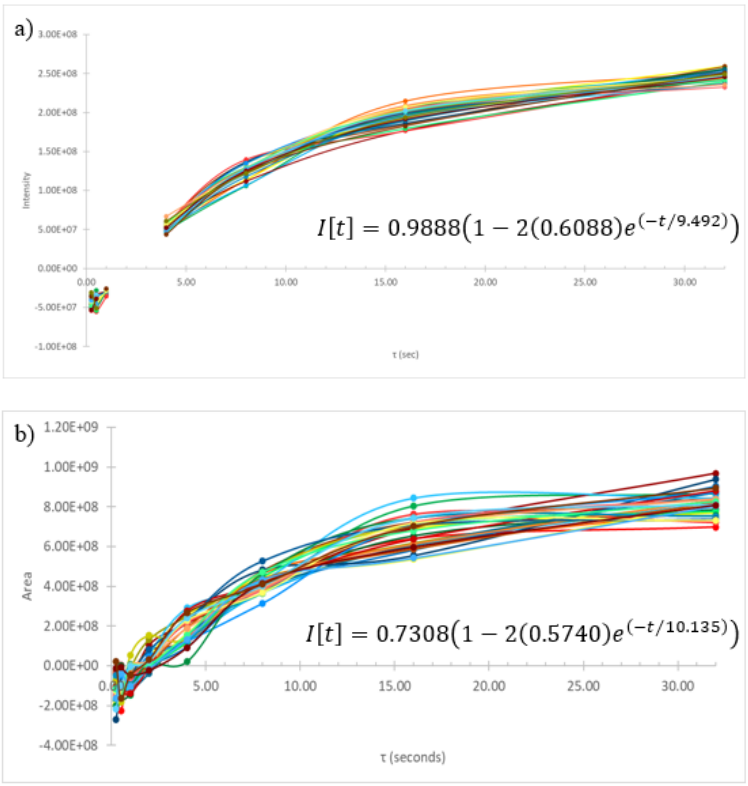

Figure 18. (a) Intensity and **(b)** area fits of the carbonyl carbon of apo-EDTA (a) with line of best fit equations. **(a)** RSS: 0.1581, SD: $2.791 \cdot 10^{-2}$, $T_1 = 9.492$ s. **(b)** RSS: 1.030, SD: $6.344 \cdot 10^{-2}$, $T_1 = 10.135$ s.

When measuring relaxation, it is common to use deoxygenated solutions. This is because molecular oxygen is paramagnetic giving it the potential to induce relaxation. To determine the relevance of oxygen to our experiments, T_1 values of the lateral peak of deoxygenated solutions apo-EDTA (a) and (b) were compared to those of apo-EDTA (c) which was not deoxygenated. The results are shown in **Table 10**. The results of the student's t test indicates that the difference seen in the two data sets are insignificant (P = 0.7442). Deoxygenation was determined to be statistically insignificant for all three peaks of the apo-EDTA solutions and Zn-EDTA solutions. As a result, it was decided that the lengthy and laborious process of deoxygenation would be forgone and this provided statistical support for the combination of T_1 measurements of the (a), (b), and (c) solutions, both Zn^{2+} bound and Zn^{2+} free.

Table 10. Comparison of T_1 Values of Intensity Fit of Lateral Peak of Deoxygenated apo-EDTA (a) and (b) with Oxygenated apo-EDTA (c)

Run	Deoxygenated (ms)	Oxygenated (ms)
1	482.099	533.100
2	487.200	513.199
3	500.399	498.200
4	560.000	
5	521.599	
6	500.299	
Average	508.599	514.833
Standard deviation	28.661	17.507

The ^{13}C T_1 values, averages, and standard deviations of apo-EDTA (a) can be seen in **Table 11** to **13**. The lateral and central peaks had shorter T_1 times than the carbonyl peak as seen with their quicker return to their equilibrium intensity in **Figure 17a** and resulting T_1 values.

Table 11. Intensity Fit T_1 Values of Carbonyl Carbon of apo-EDTA (a)

Run	Intensity measurement (s)
1	10.210
2	10.350
3	9.492
Average	10.017
Standard deviation	0.460

Table 12. Intensity Fit T_1 Values of Lateral Carbon of apo-EDTA (a)

Run	Intensity measurement (ms)
1	482.099
2	487.200
3	500.399
Average	489.899
Standard deviation	9.444

Table 13. Intensity Fit T_1 Values of Central Carbon of apo-EDTA (a)

Run	Intensity measurement (ms)
1	449.200
2	436.900
3	454.200
Average	446.767
Standard deviation	8.903

The ^{13}C NMR stacked plots of apo-EDTA and Zn-EDTA are shown in **Figure 19**. T_1 values were compared between apo-EDTA and Zn-EDTA solutions. The results of the comparison of the carbonyl peak can be seen in **Table 14**. With a p-value of less than 0.0001, the differences between the apo-EDTA solutions and Zn-EDTA solutions are statistically significant. Both the lateral and central carbon showed similar results indicating that the binding of Zn^{2+} results in quicker T_1 relaxation times for all of the carbon types in EDTA.

Table 14. Comparison of T_1 Values of Intensity Fit of Carbonyl Peak of apo-EDTA (a), (b), and (c) with Zn-EDTA (a), (b), and (c)

Run	apo-EDTA (s)	Zn-EDTA (s)
1	10.210	7.949
2	10.350	7.774
3	9.492	7.619
4	11.320	6.848
5	10.110	7.971
6	9.803	7.756
7	9.870	7.993
8	9.305	7.819
9	8.302	8.671
Average	9.862	7.822
Standard deviation	0.824	0.472

Isotopically enriched samples of metals are often only available in their metallic form, i.e., Zn^0, and this was the case for the ^{67}Zn that was purchased. Prior to converting $^{67}Zn^0$ to $ZnCl_2$, its divalent form, the method for synthesis and sample preparation was tested using isotopically unenriched solid Zn. The T_1 values for Zn-EDTA (a) and (b) were compared to those of Zn-EDTA (d) which was made with synthesized $ZnCl_2$, and the results for the lateral peak are shown in **Table 15**. The difference in the averages for the carbonyl peak of Zn-EDTA (a) and (b) compared to (d) is not statistically significant ($P = 0.2383$). This was true for all the peaks, as they showed that there was no statistical difference in T_1 values despite using the synthesized

$ZnCl_2$ to prepare the solution, giving confidence in a similar methodology for ^{67}Zn to synthesize $^{67}Zn^{2+}$.

Table 15. Comparison of T_1 Values of Intensity Fit of Lateral Peak of Zn-EDTA (a) and (b) with Zn-EDTA (d) Made with Synthesized $ZnCl_2$

Run	Zn-EDTA (a) & (b) (ms)	Zn-EDTA (d) (ms)
1	398.400	436.300
2	403.100	441.900
3	378.400	429.000
4	400.200	
5	423.900	
6	453.900	
Average	409.650	435.733
Standard deviation	26.063	6.469

A ^{13}C NMR spectra of ^{67}Zn-EDTA (e) solution made with synthesized $^{67}ZnCl_2$ is shown in **Figure 19** with the ^{13}C NMR of apo-EDTA and Zn-EDTA slightly offset to allow for distinguishability in peaks. The addition of $^{67}Zn^{2+}$ did not cause a change in the chemical shifts or appearance of a splitting pattern compared to Zn-EDTA.

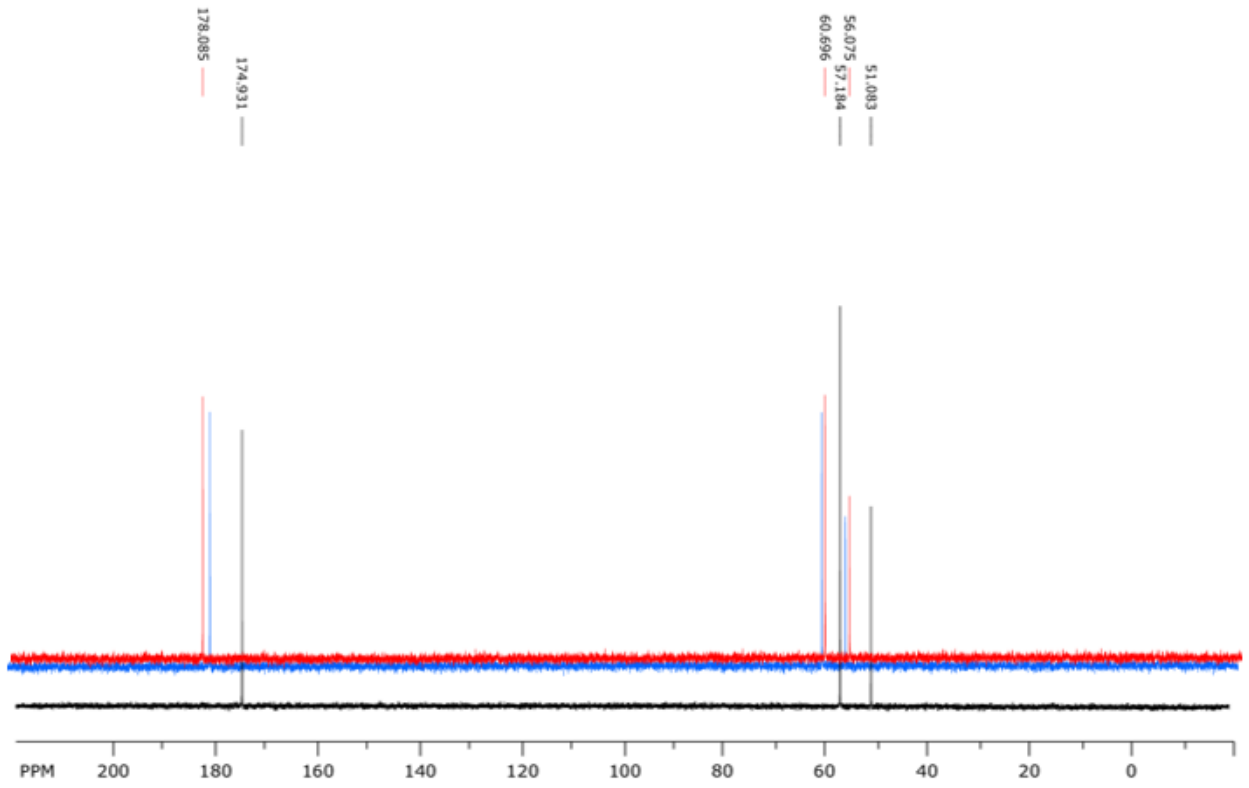

Figure 19. ^{13}C NMR of apo-EDTA in black, Zn-EDTA in red, and ^{67}Zn-EDTA in blue with peaks labeled.

In order to determine if the binding of $^{67}Zn^{2+}$ to EDTA caused a change in spin-lattice relaxation times, student's t test was used to compare T_1 values. The intensity fit values of the carbonyl peak can be seen in **Table 16**. As expected, the introduction of $^{67}Zn^{2+}$ caused the carbons to relax faster than compared to EDTA without Zn^{2+}. With a P-value of 0.0241, the difference in the values is considered to be statistically significant. All peaks showed that the change was statistically significant, except the central peak. As for the central peak, it is likely due to an inconsistency in the experimental process as the temperature could not be controlled for the duration of the experiment. Despite the inconsistency, the introduction of $^{67}Zn^{2+}$ did result in a shorter average T_1 compared to the apo-solutions.

Table 16. Comparison of T_1 Values of Intensity Fit of Carbonyl Peak of apo-EDTA (a), (b), and (c) with ^{67}Zn-EDTA (e)

Run	apo-EDTA (s)	^{67}Zn-EDTA (s)
1	10.210	9.128
2	10.350	8.300
3	9.492	8.012
4	11.320	
5	10.110	
6	9.803	
7	9.870	
8	9.305	
9	8.302	
Average	9.862	8.480
Standard deviation	0.824	0.579

T_1 values for the Zn-EDTA solutions were compared to those of ^{67}Zn-EDTA (e) as shown for the carbonyl carbon data in **Table 17**. The ^{13}C had a T1 of 7.822 in the Zn-EDTA solutions and 8.480 s in ^{67}Zn-EDTA (e). This difference was determined to be statistically insignificant (P = 0.0745). For all three peaks, there was determined to be no statistical difference in the T_1 values. Despite the quadrupolar shape of $^{67}Zn^{2+}$, there was no change in the spin-lattice relaxation times.

Table 17. Comparison of T_1 Values of Intensity Fit of Carbonyl Peak of Zn-EDTA (a), (b), and (c) with ^{67}Zn-EDTA (e)

Run	Zn-EDTA (s)	^{67}Zn-EDTA (s)
1	7.949	9.128
2	7.774	8.300
3	7.619	8.012
4	6.848	
5	7.971	
6	7.756	
7	7.993	
8	7.819	
9	8.671	
Average	7.822	8.480
Standard deviation	0.472	0.579

3.1.1 J-couplings

Since there was no apparent change to the ^{13}C NMR spectra upon EDTA binding $^{67}Zn^{2+}$ and no statistical difference between the Zn-EDTA and ^{67}Zn-EDTA spin-lattice relaxation values, ^{1}H NMR were investigated as well for potential J-couplings between ^{67}Zn and ^{1}H. Both apo-EDTA and Zn-EDTA solutions showed large peaks at 4.8 ppm due to H_2O in their standard ^{1}H NMR spectra (i.e., without solvent suppression). apo-EDTA had singlets at 3.480 and 3.079 ppm with integrals of 1.647 and 1.000, respectively. Zn-EDTA had a signal with non-first order splitting at 3.280 ppm and a singlet at 2.756 ppm with integrals of 1.774 and 1.000, respectively.

An overlay of these spectra can be seen in **Figure 20**. The singlet at 2.8 ppm does not undergo splitting upon Zn^{2+} binding. The protons on the central carbons responsible for the singlet remain chemically equivalent after Zn^{2+} binding, preventing them from splitting one another. The signal at approximately 3.3 ppm, which represents the protons located on the lateral carbons, experiences non first order splitting because the binding of Zn^{2+} locks the two protons on each carbon into different chemical environments. As a result, they become chemically inequivalent and can J-couple with one another. For two different protons coupling to one other, a pair of doublets is expected to appear in the spectrum. However, the small difference in the chemical shifts between these protons leads to their signals becoming non-first order. The general limit for non-first order splitting to occur is $\Delta\nu/J_{H,H} < 6$, meaning the chemical shift difference is small relative to the J-coupling constant between the lateral protons.[40]

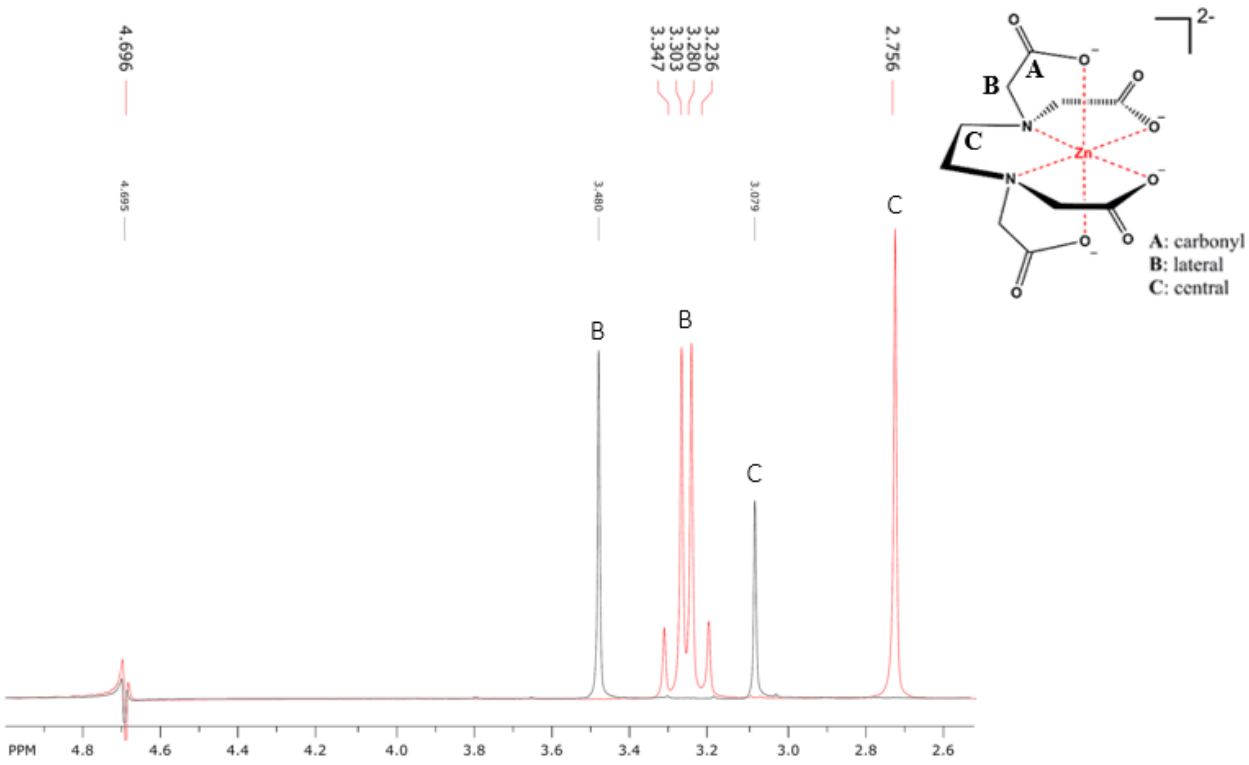

Figure 20. Overlay of ^{1}H NMR with solvent suppression of apo-EDTA in black and Zn-EDTA in red with labeled peaks that correspond to the Zn-EDTA structure shown at right.

The ^{1}H NMR of ^{67}Zn-EDTA (e) is shown overlayed with the ^{1}H NMR of Zn-EDTA in **Figure 21**. Resonance peaks did not shift upon the binding of $^{67}Zn^{2+}$ and no new splitting patterns or changes in integral values were observed. A closer look at the area around the bases of the peaks can be seen in **Figure 22**. There is no evidence of J-coupling between ^{67}Zn and ^{1}H in the resulting NMR spectra, which suggests that if a J-coupling exists, it is likely very small ($\ll$ 1Hz).

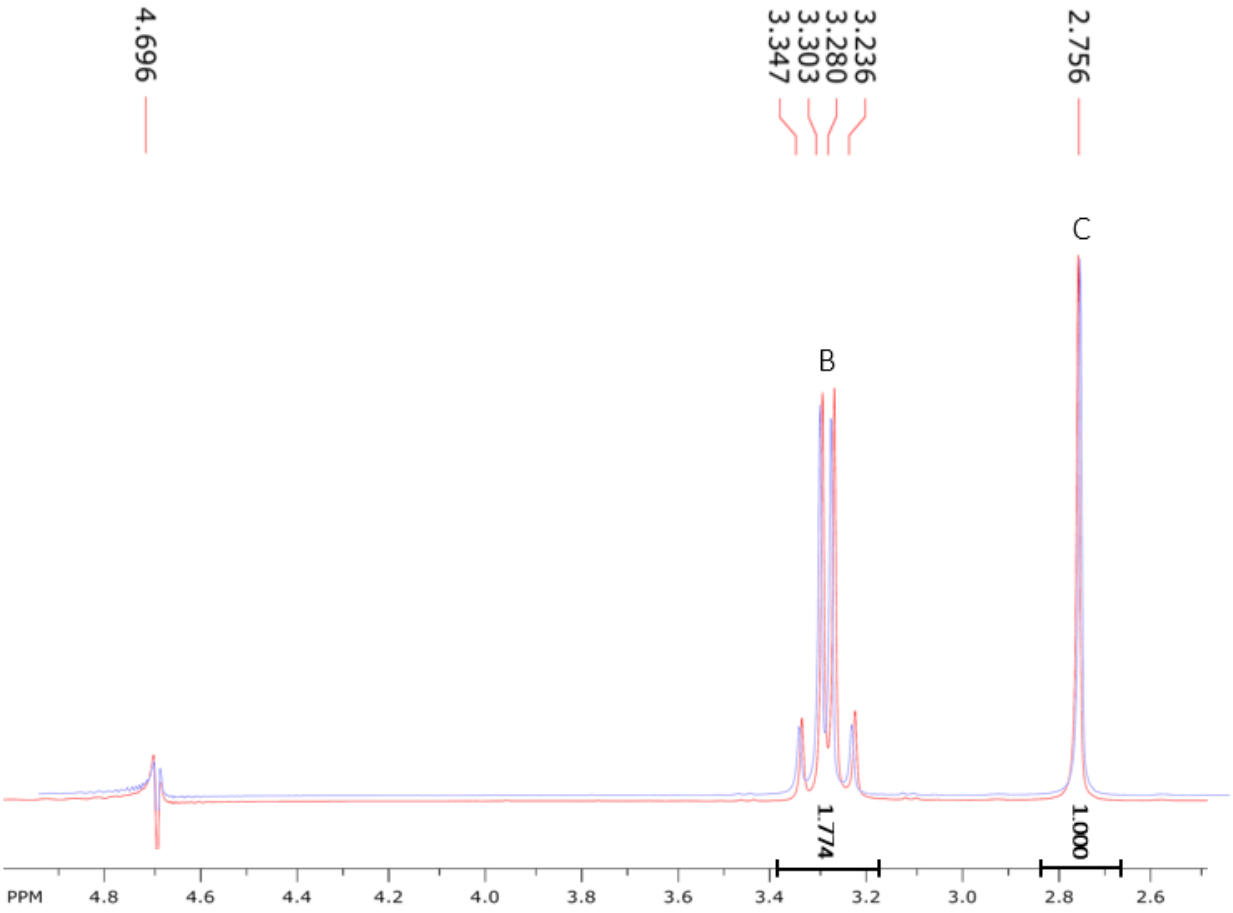

Figure 21. Overlay of ^{1}H NMR with solvent suppression of Zn-EDTA in red and ^{67}Zn-EDTA in blue with labeled peaks and integral values.

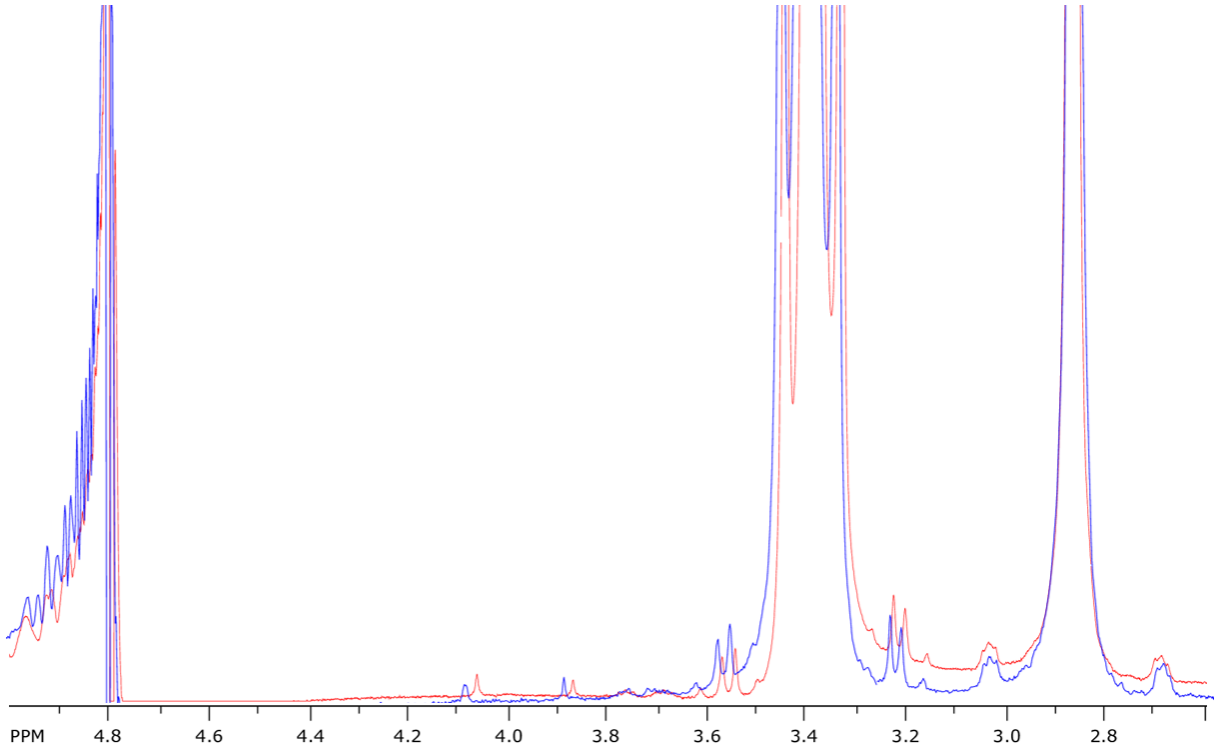

Figure 22. Enlarged overlay of ^{1}H NMR with solvent suppression of Zn-EDTA in red and ^{67}Zn-EDTA in blue.

3.2 Glycine Studies

The structures of apo-Gly and Zn-Gly can be seen in **Figure 23**. Gly has two carbon types – carboxyl and alpha, and it has the ability to bind in a bidentate manner with Zn^{2+}.

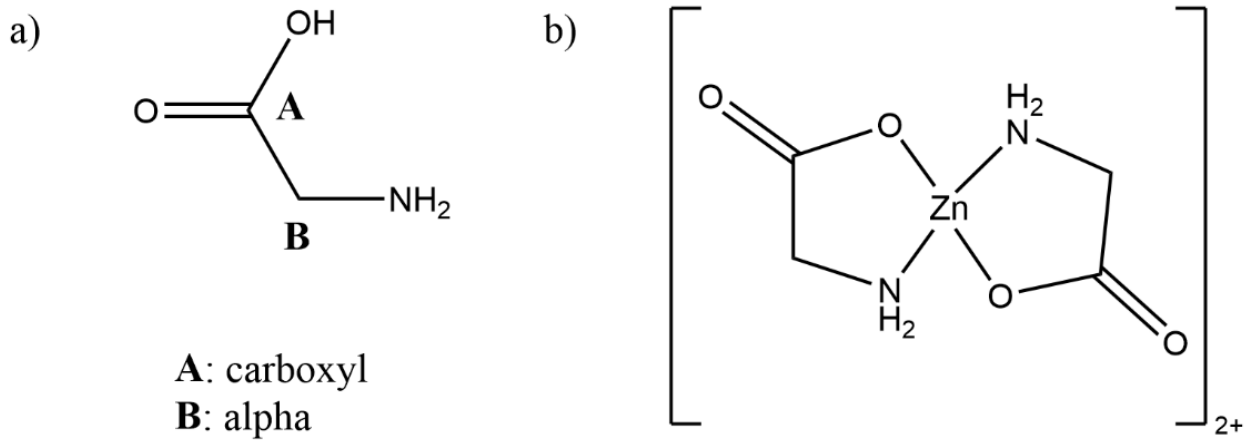

Figure 23. (a) apo-Gly and **(b)** Zn-Gly with the (A) carboxyl and (B) alpha carbons labeled.

The ^{13}C NMR spectra of apo-Gly and Zn-Gly can be seen in **Figure 24**. apo-Gly has two ^{13}C signals – 172 ppm due to the carboxyl carbon and 42 ppm due to the alpha carbon. The binding of Zn^{2+} results in the loss of the carboxyl resonance signal. This is likely due to a large number of different Zn-bound complexes existing in solution, such that the carbonyl carbon experiences many different chemical environments. This would lead to several lower intensity carbonyl peaks which may be lost in the noise (i.e., below the detection limit). Also, if the interconversion between species is fast relative to the NMR timescale, then the NMR signal may be broadened and subsequently more difficult to observe.

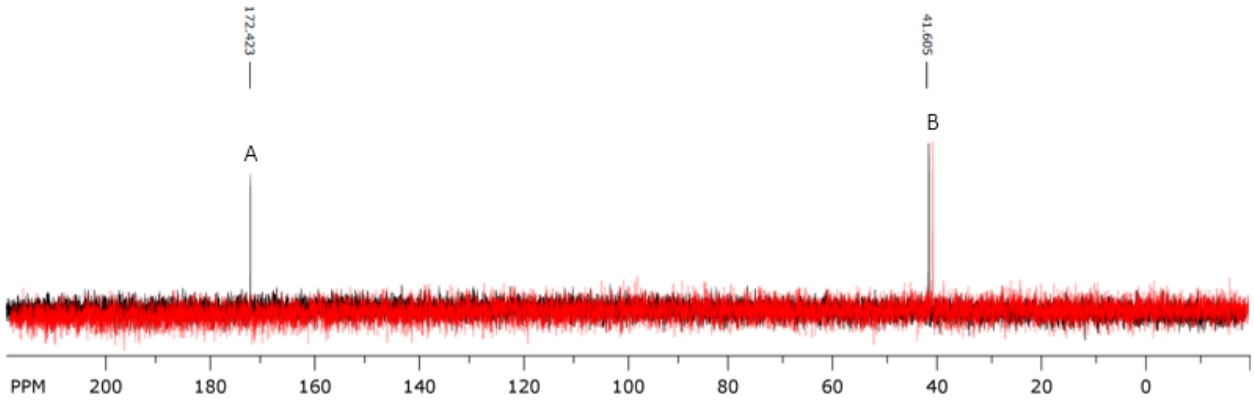

Figure 24. ^{13}C NMR of apo-Gly in black and Zn-Gly in red with (A) carboxyl and (B) resonances labeled.

The ^{13}C T_1 measurements of the carboxyl and alpha carbons of apo-Gly using intensity and area fits are shown in **Table 18** and **19**. The alpha peak had a shorter relaxation time than the carboxyl peak.

Table 18. T_1 Measurements of Carboxyl Peak of apo-Gly

Run	Intensity measurement (s)	Area measurement (s)
1	31.354	35.365
2	32.709	34.264
3	33.474	42.277
Average	32.512	37.302
Standard deviation	1.074	4.344

Table 19. T_1 Measurements of Alpha Peak of apo-Gly

Run	Intensity measurement (s)	Area measurement (s)
1	3.278	3.267
2	4.129	4.912
3	3.289	3.759
Average	3.565	3.979
Standard deviation	0.488	0.844

The ^{13}C T_1 values of Zn-Gly are shown in **Table 20**. Although the carboxyl peak cannot be seen for Zn-Gly, similar bounds were set around the apo-Gly carboxyl resonance for investigation. The intensity measurement T_1 value of the carboxyl peak of Zn-EDTA given by Bruker's TopSpin was 1.000 s, which is the value given by the program when it is unable to fit the data. This is due to the program being unable to measure intensity values since there was no signal above the noise level for all of the time points. The program was able to obtain area values for the carboxyl peak, and thus was able to give a T_1 value of 949.102 ms. This value will be ignored since the stacked plot, shows no signal at any of the time points used. The intensity measurement of the alpha carbon of Zn-Gly is beyond the time points used for the T_1 experiment and will be ignored. The area measurement of the alpha peak yielded a T_1 value of 756.282 ms. This value compared to the alpha peak T_1 of apo-Gly is significantly smaller due to the presence of Zn^{2+}, similar to what was seen with the EDTA solutions.

The Gly studies completed here suggest that Gly is poor system to use for T_1 studies as there is insufficient signal, likely due to the presence of several Zn-bound species in solution. This made obtaining accurate T_1 measurements difficult for this model system.

Table 20. T_1 Measurements of Zn-Gly

Peak	Intensity measurement (s)	Area measurement (ms)
Carboxyl	1.000[a]	949.102
Alpha	323510.901	756.282

[a]Value given when program is unable to fit data

3.3 PK9-H Peptide Studies

The resulting HPLC chromatogram of Ac-WPDEKHEL-NH_2 (PK9-H) can be seen in **Figure 25**. A single peak containing the PK9-H peptide can be seen eluting between 15 and 19 minutes. The collected peak was analyzed using ESI-MS, and the resulting mass spectrum can be seen in **Figure 26**. The presence of a peak at *m/z* of 1093.3683 $(M + H)^+$ confirms that PK9-H was successfully synthesized as it matches the predicted value (1093.508 amu). The peak at an *m/z* of 2190.6694 could be due to the formation of a dimer.

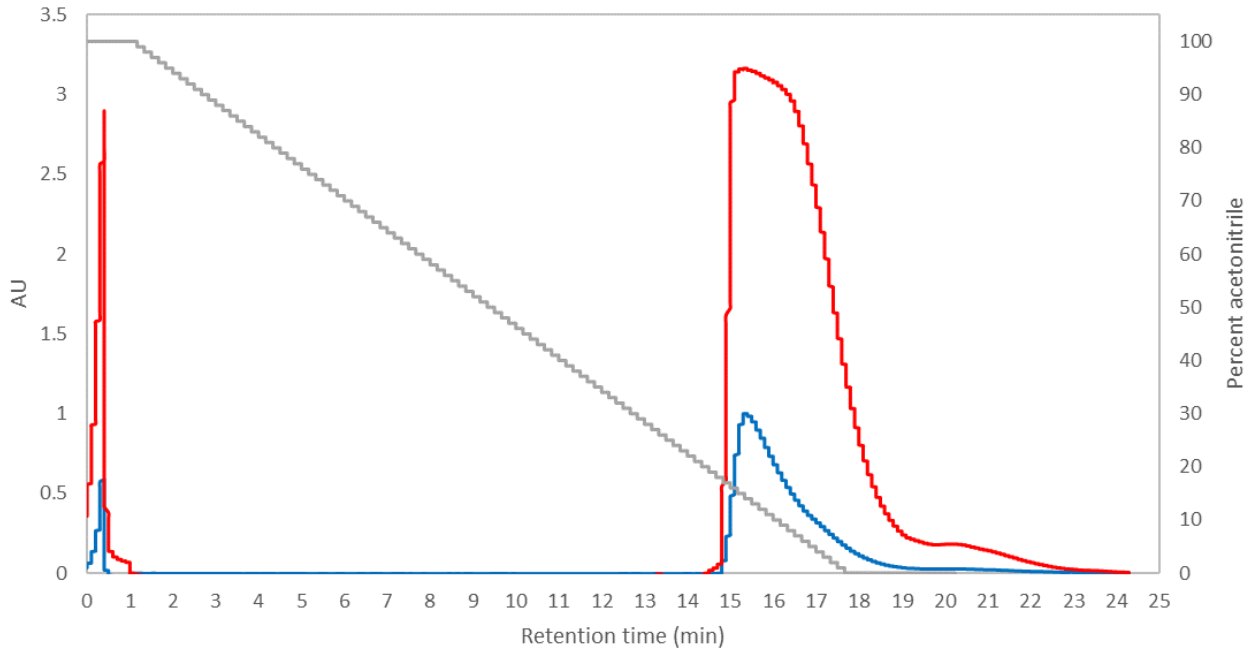

Figure 25. HPLC of PK9-H with UV-Vis absorbance at 214 nm shown in red and 280 nm shown in blue.Percent acetonitrile shown in gray. Fraction collected from 15 to 20 minutes.

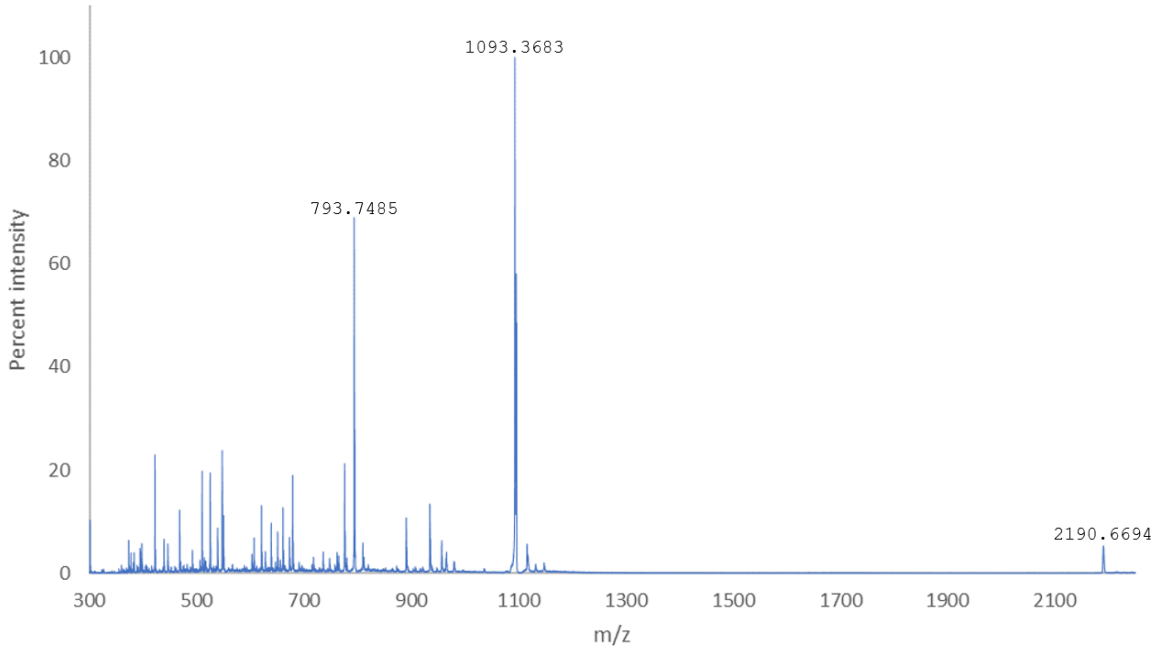

Figure 26. ESI-MS of PK9-H with the base peak at an *m/z* of 1093.3683 corresponding to the expected *m/z* shown.

Prior to attempting any NMR experiments with the peptide, its ability to bind Zn^{2+} was investigated using CD and fluorescence spectroscopy. These techniques are often used to examine ligand binding capabilities. CD is routinely used to examine peptide and protein structures, and it highly sensitive to conformational changes like those that can be induced by ligand binding. CD spectra of apo-PK9-H and Zn-PK9-H with an excess of Zn^{2+} can be seen in **Figure 27**. The lack of change in the CD signal, even with the addition of an excess of Zn^{2+} at pH 6.2 and 7.4, suggests that there is no detectable binding occurring between PK9-H and Zn^{2+}.

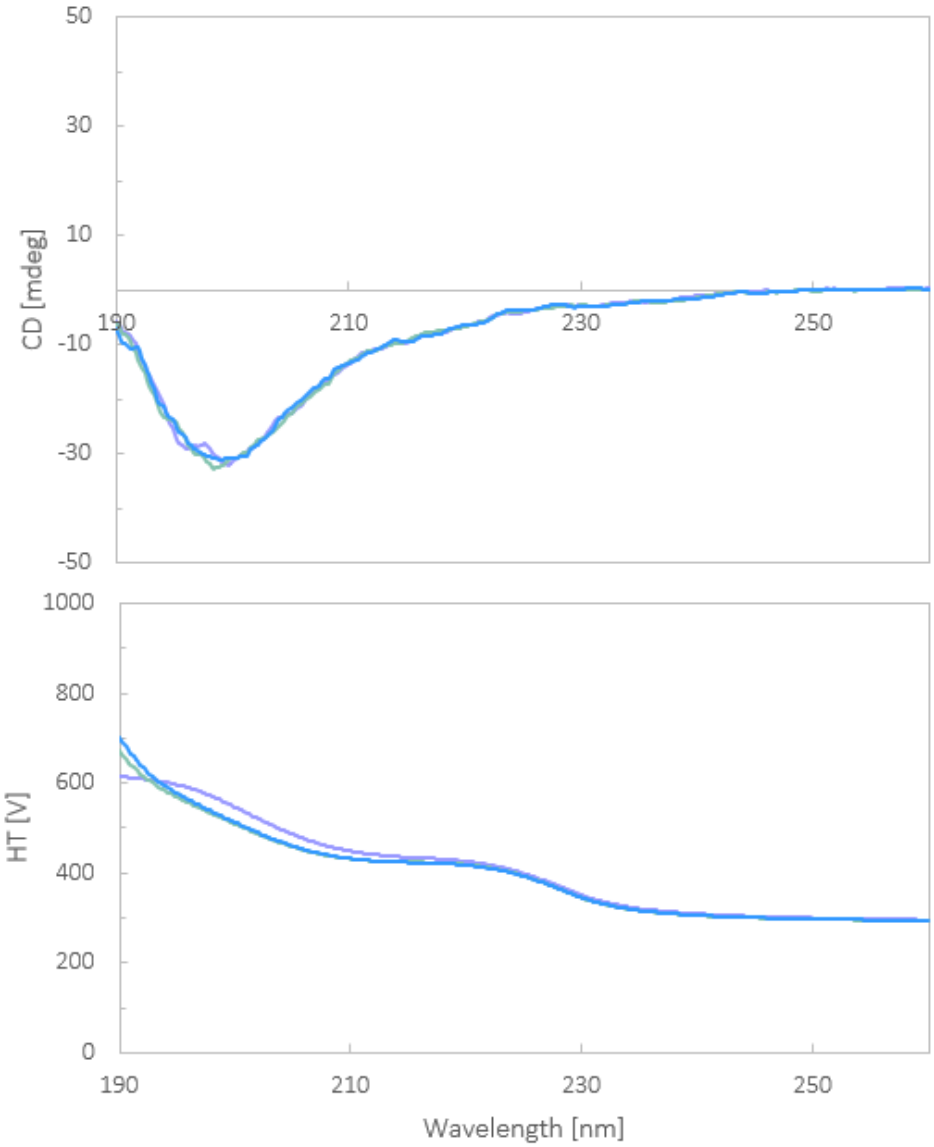

Figure 27. CD spectra and HT of apo-PK9-H at pH 6.2 in purple, Zn-PK9-H at pH 6.2 in green, and Zn-PK9-H at pH 7.4 in blue.

To further investigate potential binding interactions between PK9-H and Zn^{2+}, that could have been missed by CD, fluorescence titrations were performed in triplicate. An example of the resulting spectra can be seen in **Figure 28**. Increasing concentrations of added Zn2+ caused a decrease in the emission intensity of the peaks at approximately 350 nm and 690 nm.

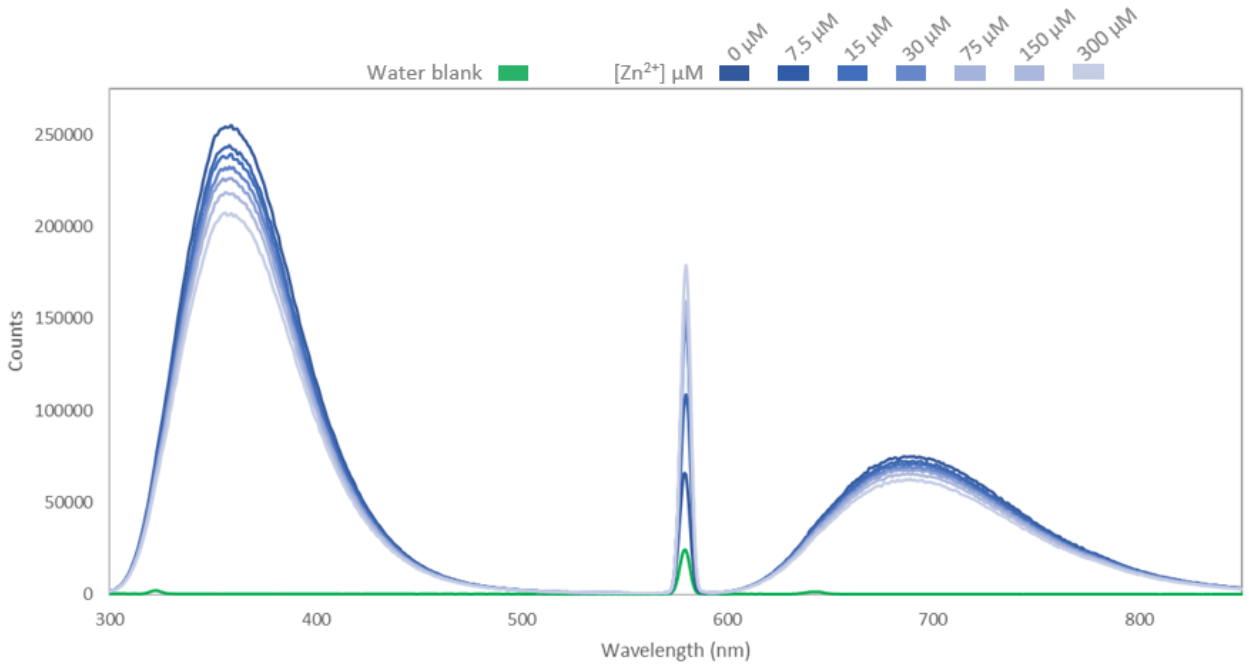

Figure 28. Fluorescence spectra of PK9-H (15 µM, pH 7.4) upon the addition of 0 to 20 equivalents of Zn^{2+}.

Graphs of the corrected fluorescence intensities of the titration experiments can be seen in **Figure 29**. Exponential fits of the data yielded K_a values of 27.555, 9.3278, and 18.891 mM. This gives an average K_a of 18.591 mM and standard deviation of 7.444, which suggests that if PK9-H is binding Zn^{2+} at all, then it is a weak binding interaction.

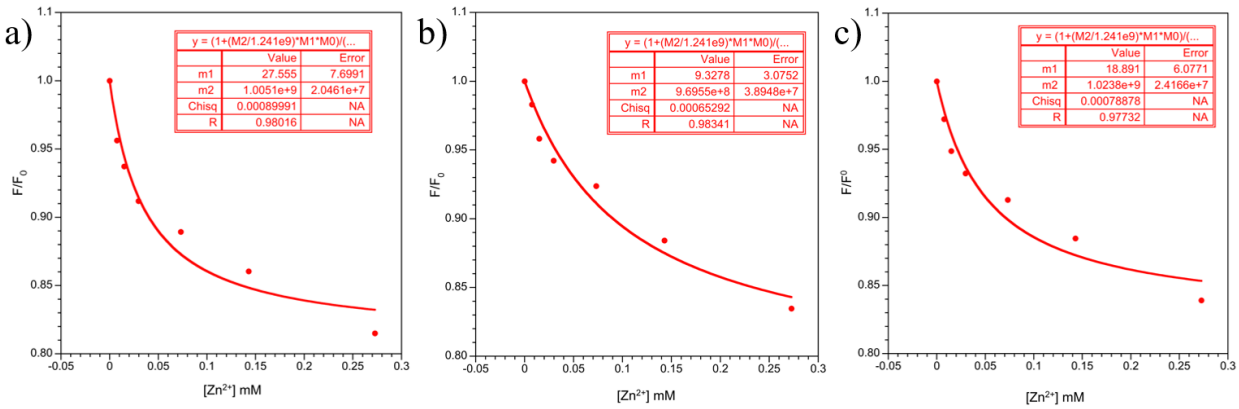

Figure 29. Fluorescence fits of Zn^{2+} titrations into PK9-H (15 μM, pH 7.4) where m1 = K_a.

A ^{13}C NMR spectrum of PK9-H can be seen in **Figure 30**. Despite the experiment being the result of 10,000 scans, the S/N ratio is poor, but some information can still be obtained. With 50 carbons in PK9-H, the observation of 43 resonances is reassuring. The missing signals are likely lost due to spectral overlap. Aliphatic carbons often appear between approximately 20 and 60 ppm. There are 21 ^{13}C signals in the aliphatic region of the spectrum. There are 10 ^{13}C signals in the aromatic region, between 110 and 140 ppm, so all the ring carbons of Trp and His are resolved.[41] Further, there are 12 signals in the carbonyl region between 170 and 185 ppm, an indication that all the carbonyl carbon signals were resolved.

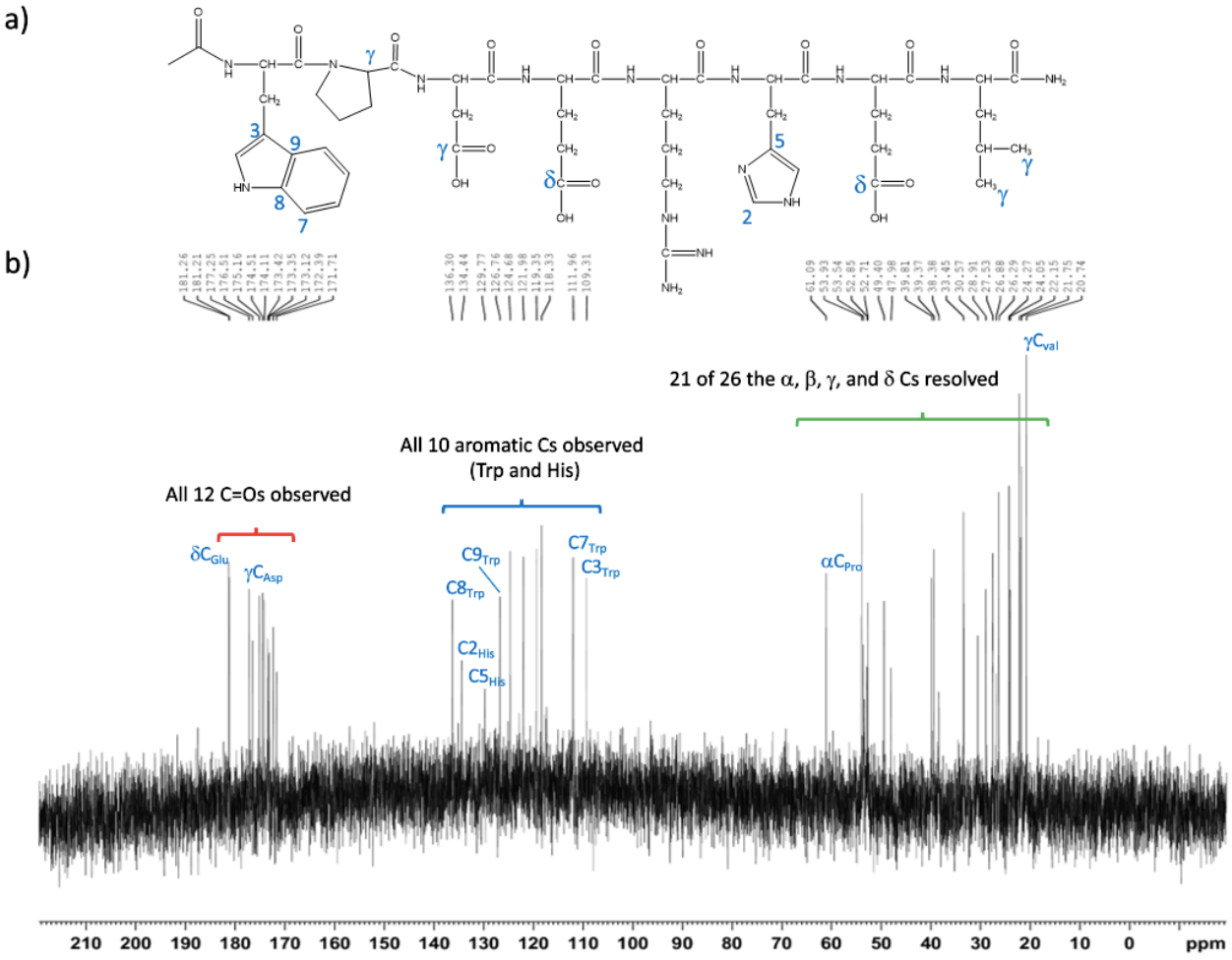

Figure 30. (a) Structure of PK9-H peptide with select carbon atoms identified. **(b)** ^{13}C NMR of PK9-H peptide with select regions and signals identified.

A ^{1}H spectrum of PK9-H can be seen in **Figure 31**. Solvent suppression of the water signal that appeared at approximately 4.8 ppm was achieved using excitation sculpting and watergate 5 (W5). Excitation sculpting uses spin or gradient echoes like W5 with its narrow notch about the solvent resonance to reduce signal distortion for nearby signals to achieve solvent suppression. W5 like watergate 3-9-19 has no effect on exchangeable protons.

Regions of ^{1}H NMR often overlap in proteins, making it difficult to identify all resonances. Amide protons appear between approximately 7 and 10 ppm and aromatic protons

appear between 6 and 8 ppm. There are several signals seen between 7 and 8.5 ppm as expected in a peptide with aromatic sidechains.[41] Alpha-protons and those due to non-aromatic side chains are typically found below 4.6 ppm, and several resonances, some well resolved and some overlapping, are observed in this region of the spectrum.[39] There is the possibility that solvent suppression could be eliminating some of the alpha-proton resonances.

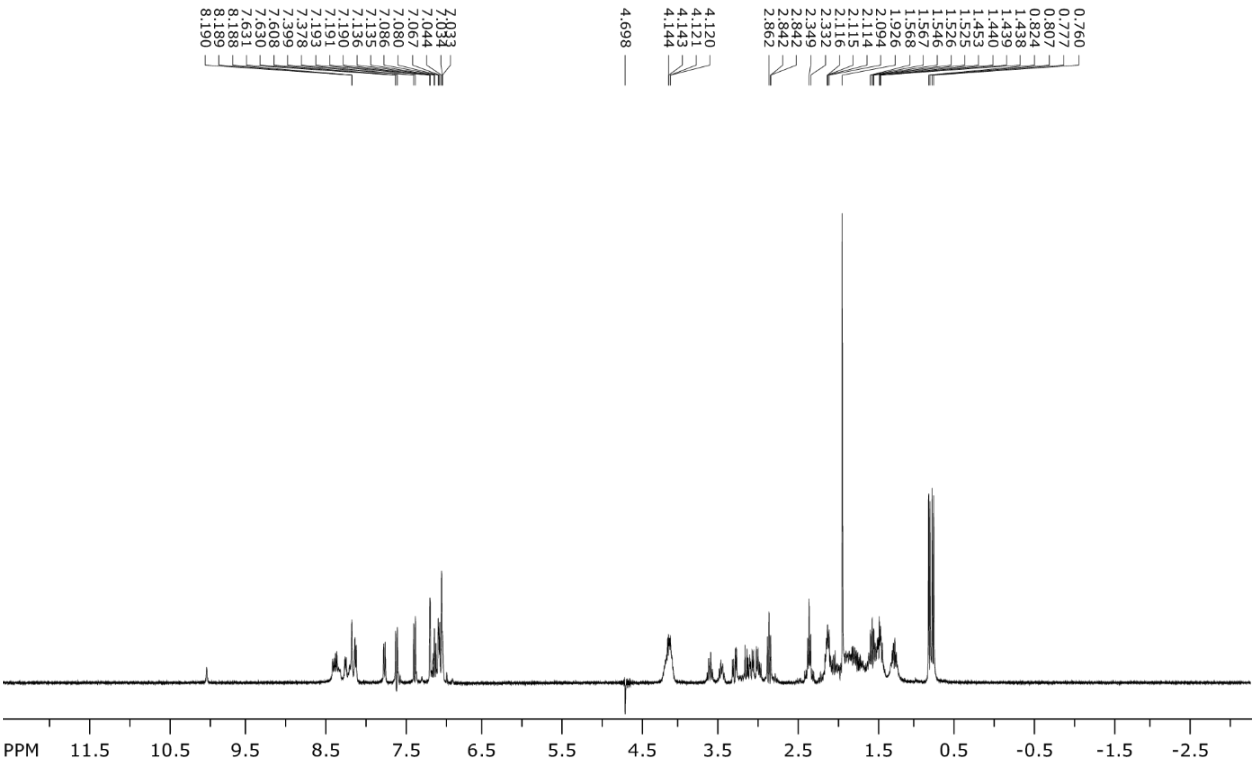

Figure 31. ^{1}H NMR of PK9-H peptide with solvent suppression using 1D excitation sculpting and W5.

A TOCSY experiment identifies signals that are from within the same spin system as its methodology allows for the spin to be transferred to atoms that are not necessarily spin coupled to one another. The 2D TOCSY is the first experiment in a suite of 2D experiments used for

protein structure determination; it allows for assignment of each signal to a specific amino acid. However, it does not necessarily identify connections between amino acids within the peptide. The 2D ^{1}H-^{1}H TOCSY of PK9-H is shown in **Figure 32**. Solvent suppression of the water peak at approximately 4.8 ppm was achieved through gradient enhancement with excitation sculpting (ES) and an MLEV-17 element. Gradient enhanced NMR are collected without phase cycling, which allows for resonances near the targeted solvent peak to be measured. MLEV-17 is a composite pulse that allows for broadband decoupling and the subsequent transfer of spin between connected atoms within the spin system. ES achieves solvent suppression using water-selective pulses.

The TOCSY spectrum in **Figure 32** shows nearly complete elimination of the water signal at 4.8 ppm and a good signal to noise ratio. However, not many cross peaks are apparent in the spectrum, especially between the amide region and the side-chain region (shown in red), so the experiment needs to be further optimized before any proper spectral assignments can be made. This issue could likely be resolved by increasing mixing times, which would allow for the magnetization to be transferred further through the spin system.

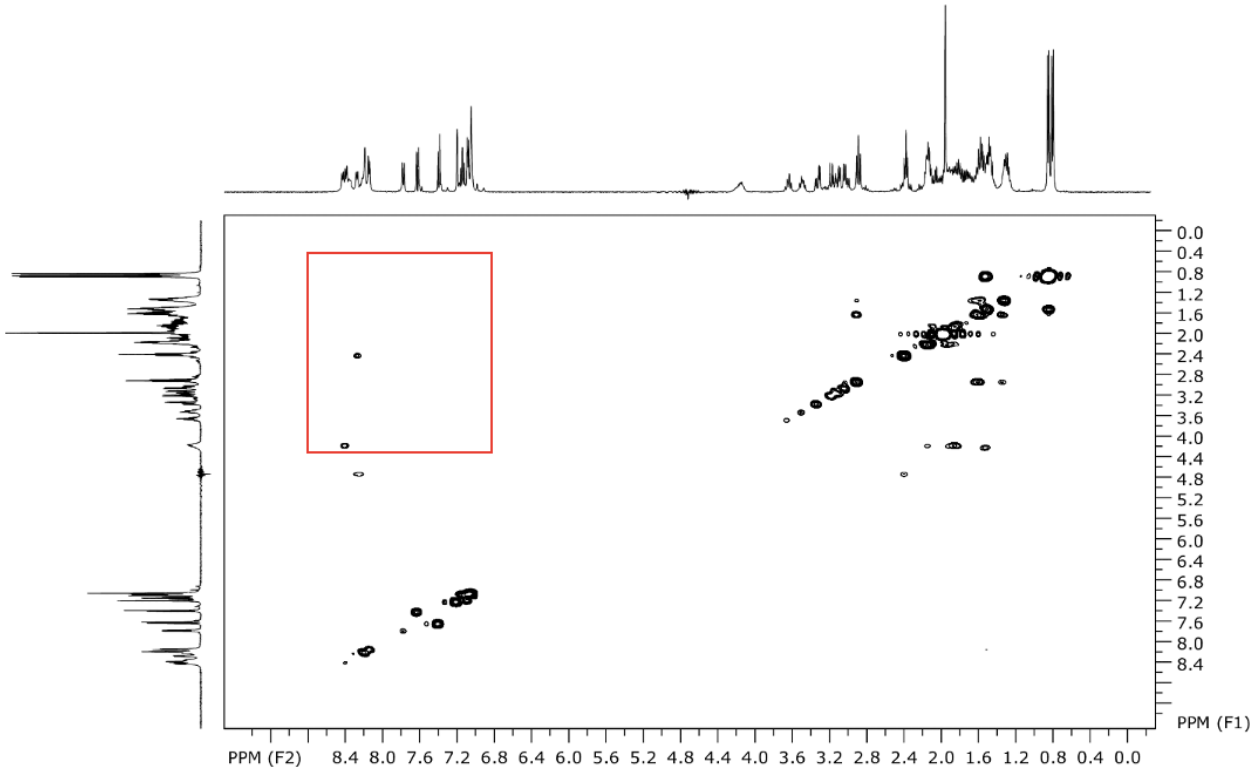

Figure 32. ge-2D ^{1}H-^{1}H TOCSY of PK9-H using excitation sculpting with MLEV-17 and ES element.

Chapter 4: Conclusions & Future Directions

The goal of this research was to evaluate whether the quadrupolar nucleus of ^{67}Zn could induce measurable changes in the ^{1}H and ^{13}C NMR spectra of various model systems – EDTA, Gly, and PK9-H. NMR spectra were analyzed for changes in ^{13}C T_1 values, the introduction of new splitting patterns or broadening of the ^{1}H and ^{13}C signals upon ^{67}Zn binding.

Zn^{2+} is an essential metal that plays a role in the cellular processes of the metabolism of DNA and RNA, gene expression, and the regulation of apoptosis.[4] Found in all three biological domains of life and the second most abundant metal in the human body, there are numerous ZBPs that serve various functions thanks to the coordination flexibility and resistance to redox reactions that zinc offers.[1-3] Its role as an intermediate Lewis acid allows it to form more covalent interactions with nitrogen, sulfur, and oxygen atoms, all of which are key coordinating atoms in the amino acids of proteins.[4,8] Although its 2+ oxidation state gives Zn^{2+} filled d-orbitals causing it to be spectroscopically silent, eliminating the use of spectroscopic methods that rely on d-to-d transitions like UV/Vis absorption spectroscopy.[9] As a result, researchers use various other methodologies like x-ray crystallography, NMR chemical shift monitoring, and amino acid substitutions analyzed by other methods like fluorescence spectroscopy. However, these have their own hindrances.

Irregular, unstructured, or large proteins can be difficult to crystallize oftentimes due to solubility issues or the abnormal structural features preventing the growth of the uniform crystals that are needed for analysis. Proteins that lack a stable secondary structure or have a high degree of homogeneity in their sequence can be difficult to study using NMR methodologies due to signal overlapping.[14] The use of amino acid substitutions can be a laborious process, and all the methodologies described to not provide site-specific binding information for Zn^{2+} creating a need

for other methodologies that yield more particular information about Zn^{2+} binding interactions with proteins.

NMR studies of EDTA established that ^{13}C T1 values obtained using area or intensity measurements had no statistical difference despite the higher standard deviation associated with the area fits. Since there was a larger spread in the area measurements and the potential for a baseline shift to further alter area measurements, intensity data fits were determined to be a better reflection of the T_1 values. A comparison of oxygenated and deoxygenated samples established that there was no statistical significance in measured values, and as a result future samples were not deoxygenated. Zn^{2+} binding to EDTA caused chemical shifts to move downfield and caused T_1 values of the ^{13}C nuclei to decrease. The introduction of $^{67}Zn^{2+}$ did result in faster T_1 times than the Zn^{2+} free sample of EDTA, but it did not cause a change in chemical shift or T_1 values in comparison to non-isotopically enriched Zn^{2+}. No irregular splitting patterns were seen as a result of $^{67}Zn^{2+}$ in either the ^{1}H or ^{13}C spectra compared to Zn^{2+}, but both Zn^{2+} and $^{67}Zn^{2+}$ did cause the protons on the lateral carbon to undergo non first order splitting induced by their steric hindrance upon Zn^{2+} binding.

The ^{13}C NMR of Gly showed two signals – carboxyl and alpha. Zn^{2+} binding caused the alpha signal to decrease in intensity and the carboxyl signal disappeared entirely. This is likely due to the presence of various species in solution that are exchanging on a time scale that is fast relative to the NMR. The remaining alpha signal did see a decrease in the T_1 value upon Zn^{2+} binding, which is consistent with the EDTA data. However, this was deemed an unsuitable system for the purpose of these studies.

PK9-H was successfully synthesized using Fmoc solid phase synthesis methods and purified using reverse phase HPLC. Synthesis was confirmed by the presence of a base peak at

an *m/z* of 1093.3683 in the ESI-MS spectrum. Despite previous NMR research that suggested that Zn^{2+} could bind to PK9-H, fluorescence and CD studies showed no evidence of a binding interaction with Zn^{2+}. A ^{13}C spectrum was recorded and solvent suppression was achieved in both the 1D and 2D ^{1}H NMR experiments.

Traditionally a 1D selective TOCSY (total correlation spectroscopy) experiment is used with small and medium-sized molecules to determine ^{1}H-^{1}H connections via scalar coupling.[24] Protons within the same coupling network are connected via J-couplings, which can allow magnetization to be transferred between the atoms yielding a 1-D spectra of all connected protons from that spin system.[24] This research investigated the feasibility and practicality of a heteronuclear 1D TOCSY utilizing quadrupolar $^{67}Zn^{2+}$ to investigate coordinating ligands. This has the potential to be particularly helpful for larger proteins and biomolecules that often contain overlapping signals as it would only identify spin-coupled atoms through magnetization transfer that occurs during the spin lock portion of the pulse sequence, shown in **Figure 33**. However, there was little evidence supporting a J-coupling between $^{67}Zn^{2+}$ and the nearby carbon and hydrogen atoms in EDTA. To perform the heteronuclear TOCSY described here, a specialized NMR probe would be needed, and a new pulse sequence would need to be created and optimized as this would be a novel experiment. ^{67}Zn NMR experiments require different radiofrequencies than those associated with ^{1}H and ^{13}C NMR and there is no pulse sequence currently available for a selective 1D TOCSY that irradiates ^{67}Zn and allows magnetization to transfer to nearby ^{13}C atoms and be detected. The cost and time commitment, along with insufficient evidence of a J-coupling between $^{67}Zn^{2+}$ and nearby spin active nuclei, suggest that it is likely not worthwhile to pursue this further.

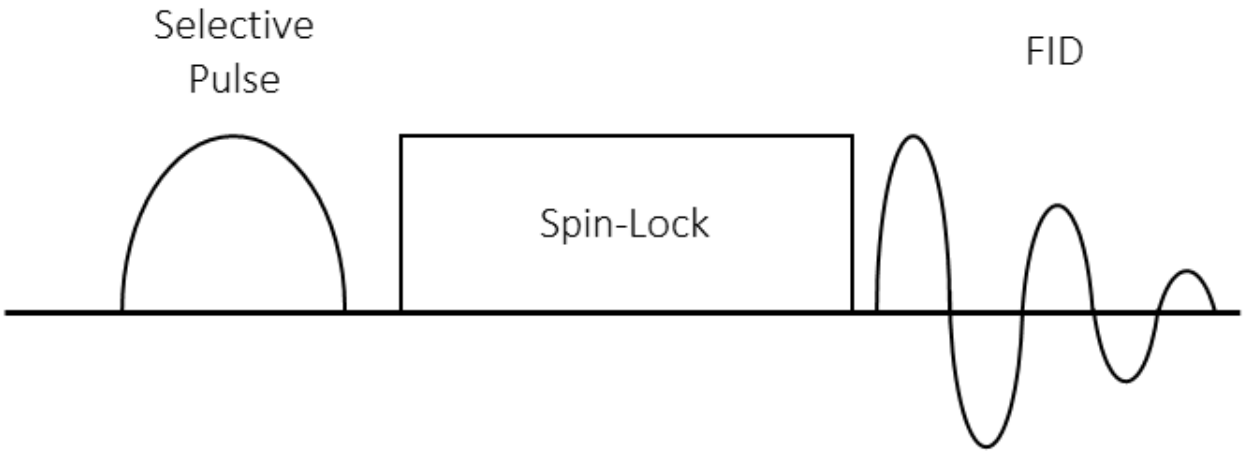

Figure 33. 1D Selective TOCSY pulse sequence.

References

1. Andreini, C.; Banci, L.; Bertini, I.; Rosato, A. Zinc through the Three Domains of Life. *J. Proteome Res.* **2006***, 5*, 3173-3178.

2. Maret, W. Zinc Biochemistry: From a Single Zinc Enzyme to a Key Element of Life12. *Advances in Nutrition* **2013***, 4*, 82-91.

3. Berg, J. M.; Shi, Y. The Galvanization of Biology: A Growing Appreciation for the Roles of Zinc. *Science* **1996***, 271*, 1081-1085.

4. Vallee, B. L.; Auld, D. S. Functional zinc-binding motifs in enzymes and DNA-binding proteins. *Faraday Discuss.* **1992***, 93*, 47-65.

5. Roohani, N.; Hurrell, R.; Kelishadi, R.; Schulin, R. Zinc and its importance for human health: An integrative review. *J Res Med Sci* **2013***, 18*, 144-157.

6. Emsley, J. *Nature's Building Blocks: An A-Z Guide to the Elements;* Oxford University Press: Oxford, 2003; .

7. Cowan, J. A. Fundamentals of Inorganic Biochemistry. In *Inorganic Biochemistry An Introduction*Wiley-VCH: 1997; pp 1-64.

8. Laitaoja, M.; Valjakka, J.; Jänis, J. Zinc Coordination Spheres in Protein Structures. *Inorg. Chem.* **2013***, 52*, 10983-10991.

9. Penner-Hahn, J. E. Characterization of “spectroscopically quiet” metals in biology. *Coordination Chemistry Reviews* **2005***, 249*, 161-177.

10. Smyth, M. S.; Martin, J. H. J. x Ray crystallography. *Mol Pathol* **2000***, 53*, 8-14.

11. Katti, S.; Her, B.; Srivastava, A. K.; Taylor, A. B.; Lockless, S. W.; Igumenova, T. I. High affinity interactions of Pb2+ with Synaptotagmin I. *Metallomics* **2018***, 10*, 1211-1222.

12. Sanders, T.; Liu, Y.; Buchner, V.; Tchounwou, P. B. Neurotoxic effects and biomarkers of lead exposure: a review. *Rev Environ Health* **2009***, 24*, 15-45.

13. Samara, P.; Ioannou, K.; Tsitsilonis, O. E. Prothymosin Alpha and Immune Responses. *Vitam Horm* **2016***, 102*, 179-207.

14. Yi, S.; Boys, B. L.; Brickenden, A.; Konermann, L.; Choy, W. Effects of Zinc Binding on the Structure and Dynamics of the Intrinsically Disordered Protein Prothymosin α: Evidence for Metalation as an Entropic Switch. *Biochemistry* **2007***, 46*, 13120-13130.

15. Reed, R.; Holmes, D.; Weyers, J.; Jones, A. Genetics. In *Practical Skills in Biomolecular Sciences*2003; pp 409-449.

16. Varadarajan, R.; Nagarajaram, H. A.; Ramakrishnan, C. A procedure for the prediction of temperature-sensitive mutants of a globular protein based solely on the amino acid?sequence. *PNAS* **1996***, 93*, 13908-13913.

17. Sacco, C.; Skowronsky, R.; Gade, S.; Kenney, J.; Spuches, A. Calorimetric investigation of copper(II) binding to Ab peptides:
thermodynamics of coordination plasticity. *JBIC Journal of Biological Inorganic Chemistry* **2012**, 531-541.

18. Macomber, R. S. Magnetic Properties of Nuclei. In *A Complete Introduction to Modern NMR Spectroscopy*John Wiley & Sons, Inc: 1998; .

19. Friebolin, H. The Physical Basis of NMR Spectroscopy. In *Basic One- and Two-Dimensional NMR Spectroscopy*Wiley-VCH: 2011; pp 1-42.

20. Harris, R. K.; Becker, E. D.; Cabral de Menezes, Sonia M; Goodfellow, R.; Granger, P. NMR Nomenclature: Nuclear Spin Properties and Conventions for Chemical Shifts: IUPAC Recommendations 2001. *Solid State Nuclear Magnetic Resonance* **2002***, 22*, 458-483.

21. Cowan, J. A. Experimental Methods. In *Inorganic Chemistry An Introduction*VHC Wiley: 1997; pp 65-132.

22. Maciel, G. E.; Simeral, L.; Ackerman, J. J. H. Effect of complexation of zinc(II) on zinc-67 chemical shifts. *J. Phys. Chem.* **1977***, 81*, 263-267.

23. Epperlein, B.; Krueger, H.; Lutz, O.; Schwenk, A. Fourier transform nuclear magnetic resonance studies of 67Zn. *Zeitschrift für Naturforschung A* **1974***, 29*, 1553-1557.

24. Friebolin, H. One-Dimensional NMR Experiments Using Complex Pulse Sequences. In *Basic One- and Two-Dimensional NMR Spectroscopy*Wiley-VHC: 2011; pp 187-238.

25. Friebolin, H. Relaxation. In *Basic One- and Two-Dimensional NMR Spectroscopy*2011; pp 167-185.

26. Balci, M. Absorption and Resonance. In *Basic 1H- and 13C-NMR Spectroscopy*Elsevier Science & Technology: 2005; pp 241-252.

27. Besecker, C. J.; Klemperer, W. G.; Maltbie, D. J.; Wright, D. A. Oxygen-17 nuclear magnetic resonance spectroscopy of polyoxometalates. 2. Heteronuclear decoupling of quadrupolar nuclei. *Inorg. Chem.* **1985***, 24*, 1027-1032.

28. wu, G.; Kroeker, S.; Wasylishen, R. Multinuclear NMR Study of Dipotassium Tetracyanometalates of the Group 12 Metals in the Solid State . *Inorganic Chemistry* **1995***, 34*, 1595-1598.

29. Bruker Avance 1D and 2D Course. **2003**, 1-208.

30. Garapati, S.; Burns, C. S.; Rodriguez, A. A. Field- and Temperature-Dependent 13C NMR Studies of the EDTA–Zn2+ Complex: Insight into Structure and Dynamics via Relaxation Measurements. *J. Phys. Chem. B* **2014***, 118*, 12960-12964.

31. Schmidt, K.; Wolfe, D. M.; Stiller, B.; Pearce, D. A. Cd2+, Mn2+, Ni2+ and Se2+ toxicity to Saccharomyces cerevisiae lacking YPK9p the orthologue of human ATP13A2. *Biochem Biophys Res Commun* **2009***, 383*, 198-202.

32. Kong, S. M. Y.; Chan, B. K. K.; Park, J.; Hill, K. J.; Aitken, J. B.; Cottle, L.; Farghaian, H.; Cole, A. R.; Lay, P. A.; Sue, C. M.; Cooper, A. A. Parkinson's disease-linked human PARK9/ATP13A2 maintains zinc homeostasis and promotes α-Synuclein externalization via exosomes. *Human Molecular Genetics* **2014***, 23*, 2816-2833.

33. Peana, M. F.; Medici, S.; Ledda, A.; Nurchi, V. M.; Zoroddu, M. A. Interaction of Cu(II) and Ni(II) with Ypk9 Protein Fragment via NMR Studies. *ScientificWorldJournal* **2014***, 2014*.

34. Medici, S.; Peana, M.; Gemma Delogu, L.; Antonietta Zoroddu, M. Mn(II) and Zn(II) interactions with peptide fragments from Parkinson's disease genes. *Dalton Transactions* **2012***, 41*, 4378-4388.

35. Remelli, M.; Peana, M.; Medici, S.; Delogu, L. G.; Zoroddu, M. A. Interaction of divalent cations with peptide fragments from Parkinson's disease genes. *Dalton Trans* **2013***, 42*, 5964-5974.

36. Remelli, M.; Peana, M.; Medici, S.; Ostrowska, M.; Gumienna-Kontecka, E.; Zoroddu, M. A. Manganism and Parkinson's disease: Mn(II) and Zn(II) interaction with a 30-amino acid fragment. *Dalton Trans.* **2016***, 45*, 5151-5161.

37. Edelhoch, H. Spectroscopic Determination of Tryptophan and Tyrosine in Proteins. *Biochemistry* **1967***, 6*, 1948-1954.

38. Garapati, S. R. Investigation of the Zinc binding region of Prothymosin-alpha: A spectroscopic and thermodynamic approach to study metal binding in Intrinsically disordered proteins, East Carolina University, 2014.

39. Moore, J. H.; Spencer, N. D. Nuclear Spin Relaxation in Liquids: Theory, Experiments, and Applications. *J. Am. Chem. Soc.* **2006***, 128*, 10630-10631.

40. Crews, P.; Rodríguez, J.; Jaspars, M. *Organic Structure Analysis;* 2009; .

41. Friebolin, H. NMR Spectroscopy and Biochemistry. In *Basic One- and Two-Dimensional NMR Spectroscopy*Wiley-VCH: 2011; pp 355-374.

Appendix A: Fitting Data of EDTA Solutions

The fitting statistics, including the T_1 values obtained through intensity fit and area fit, I[0], A, residual sum of squares (RSS), and standard deviations are included below. Data for the apo-EDTA solutions is shown in **Table A1** to **A9**, **Table A10** to **A18** contain data for Zn-EDTA (a), (b), and (c). The statistics for Zn-EDTA (d) are shown in **Table A19** to **A21**. **Table A22** to **24** includes data for ^{67}Zn-EDTA.

Table A1. Fitting Statistics of Carbonyl Peak of apo-EDTA (a)

Run	T_1 value from intensity fit (s)	I[0]	A	RSS	Std. dev.	T_1 value from area fit (s)
1	10.209	1.015E+00	6.052E-01	1.033E-01	2.213E-02	9.790
2	10.347	9.955E-01	6.018E-01	9.680E-02	2.162E-02	10.720
3	9.492	9.888E-01	6.088E-01	1.581E-01	2.791E-02	10.170
Avg.	10.016					10.227
Std. dev.	0.459					0.468

Table A2. Fitting Statistics of Lateral Peak of apo-EDTA (a)

Run	T_1 value from intensity fit (ms)	I[0]	A	RSS	Std. dev.	T_1 value from area fit (ms)
1	482.060	7.647E-01	9.688E-01	2.393E-01	3.106E-02	473.800
2	487.192	7.539E-01	9.505E-01	3.241E-01	3.586E-02	449.900
3	500.408	7.689E-01	9.485E-01	6.868E-01	5.316E-02	480.600
Avg.	489.887					468.100
Std. dev.	9.466					16.124

Table A3. Fitting Statistics of Central Peak of apo-EDTA (a

Run	T_1 value from intensity fit (ms)	I[0]	A	RSS	Std. dev.	T_1 value from area fit (ms)
1	449.209	3.645E-01	8.614E-01	1.071E-01	2.187E-02	372.599
2	436.900	3.571E-01	9.508E-01	2.268E-01	3.182E-02	383.099
3	454.160	3.585E-01	8.894E-01	2.284E-01	3.193E-02	372.000
Avg.	446.756					375.899
Std. dev.	8.888					6.242

Table A4. Fitting Statistics of Carbonyl Peak of apo-EDTA (b)

Run	T_1 value from intensity fit (s)	I[0]	A	RSS	Std. dev.	T_1 value from area fit (s)
1	11.318	1.045E+00	5.921E-01	6.789E-02	1.838E-02	10.790
2	10.114	1.001E+00	6.080E-01	9.608E-02	2.090E-02	9.157
3	9.803	9.826E-01	6.047E-01	1.104E-01	2.272E-02	10.760
Avg.	10.412					10.236
Std. dev.	0.800					0.934

Table A5. Fitting Statistics of Lateral Peak of apo-EDTA (b)

Run	T_1 value from intensity fit (ms)	I[0]	A	RSS	Std. dev.	T_1 value from area fit (ms)
1	560.012	6.997E-01	8.804E-01	4.155E-01	4.127E-02	468.500
2	521.579	7.595E-01	9.079E-01	4.664E-01	4.294E-02	474.300
3	500.316	7.392E-01	9.408E-01	1.824E-01	2.701E-02	469.400
Avg.	527.302					470.733
Std. dev.	30.257					3.121

Table A6. Fitting Statistics of Central Peak of apo-EDTA (b)

Run	T_1 value from intensity fit (ms)	I[0]	A	RSS	Std. dev.	T_1 value from area fit (ms)
1	423.986	3.282E-01	9.624E-01	1.472E-01	2.563E-02	389.400
2	405.082	3.621E-01	9.832E-01	6.861E-02	1.750E-02	400.799
3	381.027	3.492E-01	1.162E+00	2.198E-01	3.133E-02	452.599
Avg.	403.365					414.266
Std. dev.	21.531					33.683

Table A7. Fitting Statistics of Carbonyl Peak of apo-EDTA (c)

Run	T_1 value from intensity fit (s)	I[0]	A	RSS	Std. dev.	T_1 value from area fit (s)
1	9.870	9.654E-01	6.093E-01	1.256E-01	2.390E-02	9.424
2	9.304	9.656E-01	6.122E-01	1.265E-01	2.403E-02	9.944
3	8.302	9.791E-01	6.304E-01	7.000E-02	1.768E-02	9.921
Avg.	9.159					9.763
Std. dev.	0.794					0.294

Table A8. Fitting Statistics of Lateral Peak of apo-EDTA (c)

Run	T_1 value from intensity fit (ms)	I[0]	A	RSS	Std. dev.	T_1 value from area fit (ms)
1	533.100	7.326E-01	9.335E-01	9.993E-01	6.260E-02	530.200
2	513.270	7.262E-01	9.377E-01	3.392E-01	3.919E-02	532.699
3	498.189	8.346E-01	9.650E-01	1.467E-01	2.394E-02	541.800
Avg.	514.853					534.900
Std. dev.	17.509					6.105

Table A9. Fitting Statistics of Central Peak of apo-EDTA (c)

Run	T_1 value from intensity fit (ms)	I[0]	A	RSS	Std. dev.	T_1 value from area fit (ms)
1	577.694	3.520E-01	7.005E-01	2.708E-01	3.477E-02	454.600
2	429.827	3.423E-01	1.095E+00	3.374E-01	3.881E-02	510.499
3	466.618	4.031E-01	8.814E-01	7.515E-02	1.832E-02	435.400
Avg.	491.380					466.833
Std. dev.	76.981					39.015

Table A10. Fitting Statistics of Carbonyl Peak of Zn-EDTA (a)

Run	T_1 value from intensity fit (s)	I[0]	A	RSS	Std. dev.	T_1 value from area fit (s)
1	7.949	9.895E-01	6.256E-01	6.885E-02	1.790E-02	8.192
2	7.774	1.002E+00	6.295E-01	7.074E-02	1.810E-02	7.370
3	7.619	9.859E-01	6.319E-01	9.043E-02	2.032E-02	7.539
Avg.	7.781					7.700
Std. dev.	0.165					0.434

Table A11. Fitting Statistics of Lateral Peak of Zn-EDTA (a)

Run	T_1 value from intensity fit (ms)	I[0]	A	RSS	Std. dev.	T_1 value from area fit (ms)
1	398.372	5.591E-01	9.687E-01	9.191E-02	2.026E-02	430.000
2	403.132	5.811E-01	9.509E-01	8.505E-02	1.949E-02	424.300
3	378.349	5.870E-01	1.084E+00	2.661E-01	3.447E-02	395.400
Avg.	393.284					416.567
Std. dev.	13.152					18.551

Table A12. Fitting Statistics of Central Peak of Zn-EDTA (a)

Run	T_1 value from intensity fit (ms)	I[0]	A	RSS	Std. dev.	T_1 value from area fit (ms)
1	337.761	3.422E-01	1.026E+00	6.714E-02	1.731E-02	348.700
2	314.359	3.566E-01	1.217E+00	7.368E-02	1.814E-02	351.500
3	308.819	3.613E-01	1.317E+00	1.745E-01	2.791E-02	386.599
Avg.	320.313					362.266
Std. dev.	15.362					21.119

Table A13. Fitting Statistics of Carbonyl Peak of Zn-EDTA (b)

Run	T_1 value from intensity fit (s)	I[0]	A	RSS	Std. dev.	T_1 value from area fit (s)
1	6.848	9.636E-01	6.459E-01	9.932E-02	2.134E-02	8.142
2	7.971	9.991E-01	6.296E-01	9.717E-02	2.141E-02	7.889
3	7.756	9.999E-01	6.310E-01	9.045E-02	2.116E-02	9.008
Avg.	7.525					8.346
Std. dev.	0.596					0.587

Table A14. Fitting Statistics of Lateral Peak of Zn-EDTA (b)

Run	T_1 value from intensity fit (ms)	I[0]	A	RSS	Std. dev.	T_1 value from area fit (ms)
1	400.158	6.136E-01	9.902E-01	8.943E-02	1.998E-02	401.700
2	423.921	5.352E-01	9.555E-01	2.435E-01	3.297E-02	418.900
3	453.880	5.292E-01	8.320E-01	7.632E-02	1.846E-02	404.300
Avg.	425.986					408.300
Std. dev.	26.920					9.271

Table A15. Fitting Statistics of Central Peak of Zn-EDTA (b)

Run	T_1 value from intensity fit (ms)	I[0]	A	RSS	Std. dev.	T_1 value from area fit (ms)
1	348.014	3.784E-01	1.061E+00	9.054E-02	2.010E-02	360.000
2	414.883	3.286E-01	8.175E-01	7.753E-02	1.860E-02	413.300
3	334.349	3.212E-01	1.135E+00	2.048E-01	3.024E-02	396.500
Avg.	365.749					389.933
Std. dev.	43.097					27.250

Table A16. Fitting Statistics of Carbonyl Peak of Zn-EDTA (c)

Run	T_1 value from intensity fit (s)	I[0]	A	RSS	Std. dev.	T_1 value from area fit (s)
1	7.993	9.961E-01	6.295E-01	8.002E-02	1.934E-02	7.676
2	7.819	9.913E-01	6.299E-01	6.967E-02	1.800E-02	7.999
3	8.671	9.960E-01	6.201E-01	6.890E-02	1.816E-02	7.800
Avg.	8.161					7.825
Std. dev.	0.450					0.163

Table A17. Fitting Statistics of Lateral Peak of Zn-EDTA (c)

Run	T_1 value from intensity fit (ms)	I[0]	A	RSS	Std. dev.	T_1 value from area fit (ms)
1	398.382	5.868E-01	9.526E-01	8.524E-02	1.951E-02	401.700
2	382.637	5.728E-01	1.036E+00	7.538E-02	1.834E-02	398.299
3	433.271	5.525E-01	8.843E-01	9.380E-02	2.046E-02	415.700
Avg.	404.763					405.233
Std. dev.	25.913					9.223

Table A18. Fitting Statistics of Central Peak of Zn-EDTA (c)

Run	T_1 value from intensity fit (ms)	I[0]	A	RSS	Std. dev.	T_1 value from area fit (ms)
1	351.355	3.576E-01	9.855E-01	8.967E-02	2.001E-02	426.400
2	392.070	3.512E-01	8.385E-01	7.477E-02	1.827E-02	372.300
3	417.291	3.365E-01	7.950E-01	7.217E-02	1.795E-02	364.500
Avg.	386.905					387.733
Std. dev.	33.270					33.713

Table A19. Fitting Statistics of Carbonyl Peak of Zn-EDTA (d)

Run	T_1 value from intensity fit (s)	I[0]	A	RSS	Std. dev.	Area measurement (s)
1	7.322	9.596E-01	6.321E-01	1.191E-01	2.365E-02	8.096
2	8.501	9.960E-01	6.220E-01	1.045E-01	2.204E-02	8.026
3	8.527	9.809E-01	6.214E-01	1.036E-01	2.242E-02	8.141
Avg.	8.117					8.088
Std. dev.	0.688					0.058

Table A20. Fitting Statistics of Lateral Peak of Zn-EDTA (d)

Run	T_1 value from intensity fit (ms)	I[0]	A	RSS	Std. dev.	T_1 value from area fit (ms)
1	436.322	6.450E-01	8.612E-01	8.626E-02	1.962E-02	449.000
2	441.929	6.440E-01	8.781E-01	7.789E-02	1.865E-02	438.900
3	428.962	6.533E-01	9.596E-01	2.782E-01	3.524E-02	438.500
Avg.	435.738					442.133
Std. dev.	6.503					5.950

Table A21. Fitting Statistics of Central Peak of Zn-EDTA (d)

Run	T_1 value from intensity fit (ms)	I[0]	A	RSS	Std. dev.	T_1 value from area fit (ms)
1	442.613	3.890E-01	7.370E-01	8.509E-02	1.949E-02	376.000
2	399.732	3.861E-01	8.796E-01	8.479E-02	1.946E-02	457.700
3	368.082	3.900E-01	1.014E+00	8.350E-02	1.931E-02	383.400
Avg.	403.476					405.700
Std. dev.	37.406					45.185

Table A22. Fitting Statistics of Carbonyl Peak of ^{67}Zn-EDTA (e)

Run	T_1 value from intensity fit (s)	I[0]	A	RSS	Std. dev.	T_1 value from area fit (s)
1	9.128	1.003E+00	6.146E-01	6.261E-02	1.727E-02	8.062
2	8.300	9.839E-01	6.250E-01	8.865E-02	2.007E-02	8.515
3	8.012	9.581E-01	6.242E-01	9.999E-02	2.142E-02	8.218
Avg.	8.480					8.265
Std. dev.	0.579					0.230

Table A23. Fitting Statistics of Lateral Peak of ^{67}Zn-EDTA (e)

Run	T_1 value from intensity fit (ms)	I[0]	A	RSS	Std. dev.	T_1 value from area fit (ms)
1	396.218	6.087E-01	1.023E+00	9.076E-02	2.013E-02	436.000
2	457.606	6.166E-01	8.614E-01	7.064E-02	1.776E-02	480.300
3	508.672	6.297E-01	7.721E-01	8.374E-01	6.114E-02	427.900
Avg.	454.165					448.067
Std. dev.	56.306					28.207

Table A24. Fitting Statistics of Central Peak of ^{67}Zn-EDTA (e)

Run	T_1 value from intensity fit (ms)	I[0]	A	RSS	Std. dev.	T_1 value from area fit (ms)
1	472.426	3.533E-01	7.260E-01	7.834E-02	1.870E-02	454.099
2	352.289	3.619E-01	1.069E+00	6.178E-02	1.661E-02	430.400
3	361.154	3.705E-01	1.003E+00	7.198E-02	1.793E-02	393.799
Avg.	395.290					426.099
Std. dev.	66.949					30.379

Appendix B: Averages, Standard Deviations, and P-Values of EDTA Solutions

A comparison of the T_1 values from intensity fit of the carbonyl, lateral, and central peaks of apo-EDTA (a) and (b) are shown in **Table B1** through **B3**. The comparison using area fit are shown in **Table B4** through **B6**. The results of the student's t tests of apo-EDTA (a) and (b) are summarized in **Table B7**.

Table B1. T_1 Values from Intensity Fit of Carbonyl Peak of apo-EDTA (a) and (b)

Run	apo-EDTA (a) (s)	apo-EDTA (b) (s)
1	10.210	11.320
2	10.350	10.110
3	9.492	9.803
Average	10.017	10.411
Standard deviation	0.460	0.802

Table B2. T_1 Values from Intensity Fit of Lateral Peak of apo-EDTA (a) and (b)

Run	apo-EDTA (a) (ms)	apo-EDTA (b) (ms)
1	482.099	560.000
2	487.200	521.599
3	500.399	500.299
Average	489.899	527.299
Standard deviation	9.444	30.256

Table B3. T_1 Values from Intensity Fit of Central Peak of apo-EDTA (a) and (b)

Run	apo-EDTA (a) (ms)	apo-EDTA (b) (ms)
1	449.200	424.000
2	436.900	405.100
3	454.200	381.000
Average	446.767	403.367
Standard deviation	8.903	12.443

Table B4. T_1 Values from Area Fit of Carbonyl Peak of apo-EDTA (a) and (b)

Run	apo-EDTA (a) (s)	apo-EDTA (b) (s)
1	9.790	10.790
2	10.720	9.157
3	10.170	10.760
Average	10.227	10.236
Standard deviation	0.468	0.934

Table B5. T_1 Values from Area Fit of Lateral Peak of apo-EDTA (a) and (b)

Run	apo-EDTA (a) (ms)	apo-EDTA (b) (ms)
1	473.800	468.500
2	449.900	474.300
3	480.600	469.400
Average	468.100	470.733
Standard deviation	16.124	3.121

Table B6. T_1 Values from Area Fit of Central Peak of apo-EDTA (a) and (b)

Run	apo-EDTA (a) (ms)	apo-EDTA (b) (ms)
1	372.599	389.400
2	383.099	400.799
3	372.000	452.599
Average	375.899	414.266
Standard deviation	6.242	33.683

Table B7. P-values of Comparison of Deoxygenated apo-EDTA Solutions (a) & (b)

Peak	Two-Tailed P Value for Intensity	Two-Tailed P Value for Area
1 (175 ppm)	0.5018	0.9888
2 (57 ppm)	0.1105	0.7950
3 (51 ppm)	0.0322	0.1244

A comparison of the T_1 values from intensity and area fits of the carbonyl peak of apo-EDTA is shown in **Table B8**. The measurements surrounding the lateral peak are shown in **Table B9**. Central peak T_1 measurements are shown in **Table B10**. The results of student's tests of intensity and area fits of apo-EDTA are shown in **Table B11**.

Table B8. T_1 Values of Area and Intensity Fits of Carbonyl Peak of apo-EDTA (a) & (b)

Run	Intensity (s)	Area (s)
1	10.210	9.790
2	10.350	10.720
3	9.492	10.170
4	11.320	10.790
5	10.110	9.157
6	9.803	10.760
Average	10.214	10.231
Standard deviation	0.623	0.661

Table B9. T_1 Values of Area and Intensity Fits of Lateral Peak of apo-EDTA (a) & (b)

Run	Intensity (ms)	Area (ms)
1	482.099	473.800
2	487.200	449.900
3	500.399	480.600
4	560.000	468.500
5	521.599	474.300
6	500.299	469.400
Average	508.599	469.417
Standard deviation	28.661	10.487

Table B10. T_1 Values of Area and Intensity Fits of Central Peak of apo-EDTA (a) & (b)

Run	Intensity (ms)	Area (ms)
1	449.200	372.599
2	436.900	383.099
3	454.200	372.000
4	424.000	389.400
5	405.100	400.799
6	381.000	452.599
Average	425.067	395.083
Standard deviation	27.975	30.183

Table B11. P-values of Comparison of Area and Intensity Fits of apo-EDTA (a) and (b)

Peak	Two-Tailed P Value
1 (175 ppm)	0.9643
2 (57 ppm)	0.0104
3 (51 ppm)	0.1046

A comparison of the T_1 values from the intensity fit of the carbonyl, lateral, and central peaks of the deoxygenated and oxygenated apo-EDTA solutions are shown in **Table B12** to **B14**. Those associated with the area fits are shown in **Table B15** to **B17**. The P-values from student's t test are summarized in **Table B18**.

Table B12. T_1 Values of Intensity Fit of Carbonyl Peak of Deoxygenated apo-EDTA (a) and (b) with Oxygenated apo-EDTA (c)

Run	Deoxygenated (s)	Oxygenated (s)
1	10.210	9.870
2	10.350	9.305
3	9.492	8.302
4	11.320	
5	10.110	
6	9.803	
Average	10.214	9.159
Standard deviation	0.623	0.794

Table B13. T_1 Values of Intensity Fit of Lateral Peak of Deoxygenated apo-EDTA (a) and (b) with Oxygenated apo-EDTA (c)

Run	Deoxygenated (ms)	Oxygenated (ms)
1	482.099	533.100
2	487.200	513.199
3	500.399	498.200
4	560.000	
5	521.599	
6	500.299	
Average	508.599	514.833
Standard deviation	28.661	17.507

Table B14. T_1 Values of Intensity Fit of Central Peak of Deoxygenated apo-EDTA (a) and (b) with Oxygenated apo-EDTA (c)

Run	Deoxygenated (ms)	Oxygenated (ms)
1	449.200	577.699
2	436.900	429.800
3	454.200	466.600
4	424.000	
5	405.100	
6	381.000	
Average	425.067	491.366
Standard deviation	27.975	76.997

Table B15. T_1 Values of Area Fit of Carbonyl Peak of Deoxygenated apo-EDTA (a) and (b) with Oxygenated apo-EDTA (c)

Run	Deoxygenated (s)	Oxygenated (s)
1	9.790	9.424
2	10.720	9.944
3	10.170	9.921
4	10.790	
5	9.1570	
6	10.760	
Average	10.231	9.763
Standard deviation	0.661	0.294

Table B16. T_1 Values of Area Fit of Lateral Peak of Deoxygenated apo-EDTA (a) and (b) with Oxygenated apo-EDTA (c)

Run	Deoxygenated (s)	Oxygenated (s)
1	473.800	530.200
2	449.900	532.699
3	480.600	541.800
4	468.500	
5	474.300	
6	469.400	
Average	469.417	534.900
Standard deviation	10.487	6.105

Table B17. T_1 Values of Area Fit of Central Peak of Deoxygenated apo-EDTA (a) and (b) with Oxygenated apo-EDTA (c)

Run	Deoxygenated (ms)	Oxygenated (ms)
1	372.599	454.600
2	383.099	510.499
3	372.000	435.400
4	389.400	
5	400.799	
6	452.599	
Average	395.083	466.833
Standard deviation	30.183	39.015

Table B18. P-values of Comparison of Deoxygenated apo-EDTA (a) and (b) with Oxygenated apo-EDTA (c)

Peak	Two-Tailed P Value for Intensity	Two-Tailed P Value for Area
1 (175 ppm)	0.0632	0.2913
2 (57 ppm)	0.7442	0.0001
3 (51 ppm)	0.0888	0.0178

A comparison of the T_1 values from the intensity fit of the carbonyl, lateral, and central peaks of the deoxygenated and oxygenated Zn-EDTA solutions are shown in **Table B19** to **B21**. Those associated with the area fits are shown in **Table B22** to **B24**. The P-values from student's t test are summarized in **Table B25**.

Table B19. T_1 Values of Intensity Fit of Carbonyl Peak of Deoxygenated Zn-EDTA (a) and (b) and Oxygenated Zn-EDTA (c)

Run	Deoxygenated (s)	Oxygenated (s)
1	7.949	7.993
2	7.774	7.819
3	7.619	8.671
4	6.848	
5	7.971	
6	7.756	
Average	7.653	8.161
Standard deviation	0.415	0.451

Table B20. T_1 Values of Intensity Fit of Lateral Peak of Deoxygenated Zn-EDTA (a) and (b) and Oxygenated Zn-EDTA (c)

Run	Deoxygenated (ms)	Oxygenated (ms)
1	398.400	398.400
2	403.100	382.599
3	378.400	433.300
4	400.200	
5	423.900	
6	453.900	
Average	409.650	404.766
Standard deviation	26.063	25.943

Table B21. T_1 Values of Intensity Fit of Central Peak of Deoxygenated Zn-EDTA (a) and (b) and Oxygenated Zn-EDTA (c)

Run	Deoxygenated (ms)	Oxygenated (ms)
1	337.799	351.400
2	314.400	392.100
3	308.800	417.300
4	347.999	
5	414.900	
6	334.299	
Average	343.033	386.933
Standard deviation	38.171	33.252

Table B22. T_1 Values of Area Fit of Carbonyl Peak of Deoxygenated Zn-EDTA (a) and (b) and Oxygenated Zn-EDTA (c)

Run	Deoxygenated (s)	Oxygenated (s)
1	8.192	7.676
2	7.370	7.999
3	7.539	7.800
4	8.142	
5	7.889	
6	9.008	
Average	8.023	7.825
Standard deviation	0.582	0.163

Table B23. T_1 Values of Area Fit of Lateral Peak of Deoxygenated Zn-EDTA (a) and (b) and Oxygenated Zn-EDTA (c)

Run	Deoxygenated (ms)	Oxygenated (ms)
1	430.000	401.700
2	424.300	398.299
3	395.400	415.700
4	401.700	
5	418.900	
6	404.300	
Average	412.433	405.233
Standard deviation	13.876	9.223

Table B24. T_1 Values of Intensity Fit of Central Peak of Deoxygenated Zn-EDTA (a) and (b) and Oxygenated Zn-EDTA (c)

Run	Deoxygenated (ms)	Oxygenated (ms)
1	348.700	426.400
2	351.500	372.300
3	386.599	364.500
4	360.000	
5	413.300	
6	396.500	
Average	376.100	387.733
Standard deviation	26.553	33.713

Table B25. P-values for Comparison of Deoxygenated Zn-EDTA (a) and (b) with Oxygenated Zn-EDTA (c)

Peak	Two-Tailed P Value for Intensity	Two-Tailed P Value for Area
1 (175 ppm)	0.1352	0.5918
2 (57 ppm)	0.7984	0.4498
3 (51 ppm)	0.1357	0.5854

A comparison of the T_1 values from the intensity fit of the carbonyl, lateral, and central peaks of the apo-EDTA (a), (b), and (c) with Zn-EDTA (a) and (b) are shown in **Table B26** through **B28**. Those associated with the area fits are shown in **Table B29** to **B31**. Results from student's t test are included in **Table B32**.

Table B26. T_1 Values of Intensity Fit of Carbonyl Peak of apo-EDTA (a), (b), and (c) with Zn-EDTA (a) and (b)

Run	apo-EDTA (s)	Zn-EDTA (s)
1	10.210	7.949
2	10.350	7.774
3	9.492	7.619
4	11.320	6.848
5	10.110	7.971
6	9.803	7.756
7	9.870	
8	9.305	
9	8.302	
Average	9.862	7.653
Standard deviation	0.824	0.415

Table B27. T_1 Values of Intensity Fit of Lateral Peak of apo-EDTA (a), (b), and (c) with Zn-EDTA (a) and (b)

Run	apo-EDTA (ms)	Zn-EDTA (ms)
1	482.099	398.400
2	487.200	403.100
3	500.399	378.400
4	560	400.2
5	521.599	423.9
6	500.299	453.9
7	533.1	
8	513.199	
9	498.2	
Average	510.677	409.650
Standard deviation	24.490	26.063

Table B28. T_1 Values of Intensity Fit of Central Peak of apo-EDTA (a), (b), and (c) with Zn-EDTA (a) and (b)

Run	apo-EDTA (ms)	Zn-EDTA (ms)
1	449.200	337.799
2	436.900	314.400
3	454.200	308.800
4	424.000	347.999
5	405.100	414.900
6	381.000	334.299
7	577.699	
8	429.800	
9	466.600	
Average	447.167	343.033
Standard deviation	55.409	38.171

Table B29. T_1 Values of Area Fit of Carbonyl Peak of apo-EDTA (a), (b), and (c) with Zn-EDTA (a) and (b)

Run	apo-EDTA (s)	Zn-EDTA (s)
1	9.790	8.192
2	10.720	7.370
3	10.170	7.539
4	10.790	8.142
5	9.157	7.889
6	10.760	9.008
7	9.424	
8	9.944	
9	9.921	
Average	10.075	8.023
Standard deviation	0.591	0.582

Table B30. T_1 Values of Area Fit of Lateral Peak of apo-EDTA (a), (b), and (c) with Zn-EDTA (a) and (b)

Run	apo-EDTA (ms)	Zn-EDTA (ms)
1	473.800	430.000
2	449.900	424.300
3	480.600	395.400
4	468.500	401.700
5	474.300	418.900
6	469.400	404.300
7	530.200	
8	532.699	
9	541.800	
Average	491.244	412.433
Standard deviation	33.913	13.876

Table B31. T_1 Values of Area Fit of Central Peak of apo-EDTA (a), (b), and (c) with Zn-EDTA (a) and (b)

Run	apo-EDTA (ms)	Zn-EDTA (ms)
1	372.599	348.700
2	383.099	351.500
3	372.000	386.599
4	389.400	360.000
5	400.799	413.300
6	452.599	396.500
7	454.600	
8	510.499	
9	435.400	
Average	418.999	376.100
Standard deviation	47.296	26.553

Table B32. P-values of Comparison of apo-EDTA (a), (b), & (c) with Zn-EDTA (a) & (b)

Peak	Two-Tailed P Value for Intensity	Two-Tailed P Value for Area
1 (175/178 ppm)	<0.0001	<0.0001
2 (57/61 ppm)	<0.0001	<0.0001
3 (51/56 ppm)	0.0015	0.0662

A comparison of the T_1 values from the intensity fit of the carbonyl, lateral, and central peaks of apo-EDTA (a), (b), and (c) with Zn-EDTA (a), (b), and (c) are shown in **Table B33** to

B35. Those associated with the area fits are shown in **Table B36** to **B38**. The P-values from student's t test are summarized in **Table B39**.

Table B33. T_1 Values of Intensity Fit of Carbonyl Peak of apo-EDTA (a), (b), and (c) with Zn-EDTA (a), (b), and (c)

Run	apo-EDTA (s)	Zn-EDTA (s)
1	10.210	7.949
2	10.350	7.774
3	9.492	7.619
4	11.320	6.848
5	10.110	7.971
6	9.803	7.756
7	9.870	7.993
8	9.305	7.819
9	8.302	8.671
Average	9.862	7.822
Standard deviation	0.824	0.472

Table B34. T_1 Values of Intensity Fit of Lateral Peak of apo-EDTA (a), (b), and (c) with Zn-EDTA (a), (b), and (c)

Run	apo-EDTA (ms)	Zn-EDTA (ms)
1	482.099	398.400
2	487.200	403.100
3	500.399	378.400
4	560.000	400.200
5	521.599	423.900
6	500.299	453.900
7	533.100	398.400
8	513.199	382.599
9	498.200	433.300
Average	510.677	408.022
Standard deviation	24.490	24.470

Table B35. T_1 Values of Intensity Fit of Central Peak of apo-EDTA (a), (b), and (c) with Zn-EDTA (a), (b), and (c)

Run	apo-EDTA (ms)	Zn-EDTA (ms)
1	449.200	337.799
2	436.900	314.400
3	454.200	308.800
4	424.000	347.999
5	405.100	414.900
6	381.000	334.299
7	577.699	351.400
8	429.800	392.100
9	466.600	417.300
Average	447.167	357.666
Standard deviation	55.409	40.852

Table B36. T_1 Values of Area Fit of Carbonyl Peak of apo-EDTA (a), (b), and (c) with Zn-EDTA (a), (b), and (c)

Run	apo-EDTA (s)	Zn-EDTA (s)
1	9.790	8.192
2	10.720	7.370
3	10.170	7.539
4	10.790	8.142
5	9.157	7.889
6	10.760	9.008
7	9.424	7.676
8	9.944	7.999
9	9.921	7.800
Average	10.075	7.957
Standard deviation	0.591	0.477

Table B37. T_1 Values of Area Fit of Lateral Peak of apo-EDTA (a), (b), and (c) with Zn-EDTA (a), (b), and (c)

Run	apo-EDTA (ms)	Zn-EDTA (ms)
1	473.800	430.000
2	449.900	424.300
3	480.600	395.400
4	468.500	401.700
5	474.300	418.900
6	469.400	404.300
7	530.200	401.700
8	532.699	398.299
9	541.800	415.700
Average	491.244	410.033
Standard deviation	33.913	12.432

Table B38. T_1 Values of Area Fit of Central Peak of apo-EDTA (a), (b), and (c) with Zn-EDTA (a), (b), and (c)

Run	apo-EDTA (ms)	Zn-EDTA (ms)
1	372.599	348.700
2	383.099	351.500
3	372.000	386.599
4	389.400	360.000
5	400.799	413.3
6	452.599	396.500
7	454.600	426.400
8	510.499	372.300
9	435.400	364.500
Average	418.999	379.978
Standard deviation	47.296	27.543

Table B39. P-values of Comparison of apo-EDTA (a), (b), & (c) with Zn-EDTA (a), (b), & (c)

Peak	Two-Tailed P Value for Intensity	Two-Tailed P Value for Area
1 (175/178 ppm)	<0.0001	<0.0001
2 (57/61 ppm)	<0.0001	<0.0001
3 (51/56 ppm)	0.0013	0.0482

A comparison of the T_1 values from the intensity fit of the carbonyl, lateral, and central peaks of Zn-EDTA (a) and (b) with Zn-EDTA (d) made with synthesized $ZnCl_2$ are shown in

Table B40 to **B42**. Those associated with the area fits are shown in **Table B43** to **B45**. The P-values from student's t test are summarized in **Table B46**.

Table B40. of T_1 Values of Intensity Fit of Carbonyl Peak of Zn-EDTA (a) and (b) with Zn-EDTA (d) Made with Synthesized $ZnCl_2$

Run	Zn-EDTA (a) & (b) (s)	Zn-EDTA (d) (s)
1	7.949	7.322
2	7.774	8.500
3	7.619	8.527
4	6.848	
5	7.971	
6	7.756	
Average	7.653	8.116
Standard deviation	0.415	0.688

Table B41. T_1 Values of Intensity Fit of Lateral Peak of Zn-EDTA (a) and (b) with Zn-EDTA (d) Made with Synthesized $ZnCl_2$

Run	Zn-EDTA (a) & (b) (ms)	Zn-EDTA (d) (ms)
1	398.400	436.300
2	403.100	441.900
3	378.400	429.000
4	400.200	
5	423.900	
6	453.900	
Average	409.650	435.733
Standard deviation	26.063	6.469

Table B42. T_1 Values of Intensity Fit of Central Peak of Zn-EDTA (a) and (b) with Zn-EDTA (d) Made with Synthesized $ZnCl_2$

Run	Zn-EDTA (a) & (b) (ms)	Zn-EDTA (d) (ms)
1	337.799	442.599
2	314.400	399.700
3	308.800	368.099
4	347.999	
5	414.900	
6	334.299	
Average	343.033	403.466
Standard deviation	38.171	37.393

Table B43. T_1 Values of Area Fit of Carbonyl Peak of Zn-EDTA (a) and (b) with Zn-EDTA (d) Made with Synthesized $ZnCl_2$

Run	Zn-EDTA (a) & (b) (s)	Zn-EDTA (d) (s)
1	8.192	8.096
2	7.370	8.026
3	7.539	8.141
4	8.142	
5	7.889	
6	9.008	
Average	8.023	8.088
Standard deviation	0.582	0.058

Table B44. T_1 Values of Area Fit of Lateral Peak of Zn-EDTA (a) and (b) with Zn-EDTA (d) Made with Synthesized $ZnCl_2$

Run	Zn-EDTA (a) & (b) (ms)	Zn-EDTA (d) (ms)
1	430.000	449.000
2	424.300	438.900
3	395.400	438.500
4	401.700	
5	418.900	
6	404.300	
Average	412.433	442.133
Standard deviation	13.876	5.950

Table B45. T_1 Values of Area Fit of Central Peak of Zn-EDTA (a) and (b) with Zn-EDTA (d) Made with Synthesized $ZnCl_2$

Run	Zn-EDTA (a) & (b) (ms)	Zn-EDTA (d) (ms)
1	348.700	376.000
2	351.500	457.700
3	386.599	383.400
4	360.000	
5	413.300	
6	396.500	
Average	376.100	405.700
Standard deviation	26.553	45.185

Table B46. P-values of Comparison of Zn-EDTA (a) & (b) with Zn-EDTA (d) Made with Synthesized $ZnCl_2$

Peak	Two-Tailed P Value for Intensity	Two-Tailed P Value for Area
1 (178 ppm)	0.2383	0.8587
2 (61 ppm)	0.1420	0.0106
3 (56 ppm)	0.0590	0.2448

A comparison of the T_1 values from the intensity fit of the carbonyl, lateral, and central peaks of Zn-EDTA (a), (b), and (c) with Zn-EDTA (d) made with synthesized $ZnCl_2$ are shown in **Table B47** to **B49**. Those associated with the area fits are shown in **Table B50** to **B52**. The P-values from student's t test are summarized in **Table B53**.

Table B47. T_1 Values of Intensity Fit of Carbonyl Peak of Zn-EDTA (a), (b), and (c) with Zn-EDTA (d) Made with Synthesized $ZnCl_2$

Run	Zn-EDTA (a), (b), & (c) (s)	Zn-EDTA (d) (s)
1	7.949	7.322
2	7.774	8.500
3	7.619	8.527
4	6.848	
5	7.971	
6	7.756	
7	7.993	
8	7.819	
9	8.671	
Average	7.822	8.116
Standard deviation	0.472	0.688

Table B48. T_1 Values of Intensity Fit of Lateral Peak of Zn-EDTA (a), (b), and (c) with Zn-EDTA (d) Made with Synthesized $ZnCl_2$

Run	Zn-EDTA (a), (b), & (c) (ms)	Zn-EDTA (d) (ms)
1	398.400	436.300
2	403.100	441.900
3	378.400	429.000
4	400.200	
5	423.900	
6	453.900	
7	398.400	
8	382.599	
9	433.300	
Average	408.022	435.733
Standard deviation	24.470	6.469

Table B49. T_1 Values of Intensity Fit of Central Peak of Zn-EDTA (a), (b), and (c) with Zn-EDTA (d) Made with Synthesized $ZnCl_2$

Run	Zn-EDTA (a), (b), & (c) (ms)	Zn-EDTA (d) (ms)
1	337.799	442.599
2	314.400	399.700
3	308.800	368.099
4	347.999	
5	414.900	
6	334.299	
7	351.400	
8	392.100	
9	417.300	
Average	357.666	403.466
Standard deviation	40.852	37.393

Table B50. T_1 Values of Area Fit of Carbonyl Peak of Zn-EDTA (a), (b), and (c) with Zn-EDTA (d) Made with Synthesized $ZnCl_2$

Run	Zn-EDTA (a), (b), & (c) (s)	Zn-EDTA (d) (s)
1	8.192	8.096
2	7.370	8.026
3	7.539	8.141
4	8.142	
5	7.889	
6	9.008	
7	7.676	
8	7.999	
9	7.800	
Average	7.957	8.088
Standard deviation	0.477	0.058

Table B51. T_1 Values of Area Fit of Lateral Peak of Zn-EDTA (a), (b), and (c) with Zn-EDTA (d) Made with Synthesized $ZnCl_2$

Run	Zn-EDTA (a), (b), & (c) (ms)	Zn-EDTA (d) (ms)
1	430.000	449.000
2	424.300	438.900
3	395.400	438.500
4	401.700	
5	418.900	
6	404.300	
7	401.700	
8	398.299	
9	415.700	
Average	410.033	442.133
Standard deviation	12.432	5.950

Table B52. T_1 Values of Area Fit of Central Peak of Zn-EDTA (a), (b), and (c) with Zn-EDTA (d) Made with Synthesized $ZnCl_2$

Run	Zn-EDTA (a), (b), & (c) (ms)	Zn-EDTA (d) (ms)
1	348.700	376.000
2	351.500	457.700
3	386.599	383.400
4	360.000	
5	413.300	
6	396.500	
7	426.400	
8	372.300	
9	364.500	
Average	379.978	405.700
Standard deviation	27.543	45.185

Table B53. P-values of Comparison of Zn-EDTA (a), (b), & (c) with Zn-EDTA (d) Made with Synthesized $ZnCl_2$

Peak	Two-Tailed P Value for Intensity	Two-Tailed P Value for Area
1 (178 ppm)	0.4184	0.6572
2 (61 ppm)	0.0891	0.0018
3 (56 ppm)	0.1181	0.2538

A comparison of the T_1 values from the intensity fit of the carbonyl, lateral, and central peaks of apo-EDTA solutions and ^{67}Zn-EDTA made with $^{67}Zn^{2+}$ are shown in **Table B54** to **B56**.

Those associated with the area fits are shown in **Table B57** to **B59**. The P-values from student's t test are summarized in **Table B60**.

Table B54. T_1 Values of Intensity Fit of Carbonyl Peak of apo-EDTA (a), (b), and (c) with ^{67}Zn-EDTA (e)

Run	**apo-EDTA (s)**	**^{67}Zn-EDTA (s)**
1	10.210	9.128
2	10.350	8.300
3	9.492	8.012
4	11.320	
5	10.110	
6	9.803	
7	9.870	
8	9.305	
9	8.302	
Average	9.862	8.480
Standard deviation	0.824	0.579

Table B55. T_1 Values of Intensity Fit of Lateral Peak of apo-EDTA (a), (b), and (c) with ^{67}Zn-EDTA (e)

Run	apo-EDTA (ms)	^{67}Zn-EDTA (ms)
1	482.099	396.200
2	487.200	457.600
3	500.399	508.700
4	560.000	
5	521.599	
6	500.299	
7	533.100	
8	513.199	
9	498.200	
Average	510.677	454.167
Standard deviation	24.490	56.329

Table B56. T_1 Values of Intensity Fit of Central Peak of apo-EDTA (a), (b), and (c) with ^{67}Zn-EDTA (e)

Run	apo-EDTA (ms)	^{67}Zn-EDTA (ms)
1	449.200	472.400
2	436.900	352.300
3	454.200	361.099
4	424.000	
5	405.100	
6	381.000	
7	577.699	
8	429.800	
9	466.600	
Average	447.167	395.266
Standard deviation	55.409	66.944

Table B57. T_1 Values of Area Fit of Carbonyl Peak of apo-EDTA (a), (b), and (c) with ^{67}Zn-EDTA (e)

Run	apo-EDTA (s)	^{67}Zn-EDTA (s)
1	9.790	8.062
2	10.720	8.515
3	10.170	8.218
4	10.790	
5	9.157	
6	10.760	
7	9.424	
8	9.944	
9	9.921	
Average	10.075	8.265
Standard deviation	0.591	0.230

Table B58. T_1 Values of Area Fit of Lateral Peak of apo-EDTA (a), (b), and (c) with ^{67}Zn-EDTA (e)

Run	apo-EDTA (ms)	^{67}Zn-EDTA (ms)
1	473.800	436.000
2	449.900	480.300
3	480.600	427.900
4	468.500	
5	474.300	
6	469.400	
7	530.200	
8	532.699	
9	541.800	
Average	491.244	448.067
Standard deviation	33.913	28.207

Table B59. T_1 Values of Area Fit of Central Peak of apo-EDTA (a), (b), and (c) with ^{67}Zn-EDTA (e)

Run	apo-EDTA (ms)	^{67}Zn-EDTA (ms)
1	372.599	454.099
2	383.099	430.400
3	372.000	393.799
4	389.400	
5	400.799	
6	452.599	
7	454.600	
8	510.499	
9	435.400	
Average	418.999	426.099
Standard deviation	47.296	30.379

Table B60. P-values of Comparison of apo-EDTA (a), (b), & (c) with ^{67}Zn-EDTA (e)

Peak	Two-Tailed P Value for Intensity	Two-Tailed P Value for Area
1 (175/178 ppm)	0.0241	0.0005
2 (57/61 ppm)	0.0294	0.0769
3 (51/56 ppm)	0.2085	0.8154

A comparison of the T_1 values from the intensity fit of the carbonyl, lateral, and central peaks of Zn-EDTA solutions and ^{67}Zn-EDTA made with $^{67}Zn^{2+}$ are shown in **Table B61** to **B63**.

Those associated with the area fits are shown in **Table B64** to **B66**. The P-values from student's t test are summarized in **Table B67**.

Table B61. T_1 Values of Intensity Fit of Carbonyl Peak of Zn-EDTA (a), (b), and (c) with ^{67}Zn-EDTA (e)

Run	Zn-EDTA (s)	^{67}Zn-EDTA (s)
1	7.949	9.128
2	7.774	8.300
3	7.619	8.012
4	6.848	
5	7.971	
6	7.756	
7	7.993	
8	7.819	
9	8.671	
Average	7.822	8.480
Standard deviation	0.472	0.579

Table B62. T_1 Values of Intensity Fit of Lateral Peak of Zn-EDTA (a), (b), and (c) with ^{67}Zn-EDTA (e)

Run	Zn-EDTA (ms)	^{67}Zn-EDTA (ms)
1	398.400	396.200
2	403.100	457.600
3	378.400	508.700
4	400.200	
5	423.900	
6	453.900	
7	398.400	
8	382.599	
9	433.300	
Average	408.022	454.167
Standard deviation	24.470	56.329

Table B63. T_1 Values of Intensity Fit of Central Peak of Zn-EDTA (a), (b), and (c) with ^{67}Zn-EDTA (e)

Run	Zn-EDTA (ms)	^{67}Zn-EDTA (ms)
1	337.799	472.400
2	314.400	352.300
3	308.800	361.099
4	347.999	
5	414.900	
6	334.299	
7	351.400	
8	392.100	
9	417.300	
Average	357.666	395.266
Standard deviation	40.852	66.944

Table B64. T_1 Values of Area Fit of Carbonyl Peak of Zn-EDTA (a), (b), and (c) with ^{67}Zn-EDTA (e)

Run	Zn-EDTA (s)	^{67}Zn-EDTA (s)
1	8.192	8.062
2	7.370	8.515
3	7.539	8.218
4	8.142	
5	7.889	
6	9.008	
7	7.676	
8	7.999	
9	7.800	
Average	7.957	8.265
Standard deviation	0.477	0.230

Table B65. T_1 Values of Area Fit of Lateral Peak of Zn-EDTA (a), (b), and (c) with ^{67}Zn-EDTA (e)

Run	Zn-EDTA (ms)	^{67}Zn-EDTA (ms)
1	430.000	436.000
2	424.300	480.300
3	395.400	427.900
4	401.700	
5	418.900	
6	404.300	
7	401.700	
8	398.299	
9	415.700	
Average	410.033	448.067
Standard deviation	12.432	28.207

Table B66. T_1 Values of Area Fit of Central Peak of Zn-EDTA (a), (b), and (c) with ^{67}Zn-EDTA (e)

Run	Zn-EDTA (ms)	^{67}Zn-EDTA (ms)
1	348.700	454.099
2	351.500	430.400
3	386.599	393.799
4	360.000	
5	413.300	
6	396.500	
7	426.400	
8	372.300	
9	364.500	
Average	379.978	426.099
Standard deviation	27.543	30.379

Table B67. P-values of Comparison of Zn-EDTA (a), (b), & (c) with ^{67}Zn-EDTA (e)

Peak	Two-Tailed P Value for Intensity	Two-Tailed P Value for Area
1 (175/178 ppm)	0.0745	0.3180
2 (57/61 ppm)	0.0648	0.0069
3 (51/56 ppm)	0.2600	0.0337